A STUDY OF THE EFFECTS OF DISLOCATION DENSITY AND CRYSTAL ORIENTATION ON THE KINETICS OF THE CATALYZED OXIDATION OF ETHYLENE OVER A SINGLE CRYSTAL OF SILVER

Thesis by

Joe William Woodward

In Partial Fulfillment of the Requirements

For the Degree of

Doctor of Philosophy

California Institute of Technology

Pasadena, California

1965

(Submitted December 14, 1964)

ACKNOWLEDGMENTS

I wish to thank Dr. W. H. Corcoran, my research advisor, for the guidance, interest, and encouragement which he gave throughout the course of this work.

The efforts of Willard Dewitt and George Griffith during the construction of the apparatus were deeply appreciated.

The research project was supported by the Petroleum Research Fund and personal financial support was furnished by Richfield Oil Corporation, Allied Chemical Corporation, The National Science Foundation, and the Institute. This support is gratefully acknowledged.

Finally, special thanks go to my wife for her patience and encouragement.

ABSTRACT

A study of the effects of dislocation density and crystal orientation on the kinetics of the catalyzed oxidation of ethylene over a single crystal of silver was carried out in a continuous-flow microreactor. The reactor was constructed so the reacting gas stream contacted only gold surfaces and the surface of the silver crystal. A high-sensitivity gas chromatograph was developed and calibrated for the analysis of the exhaust gas from the reactor. The effect of diffusion to and from the catalyst surface on the observed kinetics was determined by solution of the partial differential equations which described diffusion and flow in the reactor geometry.

Tests of the reactor indicated ethylene oxide was oxidized on the gold surfaces. The rate was independent of the ethylene oxide concentration and had an apparent activation energy of 9.0 ± 1.3 Kcal./gm. mole. The rate of production of carbon dioxide from the oxidation of ethylene oxide at 260°C with 80% oxygen in feed gas and a pressure of 740 mm was 2.1×10^{-8} gm. moles/min. $cm.^2$

The gold surface was also active for the oxidation of ethylene. With a feed of 20% ethylene and 80% oxygen at 260°C and a pressure of 740 mm, the rate of production of carbon dioxide was 2.8×10^{-8} gm. moles/min.$cm.^2$ with an apparent activation energy of 26.0 ± 4.0 Kcal./gm. mole.

A feed composition of approximately 20% ethylene and 80% oxygen was used for all reactor runs with silver crystals, and the temperature was varied from 250 to 350°C to determine the effects of

dislocation density and crystal orientation on the temperature dependence of the reaction rate. No significant differences were observed in the rates of production of carbon dioxide on non-strained crystals with (100), (110), and (111) crystal planes parallel to the surface. In addition no significant differences were observed in the rates of production of carbon dioxide on crystals with (100), (110), and (111) planes parallel to the surface which had been strained 0.8% by rolling parallel to the axis at 45° increments around the circumference of the crystals. An apparent activation energy of 23.1 ± 1.8 Kcal./gm. mole was obtained for the strained and non-strained crystals, but the rate decreased from 6.3×10^{-8} gm. moles/min. cm.^{2} for the non-strained crystals to 3.2×10^{-8} gm. moles/min. cm.^{2} for the strained crystals, with a feed of 20% ethylene and 80% oxygen at 260°C and 740 mm pressure.

The results of chemical etching of the crystal surfaces to reveal dislocations were not considered conclusive, but if a one-to-one correspondence between etch pits and dislocations is assumed, then the dislocation density increased about 40% with the 0.8% strain. As a result it was concluded that the dislocations did not act as active sites for the oxidation of ethylene to carbon dioxide but interfered with the oxidation reaction in some manner.

Photographic materials on pp. 79-87 are essential and will not reproduce clearly on Xerox copies. Photographic copies should be ordered.

TABLE OF CONTENTS

LIST OF TABLES

LIST OF FIGURES

INTRODUCTION

Ethylene oxide is an important organic chemical used in the manufacture of ethylene glycol, polyethylene glycols, ethanolamines, plastics, surface-active agents, and other products (11, 16). Two processes are used in the commercial production of ethylene oxide: 1.) the ethylene chlorohydrin process and 2.) the catalytic partial oxidation process (11, 12). The oxidation of ethylene to ethylene oxide on a silver catalyst was first patented by Lefort (18). The commercial application of this process surpassed the chlorohydrin process capacity in 1954 (11).

The catalytic oxidation of ethylene on silver proceeds by two main overall reactions:

$$C_2H_{4(g)} + \frac{1}{2} O_{2(g)} \xrightarrow{Ag} C_2H_4O_{(g)} \quad \Delta H_{298} = -24.7 \text{ Kcal.} \qquad (1)$$

$$C_2H_{4(g)} + 3O_{2(g)} \xrightarrow{Ag} 2CO_{2(g)} + 2H_2O_{(g)} \quad \Delta H_{298} = -316.2 \text{ Kcal.} \qquad (2)$$

These reactions have been studied by various authors at temperatures from 150 to 400°C, pressures from 0.2 to 20 atmospheres, oxygen concentrations from 1.5 to 90%, ethylene concentrations from 0.6 to 60%, carbon dioxide concentrations from 0.1 to 90%, and ethylene oxide concentrations from 0.3 to 3%. Nitrogen was usually used as a diluent. A typical set of operating conditions would be a temperature of 274°C, an oxygen concentration of 20%, an ethylene concentration of 4.7%, and a total conversion of 68% of the ethylene with 52% of the

reacted ethylene converted to ethylene oxide (25). A typical catalyst would be 12% by weight of silver supported on an alundum support (3).

Much work has been done on the study of the overall rates of reactions (1) and (2) and the properties of various combinations of silver and catalyst supports. There has been little study of the kinetics and mechanism of the reactions, and much of the work reported in the literature is inconclusive because the effects of the products of the reactions and the effects of the nature of the surface of the catalyst on the kinetics and mechanisms of the reactions were not studied in sufficient detail.

Most of the work reported in the literature was concerned with studies of the overall rates of reactions (1) and (2) and the optimum operating conditions for a particular combination of silver and catalyst support prepared in a specific manner (7, 22, 23). McBee, Hass, and Wiseman (20) reported the activity, selectivity, and optimum operating conditions may vary from batch to batch of catalyst prepared in the same manner. Variation in the catalyst properties with time was a problem encountered by Orzechowski and MacCormack (25) and Buntin (3).

The work of Twigg (32) is an early study of the kinetics and mechanisms of these reactions. He used silver, plated on glass fibers, for the catalyst in both flow and static experiments. Twigg proposed the following reaction scheme on the basis of his results:

$$O_{2(g)} \rightarrow 2O_{(a)} \qquad (3)$$

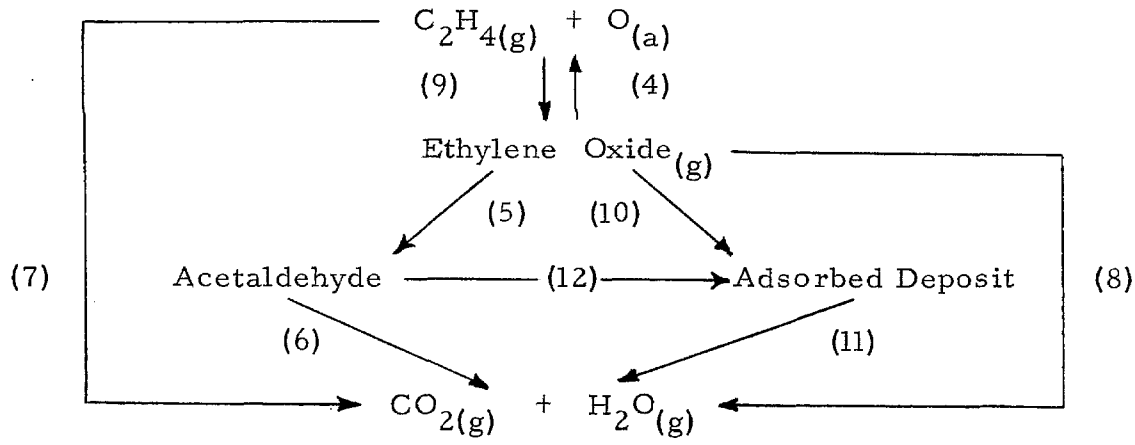

He found reaction (3) was the rate controlling step; reactions (4), (5), (6), and (7) were fast steps of the overall reactions; and the other reactions were much slower. The adsorbed deposit was a non-volatile residue of varying composition. Twigg proposed the following mechanism for the oxidation of ethylene to either ethylene oxide or to carbon dioxide and water:

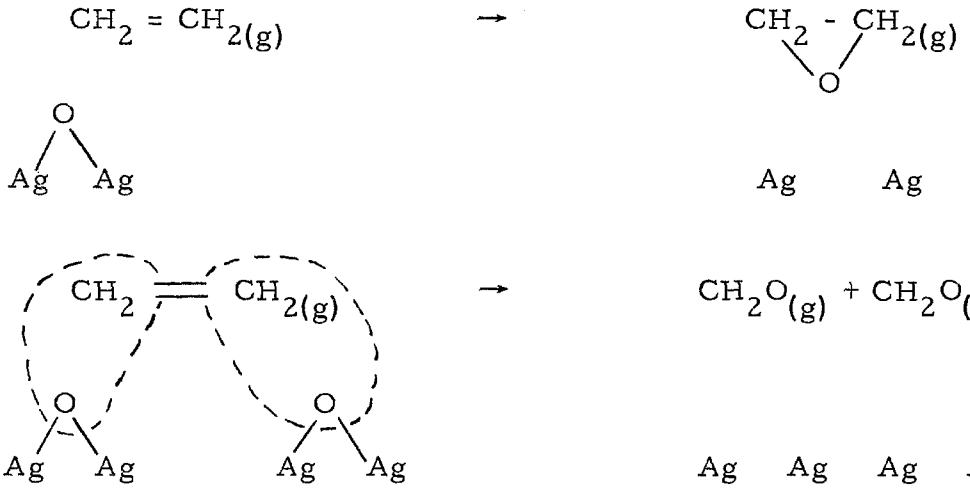

The formaldehyde formed by reaction (13) is then rapidly oxidized by the following reactions:

$$CH_2O_{(g)} \rightarrow CO_{(a)} + 2H_{(a)} \quad (14)$$

$$2H_{(a)} + O_{(a)} \rightarrow H_2O_{(g)} \quad (15)$$

$$CO_{(a)} + O_{(a)} \rightarrow CO_{2(g)} \quad (16)$$

Twigg found the concentration of ethylene oxide reached a maximum and then decreased. He proposed the oxideation of the ethylene oxide proceeded by isomerization to acetaldehyde which was rapidly oxidized.

A study of Burgoyne and Kapur (4) indicated the rate of homogeneous oxidation of ethylene oxide was large enough to produce errors in the results of Twigg's static experiments. Extrapolation of the data of Heckert and Mack (15) and Fletcher and Rollefson (9) for the rate of thermal decomposition of ethylene oxide to the temperatures used by Twigg showed the homogeneous rate of isomerization of ethylene oxide to acetaldehyde was very slow. The isomerization reaction was assumed the rate controlling step for the thermal decomposition of ethylene oxide. This would indicate the more rapid isomerization reaction observed by Twigg occurred on the catalyst surface.

Orzechowski and MacCormack (25) made a detailed study of the kinetics and mechanism of reactions (1) and (2) in a flow reactor. Their catalyst was prepared from a silver alloy containing 8.5% by weight of calcium which was removed by leaching with acetic acid. They observed slow changes in the activity and selectivity of the catalyst for periods of over 60 hours after changes in operating conditions. Their studies on the rate of oxidation of ethylene oxide in the

presence of the silver catalyst compared to the rate of isomerization of ethylene oxide on the catalyst indicated the rate controlling step was a reaction between gaseous ethylene oxide and adsorbed oxygen atoms. Their mechanism for the oxidation of ethylene involved the reaction of gaseous ethylene with a single adsorbed oxygen atom. The product of this reaction was desorbed as ethylene oxide or an isomeric compound which was rapidly oxidized to CO_2 and H_2O. They proposed different crystal planes of silver could have different values for the various rate constants involved in their mechanism and poisoning of some of these crystal planes would account for the slow processes which affected the activity and selectivity of the catalyst. Stable oxygen-silver bonds and organic deposits were suggested as possible poisons.

Some work has been done on the effects of the crystallographic orientation of the catalyst surface by Wilson, Voge, Stevenson, Smith, and Atkins (36). They compared the catalytic activity and selectivity of randomly orientated silver films evaporated onto the inside of a pyrex glass tube to the activity and selectivity of films which were orientated with the (110) crystal plane parallel to the surface. No difference in activity or selectivity was observed. They examined the structure of the film by low angle electron diffraction and found the (110) orientated film would lose its orientation after exposure to the reaction gases for a few hours. The large amount of energy released by the total oxidation of the ethylene was thought to be large enough to cause the reorientation of the film.

Kummer (17) used single silver crystals as the catalyst for the partial oxidation of ethylene and compared the activity and selectivity of the single crystals to the activity and selectivity for a sheet of poly-crystalline silver. These crystals were 0.15 cm. thick, 1.5 cm. wide, and 10 cm. long. The surfaces of these crystals were not orientated parallel to any particular crystal plane. Kummer machined a 5/8 in. sphere to expose only (111) crystal planes as the catalyst surface. He did not detect any differences in the activity or selectivity of the single crystals as compared to the poly-crystalline sheet.

The intersection of line crystal defects, dislocations, with catalyst surfaces have been suggested as active sites for catalytic reactions to explain the increase in catalytic activity of copper and nickel catalysts after cold-working and the decrease in activity of the cold-worked catalysts with annealing (33). Sosnovsky (29) proposed dislocations were the active sites for the decomposition of formic acid on silver. He based this conclusion on the increase in catalyst activity after bombardment of the silver surface with argon ions. Ions with energies above 77 ev. caused the surface of single silver crystals to break into small crystalline blocks rotated several degrees with respect to one another. The disturbed region extended 100 A. into the bulk of the crystal. The low angle boundaries between the blocks produced an overall increase in dislocation density by a factor of about 10^5. The rate constant for the reaction increased by a factor of about 100, and the activation energy increased from 12.2 Kcal./gm.

mole to 20.8 Kcal./gm. mole.

The development of methods of direct observation of the dislocations in crystals lead to further studies of the role of the dislocation in catalytic activity. Hall and Rase (13) found a considerable increase in the rate of the catalytic dehydrogenation of ethanol on single crystals of lithium fluoride with increases in the dislocation densities of the crystal surfaces. Perkins (26) found only a small increase in the rate of decomposition of formic acid on single silver crystals with large increases of the dislocation density of the surface. Perkins' measurements of the actual area of the surface by hydrogen overvoltage measurements showed a corresponding increase in the surface area with the increased dislocation density. Perkins concluded dislocations did not act as the active sites for the catalytic decomposition of formic acid on silver. The works of Perkins (26) and Sosnovsky (29) are in direct disagreement on the role of dislocations in the catalytic decomposition of formic acid on silver.

McCarty (21) studied the adsorption of ethylene, oxygen, and ethylene oxide on a silver catalyst supported on alundum. A quartz beam microbalance was used in this study. The catalyst sample was obtained from a batch of catalyst used by Buntin (3) for kinetic studies of the partial oxidation of ethylene. The adsorption data indicated the oxygen was dissociated on the silver surface. McCarty found a small amount of ethylene was rapidly adsorbed on the catalyst at 350 and 450°F. Ethylene oxide was adsorbed on the catalyst and was not completely removed by vacuum degassing. The catalyst required

treatment with oxygen and hydrogen to completely remove the ethylene oxide adsorbate.

Czanderna (5) made a recent study of the rate of adsorption and desorption of oxygen on silver powder using a vacuum ultramicrobalance. Three activation energies, 3, 8, and 22 Kcal./gm. mole, were found for different phases of the adsorption process. These were respectively: dissociative adsorption, molecular adsorption, and surface mobility of oxygen adatoms. Five levels of strength of the oxygen-silver bond were observed during the desorption studies. These were:

(1) Very weakly adsorbed oxygen probably physically adsorbed.

(2) Weakly chemisorbed oxygen possibly as charged molecules.

(3) Chemisorbed oxygen possibly as charged atoms.

(4) Strongly chemisorbed oxygen.

(5) Very tightly chemisorbed oxygen probably on high index plane adsorption sites.

Reactions of ethylene oxide on silver catalysts were found to be complex. Orzechowski and MacCormack (25) proposed the oxidation of ethylene oxide involved reactions of the ethylene oxide with adsorbed oxygen. Twigg (32) concluded ethylene oxide isomerized to acetaldehyde which was rapidly oxidized. Twigg observed the formation of deposits on the catalyst surface when it was exposed to ethylene oxide. The deposits were composed of carbon and hydrogen and varied in composition. The formation of ethylene was also observed when ethylene oxide contacted a silver catalyst.

The effects of heat and mass transfer on the observed kinetics

of the reactions have not been carefully considered. These effects might account for some of the disagreement among the results obtained by various experimenters.

In summary the results of various studies reported in the literature did not give definite information concerning the mechanism of the oxidation of ethylene on silver catalysts. There was general agreement that the rate of homogeneous oxidation of ethylene was small compared to the catalytic rate for temperatures lower than 400°C. Most studies concluded oxygen was adsorbed on the silver surface, and ethylene in the gas phase reacted with the adsorbed oxygen.

A study of the kinetics and mechanism of the partial oxidation of ethylene with a single crystal of silver as catalyst was the goal of this work. The crystal was mounted in a continuous flow microreactor and the following four points were emphasized:

1. Analysis of the product gas stream with a high sensitivity gas chromatograph.
2. Mathematical analysis of the effects of flow and diffusion in the microreactor on the observed reaction kinetics.
3. Use of crystal surfaces with specified crystal planes parallel to the surface of the catalyst to determine effects of crystal orientation on the kinetics and mechanism of the reactions.
4. Study of effects of increased dislocation density on kinetics and mechanism of the reactions.

APPARATUS

Single silver crystals for use as the catalyst in the microreactor were purchased from the Unimet Company. Each crystal had been grown in the form of a 1/2 in. cylinder with a particular crystal plane perpendicular to the axis of the cylinder. Three crystal planes, (100), (110), and (111), were obtained for use in the reactor. The cylinders were cut into 1/2 in. lengths by the manufacturer with an electric spark cutting device which minimized the strain introduced into the surfaces. Four slugs of each crystal orientation were obtained. The orientation of the crystals was confirmed by the action of the etching solution on the surface. The dislocation density of the surface was determined from the etch pit density. The details of the etching and polishing are discussed in Appendix C.

The reactor design was selected to provide a symmetric flow pattern over the catalyst surface to allow the calculation of the effects of the reactants and products to and from the surface. It was also preferable to minimize the amount of mechanical preparation of the crystals for use in the reactor because excessive strain could cause the crystal to reorient when heated (10). Radial gas flow between parallel discs with the gas feed at the center was selected as the flow geometry. This design provided the desired symmetry of flow and also required only polishing of the cylindrical face of the crystal to provide a smooth surface for use as the catalyst. The original reactor design is shown in Figure 1. This was chosen so the only

metal surface which contacted the gas stream in the reaction zone was the silver surface. The reactant gas streams entered through concentric quartz tubes centered on the axis of the reactor. The two gas streams mixed just prior to entering the reaction zone through a 0.010 in. hole in the quartz disc. Quartz tubes were positioned at the outer radius of the crystal so gas samples could be withdrawn before the gas stream contacted the metal surfaces in the remainder of the reactor. The disc spacing could be varied to check the effects of diffusion to and from the catalyst surface. Viton-A or silicone rubber O-rings were used to seal the reactor. A cement for sealing the quartz disc and tubes to the stainless-steel reactor body was difficult to find. The usual ceramic-type cements used to seal the thermocouple protector tubes were porous and also reacted with the quartz at 300°C to form a structurally weak bond. Several high-temperature, organic cements were tried including Dow D. E. N. 438 epoxy resin and Engelhard CA9R cement. The epoxy would not stick to the quartz. The Engelhard CA9R cement was porous and did not produce a gas-tight seal. Minnesota Mining and Mfg. Co. EC 1663 A/B silicone rubber sealer was found to produce a satisfactory bond which was gas-tight and held attemperatures up to 300°C. A copper-constantan thermocouple was calibrated at the freezing points of tin and lead, and then placed in one of the sample tubes which had been sealed for this purpose. The crystals were placed in crystal holders which were bored to fit each crystal. The body of the reactor and the the crystal holders were constructed from Type 304 stainless steel.

The reactor was mounted in an electric oven to provide the necessary temperature control. This reactor was abandoned when experimental runs indicated reactions of the ethylene oxide on the quartz were sufficiently rapid to make representative sampling of the reaction zone impossible. These reactions combined with diffusion in the direction of flow significantly affected the concentrations in the reaction zone. A detailed discussion of the problem of diffusion in the microreactor is included in Appendix B.

A second reactor was constructed in an attempt to eliminate the problems encountered with the initial design. A sketch of this design is shown in Figure 4. A literature search for the activity of various metals as catalysts for the oxidation of hydrocarbons showed gold was probably less active than most metals (27, 28). This information combined with the relative ease in machining gold as compared to various types of stainless steels provided the basis for the selection of 99.99% pure gold for the major construction material for the second reactor. The second reactor design had two main objectives: 1) to reduce the total reactor volume and surface area to minimize the magnitude of the side reactions and, 2) to provide a less reactive surface for the non-catalytic portion of the reactor. The feed and exhaust tubes were also gold. These were placed in a water-cooled jacket to reduce the heated length of the tubes to a minimum and further reduce the total volume of the reactor. The tubes were fused to the reactor head with pure gold. The inside surface of the support plate for the reactor was gold plated. An exploded view of the reactor

is shown in Figure 5, and views of the reactor head are shown in Figure 6. Gaskets of gold foil were used for the necessary seals in the reactor. The reactor head and support plate were assembled to give an 0.005 in. spacing between the upper disc and the catalyst surface. A crystal holder was fitted with a gold disc for use in runs to determine the catalytic activity of gold for the oxidation of ethylene and ethylene oxide.

Estimates of the reaction rate taken from the literature (3, 17) showed a yield of about 200 ppm of ethylene oxide could be expected with a flow rate of 1 cc./min. of reactants. This very low conversion combined with the low flow rate placed some restrictions on the amount of sample which was available for analysis and the sensitivity of the gas chromatograph used for the analysis. The details of the chromatograph and its calibration are given in Appendix A. A Loenco gas sampling valve was placed in the reactor exhaust stream and was used to inject 1 cc. samples into the chromatograph.

A flow chart for the reactor and the feed gas system is given in Figure 8. Gas could be fed either from the 30 ℓ. stainless steel storage tanks shown or directly from commercial gas cylinders. Matheson Model 8 two-stage regulators were used to reduce the gas pressure from the high pressure of the gas cylinders to a constant feed pressure. Matheson Model 70 low-pressure regulators were used to control the pressure of gas taken from the 30 ℓ. storage tanks. The low-pressure (3 psig.) gas was filtered through Nupro Inline Filters with 7 micron filter elements. Nupro Very Fine 1/16 in.

needle valves were used to set the gas flow. Gas flow rates of less than 1 cc./min. were maintained within 2% for up to three days without adjustment with this flow system. The gas flow rate was measured with a soap-film flow meter which was placed downstream from the gas sample valve.

The electric oven used with the first reactor was constructed with a large thermal mass which was to maintain a constant temperature in the oven without using a temperature controller. Temperature variations in the laboratory were large, and the oven temperature varied several degrees over a twenty-four hour period. The oven also required a long period of time to reach its operating temperature. Attempts to control the oven temperature with a simple on-off type controller were not successful because of the large thermal mass.
A fluidized-bed temperature bath was constructed for use with the second reactor. The design shown in Figure 7 was developed from designs given by Hall and Rase (13) and Sutcliffe (31). The bath was 4.0 in. in diameter and 7 in. deep. A 750 watt Calrod heating element was used in a double-pipe heat exchanger for preheating the air which was used to fluidize the bed. A 1000 watt Calrod heating element was used to supply heat to the walls of the bed. The bed was filled with 60-80 mesh glass beads purchased from Minnesota and MiningManufacturing Co. The output from a thermocouple placed about 1/2 in. above the distributor plate in the bed was subtracted from a reference voltage and the difference was amplified with a D. C. amplifier. The amplified difference signal was fed to a Barber-Coleman

Potentiometric Recorder with an on-off controller. The use of the reference voltage and D. C. amplifier increased the sensitivity of the controller. The total power input to the heating elements was set with Variacs. About 25% of the power to the main heating element was varied by the controller by switching a resistor into and out of series with the main heating element. Overheating of the bath was prevented with a second on-off switch controlling the total power input to the bath. This switch was set about 20°C above the control point. The bath could be controlled to ± 0.5°C with this arrangement. The bath had very rapid response and the temperature could be raised 100°C in less than 1 hour. The bath was used at temperatures above 400°C without any difficulties. The value of 60 BTU/(hr.)(°F.)(sq. in.) was obtained as a heat transfer coefficient for the bath. The bath, reactor, and preheated air temperatures were recorded on a 4-point Brown potentiometric recorder to give a continuous indication of the bath performance. The EMF produced by the thermocouple mounted in the reactor was measured on a Leeds and Northrup K-3 potentiometer for use in data calculations. The rate of heat transfer within the bath was sufficiently great that the reactor remained only about 3°C below the bath temperaure in spite of the heat losses due to conduction along the feed tubes, exhaust tube, and reactor supports.

EXPERIMENTAL

A program of experimental work was selected to determine the effects of crystal orientation and changes in density of the dislocations on the temperature dependence of the rate constants for the reactions involved in the partial oxidation of ethylene on silver. This program consisted of a series of reactor runs with constant feed composition at four temperatures: 250, 280, 320, and 350°C. One crystal of the three crystallographic orientations, (100), (110), and (111), was used in the non-strained state and one each of the three orientations was used as the catalyst after being strained 0.8%. The crystals were strained by deforming the cylindrical crystals 0.004 in. on the 0.5 in. diameter by rolling parallel to the axis of the crystal with a 3 in. hand roll. This was repeated at 45° increments around the circumference of the crystal. This method of straining produced some visible deformation over most of the face of the crystal and did not destroy the general cylindrical shape of the crystal. The three non-strained crystals and the three strained crystals were chemically polished, etched to show the dislocation density of the polished surface, photographed to record the dislocation densities, and repolished to remove the etch pits. These operations were performed on the six crystals at the same time to try to produce surfaces in the same condition for use as catalysts. The six crystals were stored in a desiccator until needed for use in the reactor. Details of the chemical polishing and etching procedure are given in Appendix C.

C. P. grade ethylene, minimum purity 99.0%, was purchased

from the Matheson Co. for use as reactor feed gas. This ethylene was analyzed by gas chromatography and found to contain at least 10 hydrocarbon impurities. These hydrocarbon impurities were removed by passing the ethylene through two columns, 1.25 in. I.D. and 4 ft. long, filled with Linde Type 5A and Type 13X Molecular Sieve. The columns were activated by heating at 250°C under vacuum for several days and were placed in a dry ice-acetone slurry during the purification operation. Purified ethylene was condensed in a liquid nitrogen trap and later boiled into a stainless-steel storage tank at about 80 psig. Ethylene obtained in this manner contained only about 1 ppm of an unsaturated C-4 hydrocarbon and about 1% nitrogen.

A feed-gas mixture of about 0.5% ethylene oxide in helium was stored in another stainless-steel tank. Matheson ethylene oxide of 99.7% minimum purity was used in this mixture. No impurities were detected by gas chromatographic analysis of the ethylene oxide used in this work. Linde helium, 99.99% minimum purity, was used for the balance of this mixture.

Oxygen, 99.5% minimum purity, for the reactor feed was used directly from Linde cylinders with no further treatment.

A constant flow rate of about 1 cc./min. measured at room conditions was used for the reactor runs. A feed composition of about 25% ethylene and 75% oxygen was selected from the results given by Buntin (3) and Wan (35) to give a reasonable reaction rate. The flow system described in the Apparatus Section maintained this com-

position and total flow rate very well. The total flow would change about 1% with changes in reactor temperature from 250°C to 350°C. This change of flow rate was probably due to the increased pressure drop through the reactor due to the increase in gas viscosity with temperature and the increase in the velocity of the gas in the reactor due to the increase in the specific volume of the gas with increased temperature. The total flow rate of gas through the reactor was measured at the exhaust side of the Loenco gas sample valve with a soap-film flow meter. This flow meter was calibrated by filling with mercury and weighing the amount of mercury contained between marks on the scale of the meter. The volume of the tube was determined to ± 0.45% in this manner. The time required for 1.5 cc. of gas to flow through the meter could be measured to the nearest 0.01 min.; so a flow rate of 1 cc./min. could be determined to within ± 1.2%.

At the beginning of a run a crystal in its holder or the gold blank was installed in the reactor which was then tested at 3 psig. for possible leaks. Usually a sample of the reactor exhaust was analyzed with the reactor at room temperature to check the feed composition. No reaction was ever observed during the room temperature composition checks. The reactor was lowered into the fluidized temperature bath which was set at about 320°C. The reactor would reach the bath temperature in less than 15 min., but no samples were taken for at least one hour after placing the reactor in the bath. Atmospheric pressure, room temperature, the EMF of the reactor thermocouple, and the gas flow rate were measured each time a sample of the

reactor exhaust was analyzed. Usually three samples of the reactor exhaust were taken at each reactor temperature. Each sample required about 30 min. to analyze so the reactor remained at one temperature for at least 2.5 hr.

Two runs with the gold disc installed in place of a silver crystal were made to determine the effects of the gold surfaces on the experimental results. One run was made with approximately the same feed conditions as used with the silver crystals. The second run was made with a feed of 80% oxygen, 0.03% ethylene oxide, and the balance helium.

The usual sequence of temperature points was 320, 350, 250, and 280°C. This sequence was used after the first crystal run because an increase in the activity of the crystal surface was observed during this run. The activity increase occurred slowly at 250°C and more rapidly at 280°C. The data taken with this sequence of temperatures were reasonably reproducible so any activity changes were rapid enough at 320°C to not be observed in the data. The reactor was removed from the temperature bath at the completion of the series of temperature runs and allowed to cool. About one hour was required for the reactor to cool enough to allow removal of the crystal. The crystal was removed from the reactor and stored in a dessicator. A chromatograph calibration sample was usually run during the time the temperature of the bath was being changed. The bath required about 15 min. to reach the new set point and the reactor was left at the new temperature for about 1 hr. before more samples were taken.

The gas flow rate, thermocouple EMF, room temperature, atmospheric pressure, and peak areas with the necessary identification and attenuation data from the chromatograph analysis were recorded on data sheets and punched on IBM data cards. The calculations necessary to convert the data to the analysis of the gas samples and the reactor operating conditions were made using an IBM 7094 Digital Computer. The sample analysis and reactor operating conditions were printed out by the computer and punched onto data cards for further use in the correlation of the results. The use of the digital computer for these rather routine calculations had several advantages such as reducing the time required for the calculation of the results of the chromatograph analysis. Small corrections such as use of experimentally-determined values for the attenuation factors of the bridge circuits for the chromatograph detectors were included in the calculations with no increase in the amount of work or time required for the calculations. The possibility of human errors in punching the calculated results for use in the rate correlations was avoided by using the computer to punch the results.

The surfaces of the crystals used as catalyst surfaces were examined with a microscope to determine any similarities among the deposits on the surfaces after the completion of the six crystal runs. Photomicrographs of possibly interesting deposits were made, and the crystals were lightly polished to remove the deposits and then etched to reveal the dislocation arrays. It was not possible to remove the

surface deposits with solvents such as methyl alcohol, ethyl alcohol, acetone, hexane, or ethylene dichloride.

These deposits were not removed when one of the crystals was placed in an ultra-sonic cleaning bath with hexane as the solvent. No attempt was made to analyze the deposits. The decomposition pressure of silver oxide is 1 atm. at 190°C so it could not be formed at the reactor operating conditions (1, 2). Twigg (32) had observed the formation of an organic deposit on the catalyst when ethylene oxide or acetaldehyde was exposed to the silver surface. Organic deposits were proposed as possible catalyst poisons by Orzechowski and MacCormack (25). Based on these observations reported in the literature the deposits observed during this work were assumed to be organic in nature.

Photomicrographs of the etch pit patterns in the same location as the photomicrographs of the surface deposits were made for comparison purposes. These are discussed in the Discussion of Results Section.

INTERPRETATION AND CORRELATION OF DATA

Temperature

The temperature indicated by the thermocouple mounted in the gold head of the reactor was assumed to be the temperature of the reacting gas stream and the catalyst surface. Energy requirements to heat the feed gas stream were negligible because the total flow rate was on the order of 5×10^{-5} gm. moles/min.; the specific heat of ethylene was 0.430 cal./(cm.)(^{o}C); the specific heat of oxygen was 0.2213 cal./(gm.)(^{o}C) (14); and the temperature rise of the feed gas was less than 400^{o}C which gave an energy requirement of 0.245 cal./min. to heat the feed gas. Energy released by the exothermic reaction of the total oxidation of the ethylene was also neglected because the oxidation rate was on the order of 1×10^{-6} gm. moles/min. and the heat of combustion of ethylene was on the order of - 316 Kcal./gm. moles which gave 0.34 cal./min. for the rate of energy release by the reaction.

Pressure

Atmospheric pressure was measured on a mercury manometer which was read to ± 0.05 in. or ± 0.2%. The pressure drop calculated for the flow of the exhaust gases from the reactor through the sample valve and exhausting to the atmosphere through the soap-film flow meter was on the order of 0.05 psi or about 0.35% of an atmosphere. Calculations of the flow pattern in the reactor discussed in Appendix B included the calculation of the pressure drop for flow between the

parallel disc section of the reactor. This pressure drop was in the range of 1×10^{-6} psi. Corrections for the pressure drop between the reactor and the end of the exhaust tube were only slightly larger than the expected experimental uncertainty in the measurement of atmospheric pressure so they were neglected. Atmospheric pressure was used as the pressure in the reactor.

Dislocation Density

The crystal surfaces were chemically etched to produce etch pits which were supposed to correspond to intersections of dislocation lines with the surface. The details of this etching procedure are given in Appendix C. Photomicrographs of the etched surfaces were made and the etch-pit densities of the surface determined by counting the pits in 5-1/4 in. square areas selected at random. The counts obtained were averaged and converted to etch-pit densities. The values of the etch-pit densities for the crystals used in the reactor are given in Table 22.

Volumetric Flow Rate

A soap-film flow meter was used to measure the volumetric flow rate of the reactor exhaust gas with an estimated uncertainty of 1.2%. The flow rate was corrected to a dry basis because the feed gases were dry and only small amounts of water were produced in the reactor. The gas in the flow meter was assumed saturated with water at the temperature of the laboratory due to the contact with the

wet walls of the tube. A molar flow rate was calculated from the volumetric flow rate with the equation of state of an ideal gas.

Analysis of Reactor Exhaust

A Loenco gas sampling valve was placed in the reactor exhaust stream between the reactor and the soap-film flow meter. The sample valve was placed in the sample pick-up position for at least 10 minutes before injecting the sample into the chromatograph. Development and calibration of the chromatograph used in this work is presented in Appendix A. The sample loop was flushed about 10 times during the waiting period by the flow of the exhaust gas through loop. Analysis of a sample required about 30 minutes. The sample valve was left in the inject position until after compounds which were measured on the hydrogen flame detector were eluted. A very small amount of sample was injected into the chromatograph when the sample valve was moved from the inject position back to the sample pick-up position. This procedure prevented any possible interference between the small sample peak and the sample analysis. This small peak was easily distinguished from the other components present in the exhaust gas samples by its sharp, symmetric shape. There was no possibility of confusing this peak with higher molecular weight compounds in the sample. Three compounds were detected during the analysis of the reactor exhaust which had not been considered during the development and calibration of the chromatograph. These were identified by comparison of their retention times with retention times determined for

27 saturated, unsaturated, and oxygenated hydrocarbon compounds. The unknown compound with a retention time of about 6.8 min. on Column III was identified as 1-butene. The other two compounds with retention times of 9.8 and 14.5 min. were identified as C-6 hydrocarbons. The column labeled C-4 in Tables 1-8 refers to the component with a retention time of 6.8 min.; column C-6,1 refers to the component with retention time of 9.8 min.; and column C-6, 2 refers to the component with retention time of 14.5 min. These identifications can not be considered as absolute because it is possible for other compounds to have the same approximate retention times on a particular chromatograph column. The retention times varied a little with the amount of material injected into the column, and this variation added to the uncertainty of the identification. Relative response factors were estimated for these compounds on the hydrogen flame detector from data given by Sternberg (30) and Ettre (8). The results of the chromatograph calculations indicated these compounds were present in the reactor exhaust in quantities of about 1 part per million.

Concentrations of Reactants and Products in Reactor

The molar concentration of gas was calculated from the equation of state for an ideal gas at atmospheric pressure and the temperature observed with the reactor thermocouple. The conversion was very low compared to the amount of reactants in the runs with ethylene-oxygen feed. The concentrations of the reactants were assumed uniform over the surface of the catalyst, and the values obtained from

the analysis of the exhaust gas were used in the correlation of the rate data. The volumetric flow rate measured at reactor conditions was in the range of 2.0-2.5 cc./min. for this run, and the diffusion coefficient of ethylene oxide was estimated to be on the order of 0.5 cm.^{2}/sec. Under these conditions the parameter β used in evaluating the effects of diffusion in the direction of flow in Appendix B ranged from 0.84 to 1.05. Figure B-6, Appendix B, gave the ratio of the area average concentration change to the total concentration change as about 0.85 for $\beta = 1$. This indicated diffusion in the direction of flow was sufficiently rapid under these conditions that the concentration of reactants in the reactor was nearly uniform over the surface independent of the degree of conversion. As a result of the analysis of diffusion effects, all reactant concentrations were considered to be uniform over the surface of the reactor with the value indicated by analysis of the exhaust gas stream.

Rate Constants

The experimental results for the six silver crystal runs and two gold blank runs are given in Tables 1-8. Examination of this data showed the total conversion of ethylene on the silver crystals was in the range expected on the basis of other kinetic studies (3, 17). The yield of ethylene oxide, less than 1% of the ethylene which reacted, was much smaller than the 30-70% yield which was expected for the silver crystals. The oxidation rate of ethylene oxide on the gold was larger than was expected from the limited data available on the catalytic activity of gold (27, 28). The rate of oxidation of ethylene

observed on the gold surfaces was about one-tenth of the rate observed on the silver surfaces. Acetaldehyde, 1-butene, and two C-6 hydrocarbons were detected in small amounts in the reactor exhaust.

The goal of this series of experimental runs was to determine the effects of dislocation density and crystal orientation of the catalyst surface on the temperature dependence of the reaction rates. Since some variation in the reactant concentrations did occur even though they were maintained as constant as possible, the possibility of obtaining some information on the dependence of the reaction rate on the reactant concentrations was investigated. The preliminary examination of the data showed only the rate of production of carbon dioxide was large enough to be measured with a reasonable degree of accuracy. An error analysis of the data is discussed later. The first step in the correlation of the rate data on the silver crystals was to determine the effects of the gold surface on the experimental results.

Oxidation of Ethylene Oxide on Gold

The oxidation of ethylene oxide on the gold surface was considered first. Since the variation in reactant concentrations were reasonably small, only simple rate expressions were fit to the experimental data. A multi-dimensional least-squares method described by Deming (6) was used to fit the experimental data to the following rate equation:

$$QC_{CO_2} = S_T k C^{o}_{O_2} C^{m}_{EO} \tag{17}$$

The reaction rate constant was assumed to have the Arrhenius form

of temperature dependence

$$k = Ae^{-E_a/RT} \tag{18}$$

where E_a is an apparent activation energy. Reaction orders of 0, 1/2, and 1 were tried for the order of the rate with respect to the oxygen concentration, and 0 and 1 were tried for the order of the reaction rate with respect to the ethylene oxide concentration. The constants obtained from the least-squares analysis of the data obtained for the oxidation of ethylene oxide on the gold surface are shown in Table 9. The variance of the fit shown in Table 9 is a measure of how well the data fit the particular rate expression. A large increase in the variance was noted for rate equations which were first-order with respect to the ethylene oxide concentration as compared to the variance of zero-order rate equations. Plots of the logarithm of the rate constant versus the reciprocal of the absolute temperature for the zero-order rate equations were reasonably linear with some experimental scatter. The plots of the rate constants for rate equations which were first-order with respect to the ethylene oxide concentration showed definite curvature. Figure 16 shows the temperature dependence of the rate constant of the rate expression which was zero-order with respect to the ethylene oxide concentration and half-order with respect to the oxygen concentration.

Attempts were made to determine the form of the rate expression for formation of acetaldehyde and ethylene from the data for ethylene oxide-oxygen feed. A first-order rate equation for production of either acetaldehyde or ethylene from the ethylene oxide

was assumed and the acetaldehyde or ethylene was assumed to react with oxygen to form carbon dioxide. Satisfactory fits of the experimental data were not obtained in this manner. Failure of simple rate expressions to fit the data was not surprising. Fletcher and Rollefson (9) found ethylene oxide was a good source of free radicals in the temperature range from 400-450°C. These were assumed to be produced by the following reactions:

$$C_2H_4O \rightarrow HCHO + \dot{C}H_2 \tag{19}$$

$$C_2H_4O \rightarrow CH_3CHO \tag{20}$$

$$\dot{C}H_2 + C_2H_4O \rightarrow 2\dot{C}H_3 + CO \tag{21}$$

$$\dot{C}H_3 + CH_3CHO \rightarrow \dot{C}H_3 + CH_4 + CO \tag{22}$$

It is possible that amounts of free radicals were produced in the range of temperatures used in this work and were responsible for the formation of the ethylene or ethane, and higher hydrocarbons which were detected in small amounts. The isomerization of ethylene oxide to acetaldehyde and the rapid decomposition of the acetaldehyde by the catalytic action of the free radicals was proposed by Fletcher and Rollefson (9) as the mechanism for the thermal decomposition of ethylene oxide. The small amounts of acetaldehyde found in the exhaust stream could have been produced in this manner.

Oxidation of Ethylene on Gold

The analysis of the data obtained for the oxidation of ethylene

on the gold surface was carried out in the same manner as the analysis of the ethylene oxide data. The results of this analysis are shown in Table 10. An "F"-test on the ratio of the variances for the different rate equations showed the differences in the variances were not statistically significant. Therefore no conclusions on the reactant concentration dependence on the rate of oxidation of ethylene on gold could be made from the results. Correction of the data for the oxidation of ethylene on silver for the contribution of the gold surface to the total rate of oxidation was made using the rate expression which was 1/2 order with respect to oxygen and 1st order with respect to ethylene. Figure 17 shows the temperature dependence of the rate constant for this rate equation. The choice of rate equation to use to correct for the reaction on the gold surface was arbitrarily made and was not critical since the correction was only about 20%.

Oxidation of Ethylene on Silver

A calculation of the rate of oxidation of ethylene oxide on the gold surfaces which were exposed to the reactant gases when the silver crystals were mounted in the reactor indicated about 100 times the amount of ethylene oxide detected in the exhaust could have been oxidized on the gold surface if it were present in the reactor. Therefore, correction of the observed rate of formation of ethylene oxide for the effects of the gold surfaces would have been about 100 times larger than the observed value. Since corrections of this magnitude were unreasonable, no attempts were made to correlate the data for the rate of production of ethylene oxide on the silver crystals.

The data for the production of carbon dioxide from ethylene was treated as if there were only two reactions producing carbon dioxide, a reaction between ethylene and oxygen on the gold surface and a reaction of ethylene and oxygen on the silver surface. The results of the analysis of the oxidation of ethylene on the gold surface showed the reaction on the gold surface would account for about 20% of the observed total rate of carbon dioxide production. The following equation was used as the form of the rate expression in the least squares calculations:

$$QC_{CO_2} = S_{Ag}k_{Ag}C^{o}_{O_2}C^{m}_{c=c} + S_{Au}k_{Au}C^{1/2}_{O_2}C_{c=c} \qquad (23)$$

A multi-dimensional least-squares method described by Deming (6) was used in all of the calculations. This method considered all of the experimental variables to have possible errors and weighted the points according to the magnitudes of the estimated experimental errors. A derivation of the least-squares equations used in this method is given in Appendix D. The results of the least-squares analysis of the rate data obtained from the runs with ethylene-oxygen feed on silver crystals are shown in Tables 11 through 16. These results are corrected for the contribution of the gold surface to the total reaction rate. Figures 18 through 23 show the temperature dependence of the rate constant for the rate equation with first-order ethylene dependence and 1/2 order oxygen dependence. Analysis of the variance of the fits of the data with equations with different ethylene and oxygen dependence did not show any significant differences in the fits so therefore no

information was obtained on the apparent order of the overall reaction of ethylene and oxygen to produce carbon dioxide.

Comparison of the curves and their 95% confidence bands in Figures 18 through 23 showed there was almost complete overlapping of the confidence bands for the three non-strained crystals as a group and the three strained crystals as a group. The combined data for the non-strained crystals and the combined data for the strained crystals was analyzed for ethylene and oxygen rate dependence in the same manner as the data for the individual crystals. The same analysis was performed on the combined data for the six runs. The results of the least squares calculations for the combined data are given in Tables 17, 18, and 19. The increase in the variance for the combined fit of the non-strained crystals as compared to the variances for the individual fits was not significant at the 5% level of the "F" test. The same result was obtained for the combined fit of the three strained crystals. The variance of the combined fit of all six crystals was significantly larger than the variances of the individual fits or the combined fits of the non-strained and strained groups of crystals. Figures 24 and 25 show the temperature dependence for the combined fits of the two groups. Figure 26 compares the two curves and their 95% confidence bands. Two rate expressions had a slight bit of overlap of the 95% confidence bands at the extremes of the range of temperatures, but none had any overlap at the 90% level. These results indicate there was a statistically significant difference in the reaction rate constant for the non-strained and strained crystals. The ratio of

the rate constant for the non-strained crystals to the rate constant for the strained crystals was about 1.4 for rate expressions which were zero-order with respect to ethylene and 1.9 for rate expressions which were first-order with respect to ethylene. No significant difference was observed between the activity of different crystal planes with the same amount of strain. The difference in the activation energy for the rate constants of the non-strained and strained crystals was not significantly different. The value of the activation energy obtained from this work is compared to the values reported by other authors in Table 21. The magnitude of the reaction rate for the disappearance of ethylene calculated from the results of this work are compared with the reaction rates of other authors in Table 20.

Etch-Pit Density and Surface Deposits

Figure 9 shows a typical deposit on the surface of the crystal where the incoming feed gases impinged on the surface. Each crystal had a similar deposit in this region. The diameter of the region is about 0.040 inch. The differences between deposits formed in the entrance region as compared to the deposits on the overall surface were probably the result of the cooler feed gas following different reactions until it reached the temperature of the reactor. The area affected in this manner was only about 1% of the total catalyst area so this should have little effect on the overall results obtained from the reactor. There was some similarity between the pattern of heavier deposits outside of the entrance region in Figure 9 for the

non-strained (110) crystal and the pattern shown in Figure 15-A for the strained (110) crystal.

Figures 10 and 11 compare the appearance of the etch pits before and after the reaction with the surface deposits formed at the same location for the non-strained and strained (111) crystals. The etch-pit density in Figure 10-A is 2.9×10^6 pits/cm.^{2} and the etch-pit density of the same surface in Figure 10-C is 7.2×10^6 pits/cm.^{2}. This corresponds to a 114% increase in the etch-pit density of the surface after the use of the surface as a catalyst. The etch-pit density of the surface of a strained (111) crystal shown in Figure 11-A is 4.2×10^6 pits/cm.^{2}. Figure 11-C shows this same surface after the surface was used as the catalyst. Very few pits of definite shape are seen. These are very distorted when compared to the almost perfect equilateral triangular pits formed on the surface shown in Figure 11-A. These photographs show definite changes in the manner the surface of the (111) crystals respond to the chemical etching solution after the surfaces were used as catalysts.

Figures 12-A and 12-B show the increase in etch-pit density of the non-strained (100) crystal surface with use as the catalyst. The pit density before reaction was 5.1×10^6 pits/cm.^{2} and was 2.1×10^7 pits/cm.^{2} after use in the reactor. This was 300% increase in pit density. Figures 13-A and 13-B compare the surface deposits on the non-strained (100) crystal with the etch-pit pattern in the same location. A longer etching time was used to clearly etch the low-angle boundary in Figure 13-B. A comparison of the surface deposits

and the etch-pit patterns on the strained (100) crystal is shown in Figures 14-A and 14-B. There is no correlation between the surface deposits and the low-angle boundaries.

Figure 15-A shows the deposits on the surface of the strained (110) crystal after use as the catalyst. Figure 15-B shows the same location after etching. Neither of the (110) crystals were attacked by the etching solution before use in the reactor. The non-strained (110) crystal did not etch after use in the reactor, but the strained (110) crystal etched slightly as seen in Figure 15-B.

The non-strained (110) crystal was used as the catalyst for two days and the non-strained (100) crystal was used as the catalyst for three days. The remaining four crystals were used in the reactor for less than one day. There did not appear to be any relationship between the amount of deposit on the surface and the length of time the crystal remained in the reactor. The activity of the surface as a catalyst did not have any correlation with the amount of deposit on the surface.

Cleaning with hexane, methyl alcohol, ethyl alcohol, acetone, and ethylene dichloride did not remove the deposits from the surfaces. The deposits on the surfaces prevented microscopic examination of the surfaces to determine if the reacting gas stream attacked the silver. A light polish lasting about 1 min. was used to remove the deposits. This amount of polishing removed about 0.001 in. of metal from the surface. Microscopic examination of the surface after the light polish did not show any differences from the polished surfaces

obtained on the crystals before use in the reactor as the catalyst.

Error Analysis

The experimental uncertainty estimated for the measurement of the flow rate was 1.2%. The uncertainty estimated for the gas chromatography analysis of the product stream was 2% of the quantity plus the minimum detection limit. Temperature variations in the reactor were of the order of 0.5°C so this was used for the uncertainty in the temperature measurement. A temperature error of 0.5°C contributed about 2% error in the value of the rate constants. Combination of the estimated errors in all of the variables used in the calculation of the experimental values of the rate constants gave an expected error of 10% for samples with high CO_2 concentrations and the error could be as high as 40% for samples with very low CO_2 concentrations. The scatter in the experimental values of the rate constants was approximately equal to the expected uncertainty calculated from this error analysis.

The standard deviation of the etch-pit density was calculated from the data used to calculate the average value for the etch-pit densities. Values of about 25% of the average were obtained. The etch-pit densities were not uniform over the face of the crystal so the error in the value for the average density could be larger than the standard deviation of the counts from a particular area of the surface. An error of 50% would not seem unreasonable.

DISCUSSION OF RESULTS AND CONCLUSIONS

The results obtained from this study of the kinetics of the oxidation of ethylene on a single crystal of silver were somewhat limited by the effects of reactions occurring on reactor surfaces other than the silver surface. One of the products of interest, ethylene oxide, was rapidly oxidized on the gold surfaces of the reactor. The rate was fast enough to oxidize almost completely any ethylene oxide formed on the silver surface.

Oxidation of Ethylene Oxide on Gold

A run with a feed of about 0.03% ethylene oxide, 80% oxygen, and about 20% helium was made with a gold disc installed in place of a silver crystal to determine the reactions of ethylene oxide on the gold surfaces. Carbon dioxide, acetaldehyde, and ethylene or ethane were detected in the reactor exhaust in addition to the reactants. Least-squares fits of various rate expressions to the experimental data showed the rate of formation of carbon dioxide was independent of the ethylene oxide concentration. No conclusions could be drawn from the experimental data on the dependence of the rate of formation of carbon dioxide on the oxygen concentration because only one oxygen concentration was used during the run. These results indicated the rate controlling step of the oxidation of ethylene oxide on gold could be the absorption of oxygen on the surface, and the ethylene oxide reacted rapidly with the adsorbed oxygen. Another possibility which would explain the zero-order dependence

of the rate on the ethylene oxide concentration would involve rapid adsorption of the ethylene oxide on the gold surface and a slower, rate controlling step of oxygen reacting with the adsorbed ethylene oxide. The second reaction scheme would seem more reasonable. The activation energy for the production of carbon dioxide from ethylene oxide on gold was 9.0 ± 1.3 Kcal./gm. mole. The stated uncertainty is the 95% confidence limit for the activation energy evaluated from the least-squares calculations.

Attempts to fit the rate of production of the acetaldehyde and ethylene or ethane found in the reactor exhaust were not successful. The failure of the attempts at fitting the rates of production of acetaldehyde and ethylene or ethane was assumed to be the result of a complex series of reactions being involved in the formation of these compounds. Fletcher and Rollefson (9) proposed the reactions shown in equations (19), (20), (21), and (22) to explain the thermal decomposition of ethylene oxide and the increase in the rate of decomposition of acetaldehyde produced by the addition of small amounts of ethylene oxide. Ethylene could be formed by the combination of two CH_2 radicals produced by reaction (19) and ethane could be formed by combination of two CH_3 radicals produced by reaction (21). Reaction (20), the isomerization of ethylene oxide to acetaldehyde, would account for the presence of acetaldehyde in the reactor exhaust.

Oxidation of Ethylene on Gold

Very small amounts of ethylene oxide and acetaldehyde, and traces of a C-4 and a C-6 hydrocarbon were detected in the reactor

exhaust in addition to carbon dioxide and the reactants during the run with 80% oxygen and 20% ethylene on the gold blank. Lehner (19) reported the formation of acetaldehyde, ethylene oxide, and some polymerization products of ethylene in addition to carbon monoxide and carbon dioxide in the homogeneous oxidation of ethylene. Lehner found the rate of homogeneous oxidation of ethylene was greatly reduced by short distances between surfaces in the reactor and concluded the homogeneous oxidation of ethylene proceeded by a chain reaction. No reaction was detected by Lehner below 450°C in reactors with less than 2 mm. distances between surfaces. The small amounts of ethylene oxide, acetaldehyde, C-4, and C-6 hydrocarbons formed in the experimental run could be explained by assuming some homogeneous oxidation was occurring in the reactor.

Analysis of the data for the production of carbon dioxide with ethylene-oxygen feed on the gold surfaces by least-squares methods did not produce any significant information on the effects of the oxygen and ethylene concentrations on the reaction rate because of the constant feed concentrations. The activation energy for the formation of carbon dioxide on the gold surface was 26.0 ± 4.0 Kcal./gm. mole.

Oxidation of Ethylene on Silver

The series of experimental runs on silver crystals was made with essentially constant feed composition of about 20% ethylene and 80% oxygen at four different temperatures, 250, 280, 320, and 350°C to determine the effects of dislocation density and crystal orientation

on the temperature dependence of the reaction rate. The data for the rate of production of carbon dioxide was fit to various rate expressions by the method of least squares. There was no significant differences in the variance of the fits so no conclusions on the order of the rate equation with respect to the reactants could be made. Examination of the curves and their 95% confidence bands, Figures 18 through 23, showed there was no statistically significant difference in the results obtained for the three orientations of the surface, (100), (110), and (111). A comparison of the combined fit of the data for the three non-strained crystals with the combined fit of the data for the three strained crystals showed a significant decrease of the reaction rate for the crystals which had been strained. The activation energy for the production of carbon dioxide from ethylene and oxygen on silver was not affected by the 0.8% strain used in this work. An activation energy of 23.0 ± 1.8 Kcal./gm. mole was obtained.

An excellent agreement between the rate of conversion of ethylene calculated from the results of this work and the rates obtained by other authors is apparent in Table 20. This would indicate that the crystal surfaces used as the catalyst in this work were not poisoned. The agreement of the results for the three non-strained crystals and for the three strained crystals is an indication of the reproducibility of the surface conditions of the silver crystals. Comparison of the value obtained for the activation energy for the production of CO_2 from ethylene on silver crystals by this work with values obtained by other authors is shown in Table 21. The value of

the activation energy agrees very closely with the values obtained by Kummer (17), Orzechowski and MacCormack (25), and Wan (36).

Etch Pits on Silver

The changes in the manner in which the etching solution attacked the crystal surfaces after use in the reactor are seen in the appearance of the etch pits shown in Figures 10-A, 10-C, 11-A, 11-C, 12-A, and 12-B. Some change in the etch-pit densities of the crystals was observed. The values obtained for the etch-pit densities are given in Table 22. The assumption of a one-to-one correspondence of etch pits to intersections of dislocations with the crystal surface, particularly for the crystals after use in the reactor, was considered somewhat questionable by Vreeland (34). Difficulties in distinguishing etch pits from the background pattern on the surface in Figure 10-C and changes in the shape of the etch pits produced on the surface after use in the reactor were the basis for his conclusion. Regardless of the relationship between the etch pits and dislocations, a definite change in the manner in which the etching solution attacked the crystal surfaces was observed after the crystal was used in the reactor.

Conclusions

1. The orientation of the crystal planes parallel to the catalyst surface did not significantly affect the rate of production of carbon dioxide from ethylene and oxygen on silver as shown in Figures 24 and 25. This conclusion was also reached by Kummer (17) and Wilson,

Voge, Stevenson, Smith and Atkins (36).

2. The rate of oxidation of ethylene on silver was significantly reduced by straining the crystal prior to use as the catalyst. The activation energy, 23.0 Kcal./gm. mole, was not affected by 0.8% strain in the crystal. The rate of production of carbon dioxide at reactor conditions of 260°C, 740 mm., 20% ethylene, and 80% oxygen feed was reduced from 6.34×10^{-8} gm. moles/(min.)(cm.^{2}) for the non-strained crystals to 3.28×10^{-8} gm. moles/(min.)(cm.^{2}) for the strained crystals. If a one-to-one correspondence of etch pits to dislocations is assumed for the crystal surfaces before use in the reactor, the dislocation densities were increased from 2.9×10^6 to 4.2×10^6 pits/cm.^{2} for the (111) crystals and from 5.1×10^6 to 6.8×10^6 pits/cm.^{2} for the (100) crystals by the strain of 0.8%. This would indicate dislocations do not act as active sites for the oxidation of ethylene on silver but interfere with the reaction in some manner.

3. The deposits which formed on the catalyst surface during use in the reactor did not affect the activity of the catalyst. The results of the rate data shown in Figure 24 agree very well even though the deposits on the surfaces in Figures 11-B, 14-A, and 15-A show considerable difference in amount and type of pattern formed on the surface. The lack of similarities between the patterns formed by the deposits and the patterns produced by the etch pits shows the regions of the surface which produce etch pits are not the same as the regions which produce the deposits on the surface.

4. Some changes in the nature of the pitting of the crystal surfaces by the etching solution were observed after the crystal was

used in the reactor. This could have been caused by physical changes of the surface of the crystal or by introduction of impurities into the crystals during use in the reactor. Wilson, Voge, Stevenson, Smith, and Atkins (36) found evaporated films of silver which were oriented with a (110) crystal plane parallel to the surface changed to randomly oriented films after use as the catalyst for the oxidation of ethylene. The polishing step which was necessary to prepare the crystals for etching after use in the reactor removed about 0.001 inch of metal. It seems improbable that physical changes produced by reaction could have extended so deep into the crystal when 77 ev argon ions used by Sosnovsky (29) only produced physical changes to a depth of 100 A. Vreeland (34) considered that introduction of impurities into the crystals during use in the reactor was a more probable explanation of the change in the way the etching solution attacked the surfaces than physical changes in the crystal surface.

5. One possible explanation for the decrease in reaction rate on the strained crystals is that the strain produced more sites where oxygen could be strongly adsorbed and the increase of strongly adsorbed oxygen reduced the amount of adsorbed oxygen which is available to react with ethylene.

RECOMMENDATIONS FOR FURTHER WORK

1. The results of the present work indicate a definite decrease of at least 30% in the rate of oxidation of ethylene to carbon dioxide is produced by 0.8% strain in the crystals used as the catalyst. Further work should be undertaken to extend these results to larger amounts of strain. Studies with crystals which were strained and then annealed to relieve the strain would also be of interest.

2. Low-energy electron diffraction studies of the adsorption of oxygen on the surface of single crystals of silver could produce more information on the behavior of the adsorbed oxygen. Comparison of the behavior of the adsorbed oxygen on strained and non-strained crystals of silver could give some insight into the manner in which the strain of the crystal affects the rate of catalytic oxidation of ethylene. Since the selectivity of the silver catalysts for the production of ethylene oxide was thought to depend upon gaseous ethylene reacting with different forms of adsorbed oxygen (25, 32), studies of the behavior of the adsorbed oxygen by low-energy electron diffraction could be very useful in the further development of the mechanism of the oxidation of ethylene on silver.

3. The studies of the homogeneous thermal decomposition of ethylene oxide, the homogeneous oxidation of ethylene oxide, and the homogeneous oxidation of ethylene found in the literature (9, 15, 19) were made before the development of gas chromatography. Further study of these reactions utilizing gas chromatography could give more

information on the kinetics and mechanisms of the reactions, particularly at low conversions.

4. Only semi-quantitative studies of the catalytic activity of gold for the oxidation of hydrocarbons was found in the literature (27, 28). Quantitative studies of the catalytic activity of gold for oxidation reactions could produce some interesting and useful information.

REFERENCES

1. Benton, A. F., and Drake, L. C., J. Am. Chem. Soc. 54, 2186 (1932).

2. Benton, A. F., and Drake, L. C., J. Am. Chem. Soc. 56, 255 (1934).

3. Buntin, R. R., Ph. D. thesis, "A Kinetic Study of the Oxidation of Ethylene on a Silver Catalyst," Purdue University (1961).

4. Burgoyne, J. H., and Kapur, P. K., Trans. Faraday Soc. 47, 234 (1952).

5. Czanderna, A. W., J. Phys. Chem. 68, 2765 (1964).

6. Deming, W. E., "Statistical Adjustment of Data," John Wiley & Sons, Inc., New York (1943).

7. Dow Chemical Co., Brit. Pat. 811,828, Apr. 15, 1959, Chem. Ab. 53, 13456e (1943).

8. Ettre, L. S., "Gas Chromatography," Chapt. 21, p. 307, Academic Press, New York (1962).

9. Fletcher, C. J. M., and Rollefson, G. K., J. Am. Chem. Soc. 58, 2135 (1936).

10. Glocher, R., and Kaupp, E., Z. Metallkunde 16, 377 (1924), Chem. Ab. 19, 1682 (1925).

11. Groggins, P. H., "Unit Processes in Organic Synthesis," p. 529, McGraw-Hill Book Company, Inc., New York (1958).

12. Ibid., p. 791.

13. Hall, J. W., and Rase, H. F., I.& E. C. Fundamentals 3, 159 (1964).

14. "Handbook of Chemistry and Physics, 39th Edition," p. 2109, Chemical Rubber Publishing Co., Cleveland, Ohio (1958).

15. Heckert, W. H., and Mack, E., Jr. J. Am. Chem. Soc. 51, 2706 (1929).

16. Jefferson Chemical Co., Inc., "Ethylene Oxide Technical Brochure," Houston, Texas.

17. Kummer, J. T., J. Phys. Chem. 60, 666 (1956).

18. Lefort, T. E., U. S. Pat. 1,998,878, Chem. Ab. 29, 4029 (1935).

19. Lehner, S., J. Am. Chem. Soc. 53, 3737 (1931).

20. McBee, E. T., Hass, H. B., and Wiseman, P. A., Ind. Eng. Chem. 37, 432 (1945).

21. McCarty, C. B., Ph.D. thesis, "The Use of a Vacuum Beam Microbalance for Adsorption Studies of Oxygen, Ethylene, and ....," Purdue University (1961).

22. Murray, K. E., Aust. J. Sci. Res. 3A, 433 (1950).

23. Nat. Res. Coun. Canada, U. S. Pat. 2,883,346, Apr. 21, 1959, Chem. Ab. 53, 20431b (1959).

24. Nault, L. G., Bolme, D. W., and Johanson, L. N., I. & E. C. Process Design and Development 1, 285 (1962).

25. Orzechowski, A., and MacCormack, K. E., Can. J. Chem. 32, 388, 415, 432, 443 (1954).

26. Perkins, T. D., Ph.D. thesis, "Effect of Dislocations upon the Catalytic Activity of Silver," The University of Oklahoma (1963).

27. Philips, J. G., J. Am. Chem. Soc. 16, 163, 255 (1964).

28. Reyerson, L. H., and Swearingen, K., J. Am. Chem. Soc. 50, 2872 (1928).

29. Sosnovsky, H. M. C., J. Phys. Chem. Solids 10, 304 (1959).

30. Sternberg, J. C., Gallaway, W. S., and Jones, D. T. L, "Gas Chromatography," Chapt. 18, p. 231, Academic Press, New York (1962).

31. Sutcliffe, H., Electronic Engineering, 94 (Feb. 1961).

32. Twigg, G. H., Proc. Roy. Soc. (London) A188, 92, 105, 123 (1946).

33. Uhara, I., Yanagimoto, S., Tani, K., and Adachi, G., Nature 192, 867 (1961).

34. Vreeland, T., Jr., Associate Professor of Materials Science, California Institute of Technology, conversations with author.

35. Wan, S., Ind. Eng. Chem. 45, 234 (1953).

36. Wilson, J. N., Voge, H. H., Stevenson, D. P., Smith, A. E., and Atkins, L. T., J. Phys. Chem. 63, 463 (1959).

NOMENCLATURE

A - Frequency factor of Arnhenius equation, gm. moles $(\text{gm. moles/cc.})^{-p}\ \text{min.}^{-1}\text{cm.}^{-2}$

C - Concentration, gm. moles/cc.

E_a - Activation energy, Kcal./gm. mole

k - Rate constant, gm. moles $(\text{gm. moles/cc.})^{-p}\ \text{min.}^{-1}\text{cm.}^{-2}$

m - Order of reaction rate, dimensionless

o - Order of reaction rate, dimensionless

p - Sum of orders of reaction rate, dimensionless

Q - Volumetric flow rate, cc./min.

R - Universal gas constant, kcal./(gm. mole)(^{o}K)

S - Surface area, cm.^2

T - Absolute temperature, ^{o}K

Subscripts

Ag - Refers to silver

Au - Refers to gold

C = C - Refers to ethylene

CO_2 - Refers to carbon dioxide

EO - Refers to ethylene oxide

T - Refers to total reactor

Table 1. Experimental Results, Ethylene Oxide-Oxygen Feed on Gold Blank

GOLD BLANK, ETHYLENE OXIDE-HELIUM-OXYGEN FEED

	DATE	SAMPLE	TOTAL CONCENTRATION (gm-moles/cc)	FLOW RATE (cc/min)	FLOW RATE (gm-moles/min)	t (°C)	T (°K)	1/T (1/°K)
1	2 SEP 64	2	2.300E-05	2.162	4.967E-05	245.57	518.75	.001927
2	2 SEP 64	3	2.299E-05	2.161	4.964E-05	245.48	518.66	.001928
3	2 SEP 64	4	2.298E-05	2.148	4.932E-05	245.72	518.90	.001927
4	2 SEP 64	6	2.190E-05	2.226	4.873E-05	269.78	542.96	.001841
5	2 SEP 64	7	2.191E-05	2.215	4.849E-05	269.85	543.03	.001841
6	2 SEP 64	8	2.195E-05	2.219	4.868E-05	268.91	542.09	.001844
7	2 SEP 64	10	2.015E-05	2.375	4.781E-05	316.29	589.47	.001696
8	2 SEP 64	11	2.016E-05	2.365	4.763E-05	316.89	590.07	.001694
9	2 SEP 64	12	2.021E-05	2.360	4.765E-05	315.40	588.58	.001699
10	2 SEP 64	14	1.925E-05	2.470	4.753E-05	344.54	617.72	.001618
11	2 SEP 64	15	1.926E-05	2.511	4.832E-05	344.46	617.64	.001619
12	2 SEP 64	16	1.923E-05	2.471	4.750E-05	345.36	618.54	.001616
13	2 SEP 64	17 - FEED	0.	0.	0.	0.	0.	.

SAMPLE ANALYSIS (mole fraction)

	O_2	C_2H_4	CO_2	Ethylene Oxide	Acetaldehyde	C-4	C-6,1	C-6,2	N_2
1	8.21E-01	1.07E-05	1.91E-04	1.71E-04	1.98E-05	0.	0.	0.	6.91E-03
2	8.17E-01	9.33E-06	1.30E-04	1.90E-04	1.56E-05	0.	0.	0.	6.90E-03
3	8.29E-01	7.31E-06	1.22E-04	2.02E-04	2.00E-05	0.	0.	0.	6.39E-03
4	8.12E-01	8.45E-06	2.53E-04	1.73E-04	2.43E-05	0.	0.	0.	6.73E-03
5	8.24E-01	5.53E-06	2.03E-04	1.47E-04	2.35E-05	0.	0.	0.	6.41E-03
6	8.22E-01	5.86E-06	2.69E-04	1.56E-04	3.44E-05	0.	0.	0.	6.30E-03
7	8.06E-01	5.29E-06	4.09E-04	6.64E-05	1.49E-05	0.	0.	0.	7.36E-03
8	8.16E-01	5.29E-06	4.14E-04	6.27E-05	1.77E-05	0.	0.	0.	6.46E-03
9	8.04E-01	3.53E-06	4.68E-04	5.13E-05	1.08E-05	0.	0.	0.	6.25E-03
10	8.33E-01	4.77E-06	6.24E-04	1.87E-05	5.72E-06	0.	0.	0.	6.83E-03
11	8.25E-01	4.40E-06	6.56E-04	1.87E-05	6.43E-06	0.	0.	0.	6.90E-03
12	7.93E-01	3.40E-06	6.01E-04	1.61E-05	4.24E-06	0.	0.	0.	6.86E-03
13	8.33E-01	0.	1.34E-05	2.82E-04	0.	0.	0.	0.	6.48E-03

TOTAL REACTION RATE (gm-moles/min)

	C_2H_4	CO_2	Ethylene Oxide	Acetaldehyde	C-4	C-6,1	C-6,2
1	5.32E-10	9.49E-09	-5.47E-09	9.84E-10	0.	0.	0.
2	4.63E-10	6.45E-09	-4.55E-09	7.76E-10	0.	0.	0.
3	3.60E-10	6.01E-09	-3.94E-09	9.86E-10	0.	0.	0.
4	4.12E-10	1.24E-08	-5.30E-09	1.18E-09	0.	0.	0.
5	2.68E-10	9.87E-09	-6.51E-09	1.14E-09	0.	0.	0.
6	2.85E-10	1.31E-08	-6.12E-09	1.67E-09	0.	0.	0.
7	2.53E-10	1.95E-08	-1.03E-08	7.10E-10	0.	0.	0.
8	2.52E-10	1.97E-08	-1.04E-08	8.42E-10	0.	0.	0.
9	1.68E-10	2.23E-08	-1.10E-08	5.15E-10	0.	0.	0.
10	2.27E-10	2.96E-08	-1.25E-08	2.72E-10	0.	0.	0.
11	2.13E-10	3.17E-08	-1.27E-08	3.11E-10	0.	0.	0.
12	1.61E-10	2.86E-08	-1.26E-08	2.01E-10	0.	0.	0.
13	0.	0.	0.	0.	0.	0.	0.

Table 2. Experimental Results, Ethylene-Oxygen Feed on Gold Blank

GOLD BLANK, ETHYLENE-OXYGEN FEED

	DATE	SAMPLE	TOTAL CONCENTRATION (gm-moles/cc)	FLOW RATE (cc/min)	FLOW RATE (gm-moles/min)	t (°C)	T (°K)	1/T (1/°K)
1	1 SEP 64	3	2.291E-05	2.141	4.901E-05	247.10	520.28	.001922
2	1 SEP 64	4	2.288E-05	2.150	4.914E-05	247.06	520.24	.001922
3	1 SEP 64	6	2.192E-05	2.192	4.802E-05	270.37	543.55	.001839
4	1 SEP 64	7	2.193E-05	2.200	4.821E-05	269.85	543.03	.001841
5	1 SEP 64	8	2.195E-05	2.201	4.828E-05	269.99	543.17	.001841
6	1 SEP 64	10	2.015E-05	2.413	4.860E-05	317.56	590.74	.001692
7	1 SEP 64	11	2.018E-05	2.375	4.788E-05	316.89	590.07	.001694
8	1 SEP 64	12	2.021E-05	2.361	4.766E-05	316.42	589.60	.001696
9	1 SEP 64	14	1.920E-05	2.448	4.696E-05	347.67	620.85	.001610
10	1 SEP 64	16	1.922E-05	2.435	4.677E-05	346.56	619.74	.001613

SAMPLE ANALYSIS (mole fraction)

	O_2	C_2H_4	CO_2	Ethylene Oxide	Acetaldehyde	C-4	C-6,1	C-6,2	N_2
1	7.87E-01	1.98E-01	1.78E-04	0.	7.35E-06	0.	0.	0.	6.60E-03
2	7.94E-01	1.96E-01	1.28E-04	0.	7.36E-06	0.	0.	0.	5.63E-03
3	7.88E-01	2.35E-01	5.80E-04	0.	1.46E-05	7.61E-07	0.	0.	6.02E-03
4	7.71E-01	2.34E-01	5.51E-04	0.	1.40E-05	0.	0.	0.	6.55E-03
5	7.92E-01	2.33E-01	5.50E-04	0.	1.27E-05	0.	0.	0.	6.17E-03
6	7.93E-01	1.68E-01	2.21E-03	8.06E-06	2.16E-05	0.	1.47E-06	0.	6.19E-03
7	7.88E-01	1.97E-01	1.76E-03	9.67E-06	2.30E-05	0.	1.77E-06	0.	6.84E-03
8	8.48E-01	1.83E-01	1.97E-03	1.05E-05	2.02E-05	0.	1.27E-06	0.	6.05E-03
9	7.75E-01	1.91E-01	7.62E-03	1.62E-05	2.52E-05	3.26E-07	2.86E-06	0.	4.93E-03
10	7.87E-01	1.94E-01	9.83E-03	1.63E-05	1.63E-05	1.16E-06	2.27E-06	0.	6.83E-03

TOTAL REACTION RATE (gm-moles/min)

	C_2H_4	CO_2	Ethylene Oxide	Acetaldehyde	C-4	C-6,1	C-6,2
1	-4.73E-09	8.74E-09	0.	3.60E-10	0.	0.	0.
2	-3.50E-09	6.29E-09	0.	3.62E-10	0.	0.	0.
3	-1.47E-08	2.79E-08	0.	7.03E-10	3.65E-11	0.	0.
4	-1.40E-08	2.66E-08	0.	6.76E-10	0.	0.	0.
5	-1.39E-08	2.66E-08	0.	6.15E-10	0.	0.	0.
6	-5.55E-08	1.08E-07	3.92E-10	1.05E-09	0.	7.12E-11	0.
7	-4.40E-08	8.45E-08	4.63E-10	1.10E-09	0.	8.47E-11	0.
8	-4.87E-08	9.40E-08	4.99E-10	9.65E-10	0.	6.07E-11	0.
9	-1.81E-07	3.58E-07	7.60E-10	1.18E-09	1.53E-11	1.34E-10	0.
10	-2.32E-07	4.60E-07	7.60E-10	7.65E-10	5.41E-11	1.06E-10	0.

Table 3. Experimental Results, Ethylene-Oxygen Feed on Crystal #1, (111), Non-strained

CRYSTAL 1, ETHYLENE-OXYGEN FEED, NON-STRAINED

	DATE	SAMPLE	TOTAL CONCENTRATION (gm-moles/cc)	FLOW RATE (cc/min)	FLOW RATE (gm-moles/min)	t (°C)	T (°K)	1/T (1/°K)
1	31 AUG 64	4	2.004E-05	2.314	4.634E-05	319.91	593.09	.001686
2	31 AUG 64	5	2.004E-05	2.335	4.677E-05	320.63	593.81	.001684
3	31 AUG 64	6	2.003E-05	2.335	4.673E-05	320.89	594.07	.001683
4	31 AUG 64	8	1.898E-05	2.394	4.540E-05	352.76	625.94	.001597
5	31 AUG 64	9	1.903E-05	2.387	4.539E-05	351.30	624.48	.001601
6	31 AUG 64	10	1.900E-05	2.410	4.574E-05	352.47	625.65	.001598
7	31 AUG 64	11	2.281E-05	2.180	4.968E-05	247.97	521.15	.001918
8	31 AUG 64	13	2.282E-05	2.139	4.880E-05	247.90	521.08	.001919
9	31 AUG 64	16	2.167E-05	2.237	4.845E-05	275.62	548.80	.001822
10	31 AUG 64	17	2.169E-05	2.239	4.853E-05	275.63	548.81	.001822
11	31 AUG 64	18	2.169E-05	2.201	4.770E-05	275.42	548.60	.001822
12	31 AUG 64	14 - FEED	0.	0.	0.	0.	0.	.

SAMPLE ANALYSIS (mole fraction)

	O_2	C_2H_4	CO_2	Ethylene Oxide	Acetaldehyde	C-4	C-6,1	C-6,2	N_2
1	7.66E-01	1.92E-01	1.43E-02	1.16E-05	6.90E-07	3.32E-07	1.51E-06	0.	8.60E-03
2	7.48E-01	1.88E-01	1.34E-02	1.57E-05	5.58E-06	3.32E-07	1.81E-06	9.09E-07	7.10E-03
3	7.84E-01	1.90E-01	1.52E-02	1.32E-05	6.89E-07	1.66E-07	1.41E-06	0.	6.45E-03
4	7.63E-01	1.85E-01	3.19E-02	2.37E-05	2.72E-06	4.92E-07	1.89E-06	1.89E-06	6.80E-03
5	7.80E-01	1.87E-01	3.07E-02	2.37E-05	3.40E-06	3.28E-07	1.79E-06	1.39E-06	6.80E-03
6	7.88E-01	1.91E-01	3.20E-02	2.13E-05	7.56E-06	3.28E-07	1.49E-06	1.89E-06	0.
7	8.21E-01	1.90E-01	9.11E-04	1.63E-05	1.87E-05	0.	0.	0.	5.82E-03
8	7.94E-01	2.00E-01	8.97E-04	0.	0.	0.	0.	0.	6.25E-03
9	7.14E-01	1.89E-01	3.21E-03	0.	4.32E-06	0.	0.	0.	5.94E-03
10	7.23E-01	1.88E-01	3.14E-03	5.14E-06	6.55E-06	0.	6.26E-07	0.	5.60E-03
11	6.86E-01	1.88E-01	3.36E-03	0.	5.83E-06	0.	0.	0.	5.37E-03
12	7.88E-01	2.01E-01	9.51E-04	0.	0.	0.	0.	0.	6.41E-03

TOTAL REACTION RATE (gm-moles/min)

	C_2H_4	CO_2	Ethylene Oxide	Acetaldehyde	C-4	C-6,1	C-6,2
1	-3.32E-07	6.62E-07	5.37E-10	3.20E-11	1.54E-11	7.00E-11	0.
2	-3.15E-07	6.27E-07	7.33E-10	2.61E-10	1.55E-11	8.46E-11	4.25E-11
3	-3.55E-07	7.08E-07	6.18E-10	3.22E-11	7.77E-12	6.59E-11	0.
4	-7.26E-07	1.45E-06	1.08E-09	1.24E-10	2.24E-11	8.56E-11	8.56E-11
5	-6.99E-07	1.39E-06	1.08E-09	1.55E-10	1.49E-11	8.11E-11	6.32E-11
6	-7.33E-07	1.46E-06	9.72E-10	3.46E-10	1.50E-11	6.82E-11	8.63E-11
7	-2.44E-08	4.52E-08	8.09E-10	9.31E-10	0.	0.	0.
8	-2.19E-08	4.38E-08	0.	0.	0.	0.	0.
9	-2.09E-10	1.56E-07	0.	2.09E-10	0.	0.	0.
10	-7.68E-08	1.52E-07	2.50E-10	3.18E-10	0.	3.04E-11	0.
11	-8.03E-08	1.60E-07	0.	2.78E-10	0.	0.	0.
12	0.	0.	0.	0.	0.	0.	0.

Table 4. Experimental Results, Ethylene-Oxygen Feed on Crystal #2, (100), Non-strained

CRYSTAL 2, ETHYLENE-OXYGEN FEED NON-STRAINED

	DATE	SAMPLE	TOTAL CONCENTRATION (gm-moles/cc)	FLOW RATE (cc/min)	FLOW RATE (gm-moles/min)	t (°C)	T (°K)	1/T (1/°K)
1	26 AUG 64	8	2.162E-05	2.209	4.774E-05	277.26	550.44	.001816
2	26 AUG 64	9	2.165E-05	2.210	4.780E-05	277.26	550.44	.001816
3	26 AUG 64	11	2.160E-05	2.190	4.726E-05	277.07	550.25	.001817
4	26 AUG 64	15	2.014E-05	2.317	4.664E-05	316.67	589.85	.001695
5	26 AUG 64	16	2.013E-05	2.322	4.671E-05	317.13	590.31	.001694
6	27 AUG 64	2	2.014E-05	2.292	4.613E-05	317.36	590.54	.001693
7	27 AUG 64	4	1.895E-05	2.419	4.582E-05	353.64	626.82	.001595
8	27 AUG 64	5	1.894E-05	2.426	4.592E-05	354.77	627.95	.001592
9	27 AUG 64	6	1.898E-05	2.400	4.553E-05	353.77	626.95	.001595
10	28 AUG 64	2	2.304E-05	2.085	4.800E-05	244.79	517.97	.001930
11	28 AUG 64	3	2.304E-05	2.085	4.800E-05	244.79	517.97	.001930
12	28 AUG 64	5	2.198E-05	2.177	4.782E-05	269.27	542.45	.001843
13	28 AUG 64	6	2.197E-05	2.157	4.735E-05	269.24	542.42	.001843

SAMPLE ANALYSIS (mole fraction)

	O_2	C_2H_4	CO_2	Ethylene Oxide	Acetaldehyde	C-4	C-6,1	C-6,2	N_2
1	7.12E-01	1.94E-01	2.03E-03	0.	0.	0.	0.	0.	6.99E-03
2	7.29E-01	1.92E-01	2.28E-03	0.	0.	0.	0.	0.	7.14E-03
3	7.80E-01	1.81E-01	2.72E-03	0.	0.	0.	0.	0.	7.58E-03
4	8.05E-01	1.93E-01	1.33E-02	2.30E-05	9.21E-06	0.	0.	0.	8.35E-03
5	8.05E-01	1.97E-01	1.33E-02	0.	1.10E-05	0.	0.	0.	7.83E-03
6	7.42E-01	1.90E-01	1.48E-02	1.25E-05	1.05E-05	0.	2.03E-06	0.	6.71E-03
7	7.54E-01	1.74E-01	2.95E-02	4.54E-05	2.21E-05	5.70E-07	2.07E-06	0.	7.15E-03
8	7.62E-01	1.74E-01	2.55E-02	3.97E-05	1.78E-05	5.69E-07	1.99E-06	0.	6.92E-03
9	7.56E-01	1.80E-01	2.51E-02	4.61E-05	2.20E-05	1.01E-06	1.81E-06	0.	6.70E-03
10	7.82E-01	1.91E-01	6.65E-04	0.	0.	0.	0.	0.	5.85E-03
11	7.84E-01	1.95E-01	6.78E-04	0.	0.	0.	0.	0.	5.91E-03
12	7.67E-01	1.86E-01	2.00E-03	1.02E-05	5.12E-06	1.91E-06	7.42E-07	0.	6.11E-03
13	7.84E-01	1.89E-01	2.01E-03	8.11E-06	6.81E-06	0.	4.16E-07	0.	6.33E-03

TOTAL REACTION RATE (gm-moles/min)

	C_2H_4	CO_2	Ethylene Oxide	Acetaldehyde	C-4	C-6,1	C-6,2
1	-4.84E-08	9.67E-08	0.	0.	0.	0.	0.
2	-5.45E-08	1.09E-07	0.	0.	0.	0.	0.
3	-6.42E-08	1.28E-07	0.	0.	0.	0.	0.
4	-3.13E-07	6.22E-07	1.07E-09	4.30E-10	0.	0.	0.
5	-3.11E-07	6.21E-07	0.	5.15E-10	0.	0.	0.
6	-3.43E-07	6.83E-07	5.77E-10	4.84E-10	0.	9.38E-11	0.
7	-6.80E-07	1.35E-06	2.08E-09	1.01E-09	2.61E-11	9.51E-11	0.
8	-5.89E-07	1.17E-06	1.82E-09	8.19E-10	2.61E-11	9.12E-11	0.
9	-5.74E-07	1.14E-06	2.10E-09	1.00E-09	4.60E-11	8.26E-11	0.
10	-1.60E-08	3.19E-08	0.	0.	0.	0.	0.
11	-1.63E-08	3.26E-08	0.	0.	0.	0.	0.
12	-4.88E-08	9.56E-08	4.87E-10	2.45E-10	9.13E-11	3.55E-11	0.
13	-4.84E-08	9.54E-08	3.84E-10	3.22E-10	0.	1.97E-11	0.

Table 5. Experimental Results, Ethylene-Oxygen Feed on Crystal #3, (111), Strained 0.8%

CRYSTAL 3, ETHYLENE-OXYGEN FEED, STRAINED

	DATE	SAMPLE	TOTAL CONCENTRATION (gm-moles/cc)	FLOW RATE (cc/min)	FLOW RATE (gm-moles/min)	t (°C)	T (°K)	1/T (1/°K)
1	11 SEP 64	2	2.030E-05	2.526	5.123E-05	315.23	588.41	.001699
2	11 SEP 64	4	2.026E-05	2.527	5.116E-05	316.06	589.24	.001697
3	11 SEP 64	5	2.025E-05	2.500	5.061E-05	316.41	589.59	.001696
4	11 SEP 64	6	1.930E-05	2.575	4.967E-05	345.34	618.52	.001616
5	11 SEP 64	7	1.934E-05	2.564	4.955E-05	344.34	617.52	.001619
6	11 SEP 64	9	1.925E-05	2.611	5.023E-05	345.68	618.86	.001615
7	11 SEP 64	10	2.294E-05	2.304	5.282E-05	245.77	518.95	.001927
8	11 SEP 64	12	2.301E-05	2.296	5.279E-05	244.79	517.97	.001930
9	11 SEP 64	13	2.303E-05	2.272	5.229E-05	244.46	517.64	.001931
10	11 SEP 64	14	2.192E-05	2.387	5.229E-05	270.64	543.82	.001838
11	11 SEP 64	16	2.196E-05	2.412	5.293E-05	270.22	543.40	.001840
12	11 SEP 64	18	2.193E-05	2.409	5.278E-05	270.44	543.62	.001839
13	11 SEP 64	1 - FEED	0.	0.	0.	0.	0.	.

SAMPLE ANALYSIS (mole fraction)

	O_2	C_2H_4	CO_2	Ethylene Oxide	Acetaldehyde	C-4	C-6,1	C-6,2	N_2
1	7.18E-01	2.62E-01	9.43E-03	1.40E-05	5.91E-06	0.	2.09E-06	2.47E-06	6.63E-03
2	7.17E-01	2.63E-01	8.81E-03	1.09E-05	0.	0.	1.90E-06	3.42E-06	6.12E-03
3	6.65E-01	2.68E-01	1.07E-02	1.17E-05	3.90E-06	0.	1.71E-06	3.14E-06	6.33E-03
4	6.93E-01	2.54E-01	2.14E-02	2.05E-05	2.63E-06	1.58E-07	1.82E-06	6.33E-06	5.87E-03
5	7.03E-01	2.59E-01	2.02E-02	1.74E-05	3.29E-06	0.	1.54E-06	6.92E-06	6.13E-03
6	6.92E-01	2.53E-01	1.93E-02	1.82E-05	3.30E-06	3.18E-07	2.22E-06	6.75E-06	6.22E-03
7	7.09E-01	2.61E-01	4.99E-04	0.	0.	0.	0.	0.	5.67E-03
8	7.13E-01	2.61E-01	5.12E-04	0.	0.	0.	0.	0.	5.90E-03
9	7.05E-01	2.66E-01	4.73E-04	0.	0.	0.	0.	0.	6.28E-03
10	7.05E-01	2.72E-01	1.76E-03	2.38E-06	0.	0.	3.86E-07	0.	5.74E-03
11	7.06E-01	2.74E-01	1.81E-03	0.	0.	0.	0.	0.	5.85E-03
12	7.06E-01	2.77E-01	1.90E-03	4.76E-06	3.33E-06	0.	0.	0.	5.81E-03
13	7.16E-01	2.63E-01	0.	0.	0.	0.	0.	0.	8.76E-03

TOTAL REACTION RATE (gm-moles/min)

	C_2H_4	CO_2	Ethylene Oxide	Acetaldehyde	C-4	C-6,1	C-6,2
1	-2.43E-07	4.83E-07	7.18E-10	3.03E-10	0.	1.07E-10	1.26E-10
2	-2.27E-07	4.51E-07	5.59E-10	0.	0.	9.74E-11	1.75E-10
3	-2.72E-07	5.42E-07	5.93E-10	1.98E-10	0.	8.64E-11	1.59E-10
4	-5.35E-07	1.06E-06	1.02E-09	1.31E-10	7.86E-12	9.03E-11	3.15E-10
5	-5.03E-07	1.00E-06	8.62E-10	1.63E-10	0.	7.61E-11	3.43E-10
6	-4.88E-07	9.72E-07	9.17E-10	1.66E-10	1.60E-11	1.12E-10	3.39E-10
7	-1.32E-08	2.64E-08	0.	0.	0.	0.	0.
8	-1.35E-08	2.70E-08	0.	0.	0.	0.	0.
9	-1.24E-08	2.47E-08	0.	0.	0.	0.	0.
10	-4.61E-08	9.19E-08	1.24E-10	0.	0.	2.02E-11	0.
11	-4.78E-08	9.56E-08	0.	0.	0.	0.	0.
12	-5.06E-08	1.00E-07	2.51E-10	1.76E-10	0.	0.	0.
13	0.	0.	0.	0.	0.	0.	0.

Table 6. Experimental Results, Ethylene-Oxygen Feed on Crystal #4, (100), Strained 0.8%

CRYSTAL 4, ETHYLENE-OXYGEN FEED, STRAINED

	DATE	SAMPLE	TOTAL CONCENTRATION (gm-moles/cc)	FLOW RATE (cc/min)	FLOW RATE (gm-moles/min)	t (°C)	T (°K)	$1/T$ ($1/°K$)
1	15 SEP 64	2	2.019E-05	2.539	5.124E-05	316.82	590.00	.001694
2	15 SEP 64	4	2.014E-05	2.532	5.095E-05	317.72	590.90	.001692
3	15 SEP 64	5	2.018E-05	2.531	5.105E-05	316.54	589.72	.001695
4	15 SEP 64	6	1.932E-05	2.657	5.129E-05	343.16	616.34	.001622
5	15 SEP 64	7	1.927E-05	2.629	5.061E-05	344.80	617.98	.001618
6	15 SEP 64	9	1.926E-05	2.651	5.103E-05	345.04	618.22	.001617
7	15 SEP 64	10	2.298E-05	1.404	3.223E-05	245.67	518.85	.001927
8	15 SEP 64	11	2.305E-05	2.293	5.282E-05	244.56	517.74	.001931
9	15 SEP 64	13	2.297E-05	2.315	5.314E-05	246.11	519.29	.001925
10	15 SEP 64	14	2.204E-05	2.394	5.274E-05	268.22	541.40	.001847
11	15 SEP 64	15	2.208E-05	2.437	5.378E-05	267.36	540.54	.001850

SAMPLE ANALYSIS (mole fraction)

	O_2	C_2H_4	CO_2	Ethylene Oxide	Acetaldehyde	C-4	C-6,1	C-6,2	N_2
1	7.04E-01	2.66E-01	7.32E-03	1.98E-05	7.68E-06	1.53E-07	2.60E-06	1.76E-06	6.82E-03
2	7.04E-01	2.66E-01	7.57E-03	1.68E-05	5.15E-06	1.53E-07	2.60E-06	1.48E-06	6.03E-03
3	6.97E-01	2.66E-01	7.96E-03	1.45E-05	8.97E-06	0.	2.33E-06	2.60E-06	6.41E-03
4	5.41E-01	2.74E-01	1.72E-02	1.90E-05	1.02E-05	3.06E-07	1.66E-06	3.34E-06	6.57E-03
5	7.06E-01	2.60E-01	1.80E-02	1.81E-05	7.98E-06	3.46E-07	2.21E-06	3.35E-06	6.57E-03
6	6.94E-01	2.61E-01	1.72E-02	1.99E-05	1.08E-05	3.46E-07	1.89E-06	4.41E-06	6.68E-03
7	7.06E-01	2.59E-01	5.04E-04	0.	0.	0.	0.	0.	6.23E-03
8	7.08E-01	2.65E-01	4.03E-04	0.	0.	0.	0.	0.	6.05E-03
9	6.98E-01	2.65E-01	5.17E-04	0.	0.	0.	0.	0.	6.00E-03
10	6.96E-01	2.63E-01	1.32E-03	0.	0.	0.	0.	0.	6.15E-03
11	7.04E-01	2.70E-01	1.26E-03	0.	0.	0.	0.	0.	6.21E-03

TOTAL REACTION RATE (gm-moles/min)

	C_2H_4	CO_2	Ethylene Oxide	Acetaldehyde	C-4	C-6,1	C-6,2
1	-1.90E-07	3.75E-07	1.02E-09	3.94E-10	7.84E-12	1.33E-10	9.01E-11
2	-1.95E-07	3.85E-07	8.57E-10	2.63E-10	7.81E-12	1.33E-10	7.57E-11
3	-2.05E-07	4.07E-07	7.40E-10	4.58E-10	0.	1.19E-10	1.33E-10
4	-4.44E-07	8.84E-07	9.77E-10	5.24E-10	1.57E-11	8.54E-11	1.71E-10
5	-4.57E-07	9.10E-07	9.19E-10	4.04E-10	1.75E-11	1.12E-10	1.70E-10
6	-4.42E-07	8.78E-07	1.01E-09	5.54E-10	1.77E-11	9.63E-11	2.25E-10
7	-8.12E-09	1.62E-08	0.	0.	0.	0.	0.
8	-1.06E-08	2.13E-08	0.	0.	0.	0.	0.
9	-1.37E-08	2.75E-08	0.	0.	0.	0.	0.
10	-3.49E-08	6.97E-08	0.	0.	0.	0.	0.
11	-3.39E-08	6.77E-08	0.	0.	0.	0.	0.

Table 7. Experimental Results, Ethylene-Oxygen Feed on Crystal #5, (110), Strained 0.8%

CRYSTAL 5, ETHYLENE-OXYGEN FEED, STRAINED

	DATE	SAMPLE	TOTAL CONCENTRATION (gm-moles/cc)	FLOW RATE (cc/min)	FLOW RATE (gm-moles/min)	t (^oC)	T (^oK)	$1/T$ ($1/^oK$)
1	16 SEP 64	4	1.775E-05	2.753	4.884E-05	399.12	672.30	.001487
2	16 SEP 64	5	1.775E-05	2.677	4.747E-05	399.31	672.49	.001487
3	16 SEP 64	6	1.932E-05	2.644	5.104E-05	343.66	616.84	.001621
4	16 SEP 64	8	1.930E-05	2.614	5.042E-05	344.41	617.59	.001619
5	16 SEP 64	9	1.932E-05	2.613	5.045E-05	343.52	616.70	.001621
6	16 SEP 64	10	2.029E-05	2.578	5.228E-05	314.24	587.42	.001702
7	16 SEP 64	13	2.031E-05	2.546	5.166E-05	314.46	587.64	.001701
8	16 SEP 64	14	2.032E-05	2.545	5.169E-05	314.05	587.23	.001702
9	16 SEP 64	15	2.206E-05	2.413	5.320E-05	267.95	541.13	.001848
10	16 SEP 64	16	2.196E-05	2.422	5.315E-05	270.57	543.75	.001839
11	16 SEP 64	18	2.203E-05	2.411	5.309E-05	268.05	541.23	.001847
12	16 SEP 64	19	2.301E-05	2.313	5.316E-05	245.39	518.57	.001928
13	16 SEP 64	20	2.292E-05	2.342	5.362E-05	247.24	520.42	.001921

SAMPLE ANALYSIS (mole fraction)

	O_2	C_2H_4	CO_2	Ethylene Oxide	Acetaldehyde	C-4	C-6,1	C-6,2	N_2
1	6.82E-01	2.53E-01	4.54E-02	3.49E-05	9.53E-06	0.	2.76E-06	8.69E-06	7.91E-03
2	6.82E-01	2.60E-01	4.69E-02	3.09E-05	1.22E-05	0.	2.97E-06	1.08E-05	7.51E-03
3	7.15E-01	2.52E-01	1.51E-02	1.68E-05	2.09E-06	0.	1.42E-06	6.11E-06	6.71E-03
4	7.15E-01	2.57E-01	1.72E-02	2.43E-05	0.	0.	1.63E-06	5.60E-06	6.93E-03
5	7.23E-01	2.61E-01	1.58E-02	1.59E-05	0.	0.	1.22E-06	5.70E-06	7.40E-03
6	7.17E-01	2.66E-01	6.72E-03	1.11E-05	0.	0.	4.14E-07	4.69E-06	6.88E-03
7	7.00E-01	2.70E-01	7.05E-03	1.62E-05	0.	0.	4.14E-07	4.17E-06	6.89E-03
8	7.05E-01	2.73E-01	7.41E-03	7.74E-06	0.	0.	7.35E-07	4.17E-06	6.63E-03
9	7.05E-01	2.78E-01	1.57E-03	2.55E-06	0.	0.	1.03E-07	1.56E-06	6.83E-03
10	7.07E-01	2.75E-01	1.56E-03	7.26E-06	0.	0.	0.	1.65E-06	6.97E-03
11	6.98E-01	2.77E-01	1.43E-03	0.	0.	0.	0.	0.	6.46E-03
12	7.03E-01	2.73E-01	4.69E-04	0.	0.	0.	0.	0.	5.95E-03
13	7.09E-01	2.76E-01	5.47E-04	0.	0.	0.	0.	0.	6.82E-03

TOTAL REACTION RATE (gm-moles/min)

	C_2H_4	CO_2	Ethylene Oxide	Acetaldehyde	C-4	C-6,1	C-6,2
1	-1.11E-06	2.22E-06	1.70E-09	4.65E-10	0.	1.35E-10	4.25E-10
2	-1.12E-06	2.22E-06	1.47E-09	5.82E-10	0.	1.41E-10	5.12E-10
3	-3.88E-07	7.72E-07	8.55E-10	1.07E-10	0.	7.27E-11	3.12E-10
4	-4.36E-07	8.68E-07	1.22E-09	0.	0.	8.21E-11	2.83E-10
5	-4.00E-07	7.97E-07	8.01E-10	0.	0.	6.18E-11	2.88E-10
6	-1.77E-07	3.51E-07	5.82E-10	0.	0.	2.16E-11	2.45E-10
7	-1.84E-07	3.64E-07	8.39E-10	0.	0.	2.14E-11	2.16E-10
8	-1.93E-07	3.83E-07	4.00E-10	0.	0.	3.80E-11	2.16E-10
9	-4.22E-08	8.36E-08	1.36E-10	0.	0.	5.50E-12	8.31E-11
10	-4.22E-08	8.32E-08	3.86E-10	0.	0.	0.	8.75E-11
11	-3.81E-08	7.61E-08	0.	0.	0.	0.	0.
12	-1.25E-08	2.49E-08	0.	0.	0.	0.	0.
13	-1.47E-08	2.94E-08	0.	0.	0.	0.	0.

Figure 8. Experimental Results, Ethylene-Oxygen Feed on Crystal #6, (110), Non-strained

CRYSTAL 6, ETHYLENE-OXYGEN FEED, NON-STRAINED

	DATE	SAMPLE	TOTAL CONCENTRATION (gm-moles/cc)	FLOW RATE (cc/min)	FLOW RATE (gm-moles/min)	t (°C)	T (°K)	$1/T$ ($1/°K$)
1	9 SEP 64	7	2.017E-05	2.348	4.734E-05	316.12	589.30	.001696
2	9 SEP 64	8	2.016E-05	2.330	4.692E-05	317.28	590.46	.001693
3	10 SEP 64	3	2.023E-05	2.245	4.537E-05	316.55	589.73	.001695
4	10 SEP 64	4	2.024E-05	2.238	4.527E-05	316.41	589.59	.001696
5	10 SEP 64	5	2.023E-05	2.273	4.596E-05	316.65	589.82	.001695
6	10 SEP 64	7	1.928E-05	2.352	4.530E-05	345.09	618.27	.001617
7	10 SEP 64	8	1.926E-05	2.353	4.528E-05	345.67	618.85	.001615
8	10 SEP 64	9	1.927E-05	2.368	4.560E-05	344.97	618.15	.001617
9	10 SEP 64	10	2.296E-05	2.187	5.017E-05	245.53	518.71	.001927
10	10 SEP 64	12	2.299E-05	1.839	4.224E-05	245.63	518.81	.001927
11	10 SEP 64	13	2.298E-05	2.146	4.928E-05	245.81	518.99	.001926
12	10 SEP 64	14	2.192E-05	2.232	4.890E-05	270.94	544.12	.001837
13	10 SEP 64	16	2.194E-05	2.231	4.892E-05	270.78	543.96	.001838
14	10 SEP 64	17	2.193E-05	2.289	5.015E-05	271.09	544.27	.001837
15	10 SEP 64	1 - FEED	0.	0.	0.	0.	0.	.

SAMPLE ANALYSIS (mole fraction)

	O_2	C_2H_4	CO_2	Ethylene Oxide	Acetaldehyde	C-4	C-6,1	C-6,2	N_2
1	7.91E-01	1.86E-01	1.27E-02	1.26E-05	0.	2.56E-07	1.38E-06	1.53E-06	7.01E-03
2	8.01E-01	1.93E-01	1.29E-02	7.52E-06	1.06E-06	2.56E-07	1.22E-06	1.53E-06	7.46E-03
3	7.75E-01	1.83E-01	1.29E-02	3.89E-06	0.	3.08E-07	1.12E-06	1.22E-06	6.76E-03
4	7.72E-01	1.91E-01	1.27E-02	7.71E-06	0.	3.09E-07	9.39E-07	1.40E-06	6.70E-03
5	7.70E-01	1.86E-01	1.29E-02	6.95E-06	0.	3.09E-07	9.39E-07	1.40E-06	7.12E-03
6	7.19E-01	2.15E-01	2.73E-02	1.49E-05	2.63E-06	6.33E-07	1.53E-06	2.88E-06	6.46E-03
7	7.03E-01	2.42E-01	2.74E-02	1.58E-05	7.95E-06	7.92E-07	1.53E-06	3.17E-06	6.95E-03
8	7.12E-01	2.31E-01	2.66E-02	1.82E-05	1.06E-05	6.34E-07	1.63E-06	2.97E-06	4.80E-03
9	7.05E-01	2.56E-01	6.73E-04	0.	0.	0.	0.	0.	5.78E-03
10	7.09E-01	2.66E-01	7.27E-04	0.	0.	0.	0.	0.	5.92E-03
11	6.97E-01	2.65E-01	7.92E-04	0.	0.	0.	0.	0.	5.65E-03
12	6.92E-01	2.69E-01	2.32E-03	0.	0.	0.	1.95E-07	0.	5.51E-03
13	6.92E-01	2.65E-01	2.40E-03	0.	0.	0.	0.	0.	6.63E-03
14	7.10E-01	2.63E-01	2.13E-03	0.	0.	0.	0.	0.	6.47E-03
15	7.86E-01	1.85E-01	0.	0.	0.	0.	0.	0.	6.15E-03

TOTAL REACTION RATE (gm-moles/min)

	C_2H_4	CO_2	Ethylene Oxide	Acetaldehyde	C-4	C-6,1	C-6,2
1	-3.01E-07	5.99E-07	5.96E-10	0.	1.21E-11	6.52E-11	7.25E-11
2	-3.04E-07	6.06E-07	3.53E-10	4.99E-11	1.20E-11	5.74E-11	7.18E-11
3	-2.93E-07	5.85E-07	1.76E-10	0.	1.40E-11	5.10E-11	5.52E-11
4	-2.87E-07	5.73E-07	3.49E-10	0.	1.40E-11	4.25E-11	6.35E-11
5	-2.98E-07	5.95E-07	3.20E-10	0.	1.42E-11	4.32E-11	6.45E-11
6	-6.20E-07	1.24E-06	6.77E-10	1.19E-10	2.87E-11	6.94E-11	1.30E-10
7	-6.21E-07	1.24E-06	7.16E-10	3.60E-10	3.59E-11	6.95E-11	1.44E-10
8	-6.08E-07	1.21E-06	8.29E-10	4.82E-10	2.89E-11	7.43E-11	1.36E-10
9	-1.69E-08	3.38E-08	0.	0.	0.	0.	0.
10	-1.53E-08	3.07E-08	0.	0.	0.	0.	0.
11	-1.95E-08	3.90E-08	0.	0.	0.	0.	0.
12	-5.68E-08	1.14E-07	0.	0.	0.	9.56E-12	0.
13	-5.87E-08	1.17E-07	0.	0.	0.	0.	0.
14	-5.33E-08	1.07E-07	0.	0.	0.	0.	0.

Table 9

Results from Least Squares Fits of Data for Rate of Production of Carbon Dioxide with Ethylene Oxide-Oxygen Feed on Gold

Oxygen Order	Ethylene Oxide Order	ln A[a]	Activation Energy (Kcal./gm. mole)	Variance of Fit
0.5	0.0	- 6.0 ± 1.1[b]	9.01 ± 1.3[b]	0.83
0.0	0.0	-12.0 ± 1.1	8.42 ± 1.3	0.86
1.0	0.0	0.03 ± 1.1	9.60 ± 1.3	0.81
1.0	1.0	36.8 ± 3.9	28.2 ± 4.5	9.2
0.5	1.0	30.8 ± 3.9	27.6 ± 4.5	9.3
0.0	1.0	24.8 ± 3.9	27.4 ± 4.6	9.5

[a]Units of A are [gm. moles (gm. moles/cc.)$^{-p}$ min.$^{-1}$ cm.$^{-2}$] where p is the sum of the orders for the oxygen and ethylene oxide concentrations.

[b]The uncertainties shown are 95% confidence limits for the constant calculated from the least squares fit.

Table 10

Results from Least Squares Fits of Data for Rate of Production of Carbon Dioxide with Ethylene-Oxygen Feed on Gold

Oxygen Order	Ethylene Order	ln A[a]	Activation Energy (Kcal./gm. mole)	Variance of Fit
0.5	1.0	23.9 ± 3.6[b]	27.3 ± 4.3[b]	17.0
0.0	0.0	3.42 ± 4.2	24.3 ± 5.0	25.0
1.0	0.0	15.5 ± 4.4	25.5 ± 5.2	27.0
1.0	1.0	30.0 ± 3.8	27.9 ± 4.4	18.0
0.0	1.0	17.9 ± 3.6	26.7 ± 4.2	16.0

[a]Units of A are $[\text{gm. moles}(\text{gm. moles/cc.})^{-p}\text{min.}^{-1}\text{cm.}^{-2}]$ where p is the sum of the orders for the oxygen and ethylene concentrations.

[b]The uncertainties shown are 95% confidence limits for the constant calculated from the least squares fit.

Table 11

Results from Least Squares Fit of Data for Rate of Production of Carbon Dioxide with Ethylene-Oxygen Feed on Silver Crystal #1, (111), Non-strained

Oxygen Order	Ethylene Order	ln A[a]	Activated Energy (Kcal./gm. mole)	Variance of Fit
0.5	1.0	21.8 ± 1.6[b]	21.7 ± 1.9[b]	8.9
0.0	0.0	2.32 ± 1.4	20.0 ± 1.6	7.5
1.0	0.0	14.2 ± 1.7	20.9 ± 2.0	11.0
1.0	1.0	27.8 ± 1.8	22.2 ± 2.1	10.9
0.0	1.0	15.9 ± 1.4	21.3 ± 1.7	7.3

[a]Units of A are [gm. moles (gm. moles/cc.)$^{-p}$ min.$^{-1}$ cm.$^{-2}$] where p is the sum of the orders for the oxygen and ethylene concentrations.

[b]The uncertainties shown are 95% confidence limits for the constant calculated from the least squares fit.

Table 12

Results from Least Squares Fit of Data for Rate of Production of Carbon Dioxide with Ethylene-Oxygen Feed on Silver Crystal #2, (100), Non-strained

Oxygen Order	Ethylene Order	ln A[a]	Activation Energy (Kcal./gm. mole)	Variance of Fit
0.5	1.0	22.8 ± 2.3[b]	23.0 ± 2.7[b]	23.
0.0	0.0	2.28 ± 2.6	20.8 ± 3.1	33.
1.0	0.0	14.9 ± 2.5	22.0 ± 2.9	28.
1.0	1.0	29.8 ± 2.2	23.6 ± 2.6	21.
0.0	1.0	16.7 ± 2.4	22.4 ± 2.8	26.

[a]Units of A are [gm. moles (gm. moles/cc.)$^{-p}$min.$^{-1}$cm.$^{-2}$] where p is the sum of the orders for the oxygen and ethylene concentrations.

[b]The uncertainties shown are 95% confidence limits for the constant calculated from the least squares fit.

Table 13

Results from Least Squares Fit of Data for Rate of Production of Carbon Dioxide with Ethylene-Oxygen Feed on Silver Crystal #3, (111), Strained 0.8%

Oxygen Order	Ethylene Order	ln A[a]	Activation Energy (Kcal./gm. mole)	Variance of Fit
0.5	1.0	22.7 ± 1.6[b]	23.5 ± 1.8[b]	7.0
0.0	0.0	3.09 ± 1.8	21.2 ± 2.0	9.4
1.0	0.0	15.1 ± 1.8	22.5 ± 2.1	9.8
1.0	1.0	28.9 ± 1.6	24.1 ± 1.9	7.2
0.0	1.0	16.6 ± 1.6	22.8 ± 1.8	6.9

[a]Units of A are [gm. moles (gm. moles/cc.)$^{-p}$min.$^{-1}$cm.$^{-2}$] where p is the sum of the orders for the oxygen and ethylene concentrations.

[b]The uncertainties shown are 95% confidence limits for the constant calculated from the least squares fit.

Table 14

Results from Least Squares Fit of Data for Rate of Production of Carbon Dioxide with Ethylene-Oxygen Feed on Silver Crystal #4, (100), Strained 0.8%

Oxygen Order	Ethylene Order	ln A[a]	Activation Energy (Kcal./gm. mole)	Variation of Fit
0.5	1.0	23.2 ± 1.6[b]	24.3 ± 1.8[b]	5.0
0.0	0.0	3.71 ± 1.5	22.3 ± 1.8	5.0
1.0	0.0	16.5 ± 2.0	24.1 ± 2.4	8.7
1.0	1.0	29.6 ± 1.9	25.3 ± 2.2	7.0
0.0	1.0	16.7 ± 1.4	23.5 ± 1.7	4.3

[a] Units of A are [gm. moles (gm. moles/cc.)$^{-p}$ min.$^{-1}$ cm.$^{-2}$] where p is the sum of the orders for the oxygen and ethylene concentrations.

[b] The uncertainties shown are 95% confidence limits for the constant calculated from the least squares fit.

Table 15

Results from Least Squares Fits of Data for Rate of Production of Carbon Dioxide with Ethylene-Oxygen Feed on Silver Crystal #5, (110), Strained 0.8%

Oxygen Order	Ethylene Order	ln A[a]	Activation Energy (Kcal./gm. mole)	Variance of Fit
0.5	1.0	21.0 ± 1.1[b]	21.8 ± 1.3[b]	3.0
0.0	0.0	1.34 ± 1.3	19.5 ± 1.5	4.1
1.0	0.0	13.4 ± 1.3	20.5 ± 1.6	4.3
1.0	1.0	27.0 ± 1.2	22.3 ± 1.4	3.1
0.0	1.0	14.0 ± 1.1	21.2 ± 1.3	2.9

[a]Units of A are [gm. moles (gm. moles/cc.)$^{-p}$ min.$^{-1}$ cm.$^{-2}$] where p is the sum of the orders for the oxygen and ethylene concentrations.

[b]The uncertainties shown are 95% confidence limits for the constant calculated from the least squares fit.

Table 16

Results from Least Squares Fit of Data for Rate of Production of Carbon Dioxide with Ethylene-Oxygen Feed on Silver Crystal #6, (110), Non-strained

Oxygen Order	Ethylene Order	ln A[a]	Activation Energy (Kcal./gm. mole)	Variance of Fit
0.5	1.0	24.7 ± 2.3[b]	25.2 ± 2.7[b]	19.0
0.0	0.0	4.10 ± 1.4	22.1 ± 1.6	7.6
1.0	0.0	15.9 ± 1.0	22.9 ± 1.1	3.7
1.0	1.0	30.6 ± 2.1	25.7 ± 2.4	15.0
0.0	1.0	18.8 ± 2.6	24.8 ± 3.0	24.0

[a]Units of A are [gm. moles (gm. moles/cc.)$^{-p}$ min.$^{-1}$ cm.$^{-2}$] where p is the sum of the orders for the oxygen and ethylene concentrations.

[b]The uncertainties shown are 95% confidence limits for the constant calculated from the least squares fit.

Table 17

Results from Least Squares Fit of Data for Rate of Production of Carbon Dioxide with Ethylene-Oxygen Feed, Silver Crystals #1, #2, and #6

Oxygen Order	Ethylene Oxide	ln A[a]	Activation Energy (Kcal/gm. mole)	Variance of Fit
0.5	1.0	23.1 ± 1.2[b]	23.3 ± 1.1[b]	27.0
0.0	0.0	3.02 ± 1.1	20.9 ± 1.3	24.0
1.0	0.0	14.0 ± 1.1	21.9 ± 1.3	21.0
1.0	1.0	29.0 ± 1.2	23.8 ± 1.4	24.0
0.0	1.0	17.1 ± 1.3	22.8 ± 1.5	30.0

[a]Units of A are [gm. moles (gm. moles/cc.)$^{-p}$ min.$^{-1}$ cm.$^{-2}$] where p is the sum of the orders for the oxygen and ethylene concentrations.

[b]The uncertainties shown are 95% confidence limits for the constant calculated from the least squares fit.

Table 18

Results from Least Squares Fit of Data for Rate of Production of Carbon Dioxide with Ethylene-Oxygen Feed, Silver Crystals #3, #4, and #5

Oxygen Order	Ethylene Order	ln A[a]	Activation Energy (Kcal./gm. mole)	Variance of Fit
0.5	1.0	22.1 ± 1.1[b]	23.0 ± 1.3[b]	15.0
0.0	0.0	2.49 ± 1.2	20.7 ± 1.4	17.0
1.0	0.0	14.8 ± 1.3	22.1 ± 1.5	19.0
1.0	1.0	28.2 ± 1.2	23.6 ± 1.4	16.0
0.0	1.0	15.9 ± 1.1	22.2 ± 1.3	15.0

[a] Units of A are [gm. moles (gm. moles/cc.)$^{-p}$ min.$^{-1}$ cm.$^{-2}$] where p is the sum of the orders for the oxygen and ethylene concentrations.

[b] The uncertainties shown are 95% confidence limits for the constant calculated from the least squares fit.

Table 19

Results from Least Squares Fit of Data for Rate of Production of Carbon Dioxide with Ethylene-Oxygen Feed, All Six Silver Crystals

Oxygen Order	Ethylene Order	ln A[a]	Activation Energy (Kcal/gm. mole)	Variance of Fit
0.5	1.0	22.6 ± 1.6[b]	23.1 ± 1.8[b]	77.0
0.0	0.0	2.28 ± 1.1	20.8 ± 1.3	43.0
1.0	0.0	14.9 ± 1.0	21.9 ± 1.2	33.0
1.0	1.0	28.6 ± 1.5	23.7 ± 1.7	68.0
0.0	1.0	16.5 ± 1.7	22.5 ± 1.9	87.0

[a]Units of A are [gm. moles (gm. moles/cc.)$^{-p}$ min.$^{-1}$ cm.$^{-2}$] where p is the sum of the orders for the oxygen and ethylene concentrations.

[b]The uncertainties shown are 95% confidence limits for the constant calculated from the least squares fit.

Table 20

Comparison of Reaction Rates

Reactor Conditions

20% Ethylene
80% Oxygen
Temperature - 260°C
Pressure - 740 mm.

	Rate of Disappearance of Ethylene (gm. moles/min. cm.^{2})
Buntin (3)	1.3×10^{-8}
Kummer (17)	1.1×10^{-6} [a]
Orzechowski and MacCormack (25)	6.5×10^{-8}
Wan (35)	1.0×10^{-8} [b]
This work, Non-strained crystals	3.2×10^{-8}
This work, Strained crystals	1.6×10^{-8}

[a]Total reactor pressure 165 mm., 33% ethylene, and 67% oxygen.

[b]Based on an assumed value of specific surface area of 1 m.^{2}/gm.

Table 21

Comparison of Activation Energies
for Production of Carbon Dioxide

	Activation Energy (Kcal./gm. mole)
Buntin (3)	15.0
Kummer (17)	22.9
Orzechowski and MacCormack (25)	20.3
Twigg (32)	10.0
Wan (35)	19.3
This work	23.0

Table 22

Etch Pit Densities of the Crystals

Crystal		Etch Pit Density (pits/cm.^{2}) Before Reaction	After Reaction
#1	(111), Non-strained	2.9×10^6	7.2×10^6
#2	(100), Non-strained	5.1×10^6	2.1×10^7
#3	(111), Strained 0.8%	4.2×10^6	Few definite pits
#4	(100), Strained 0.8%	6.81×10^6	6.1×10^6
#5	(110), Strained 0.8%	Did not etch	Slight pitting
#6	(110), Non-strained	Did not etch	Did not etch

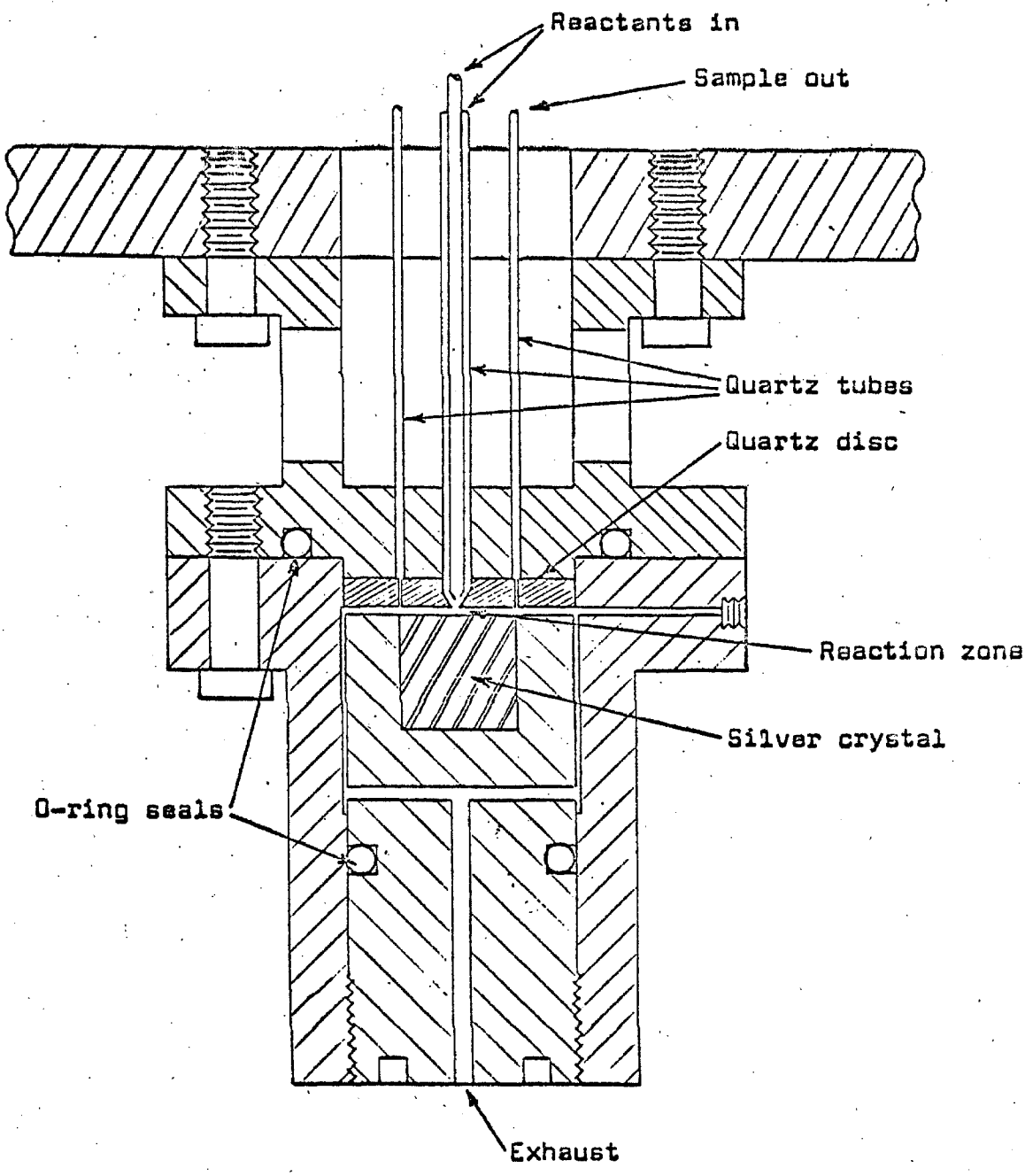

Figure 1. Sketch of Original Reactor
Approximate Scale 3:2

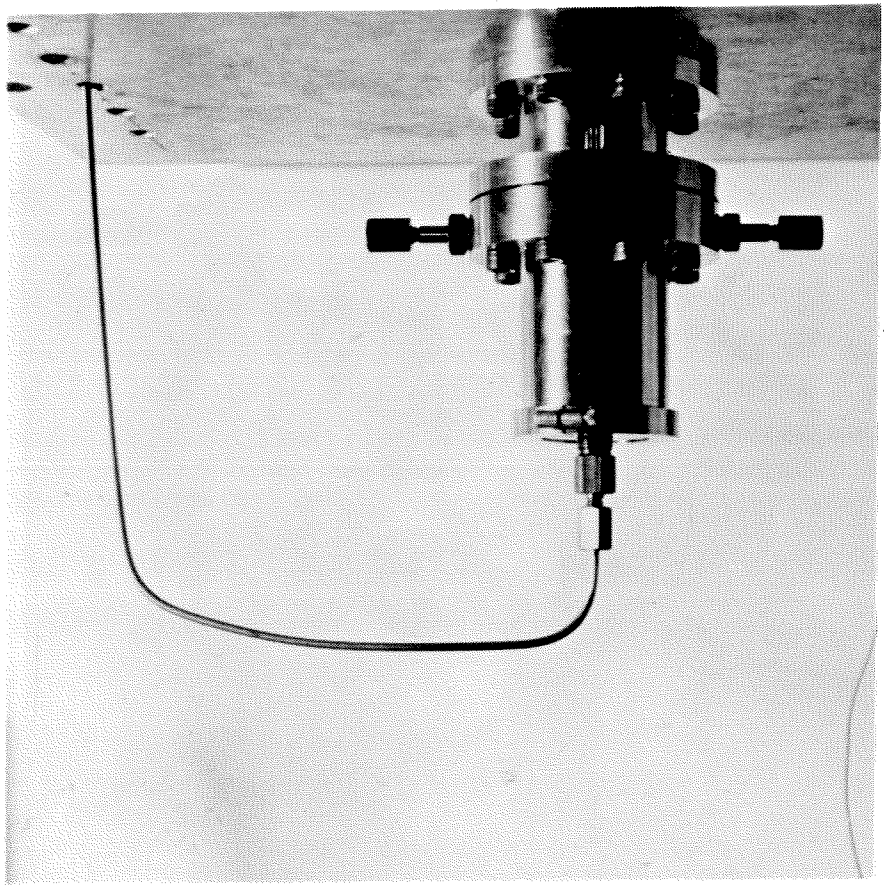

Figure 2. View of Original Reactor Mounted in Oven

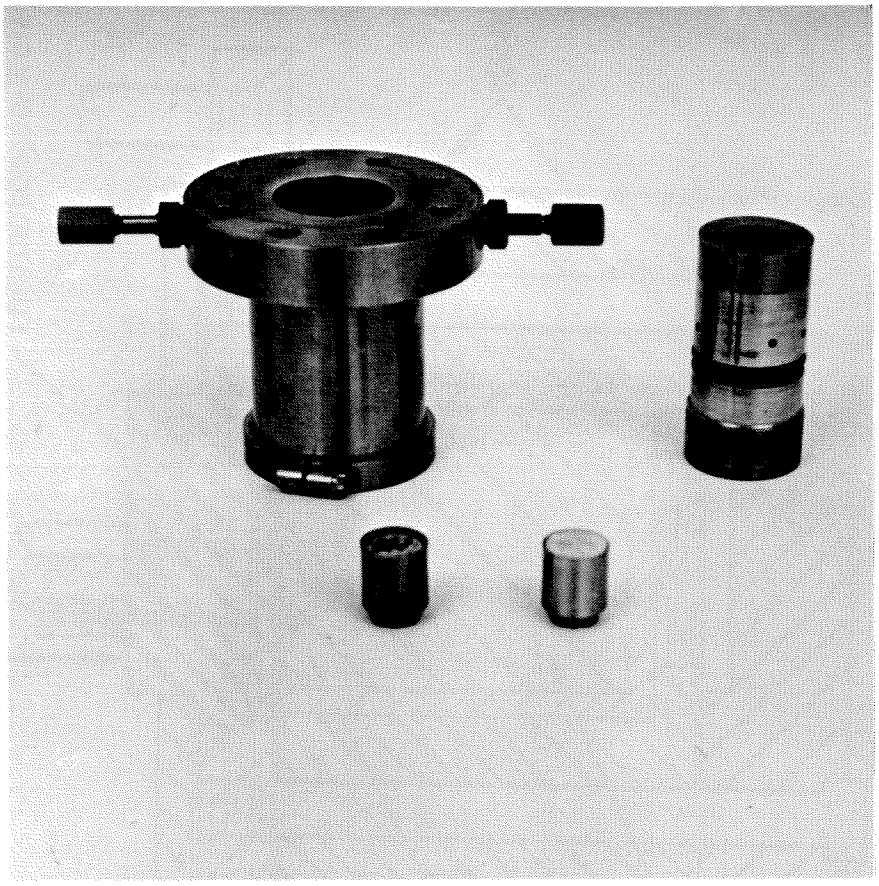

Figure 3. View of Lower Section of Original Reactor

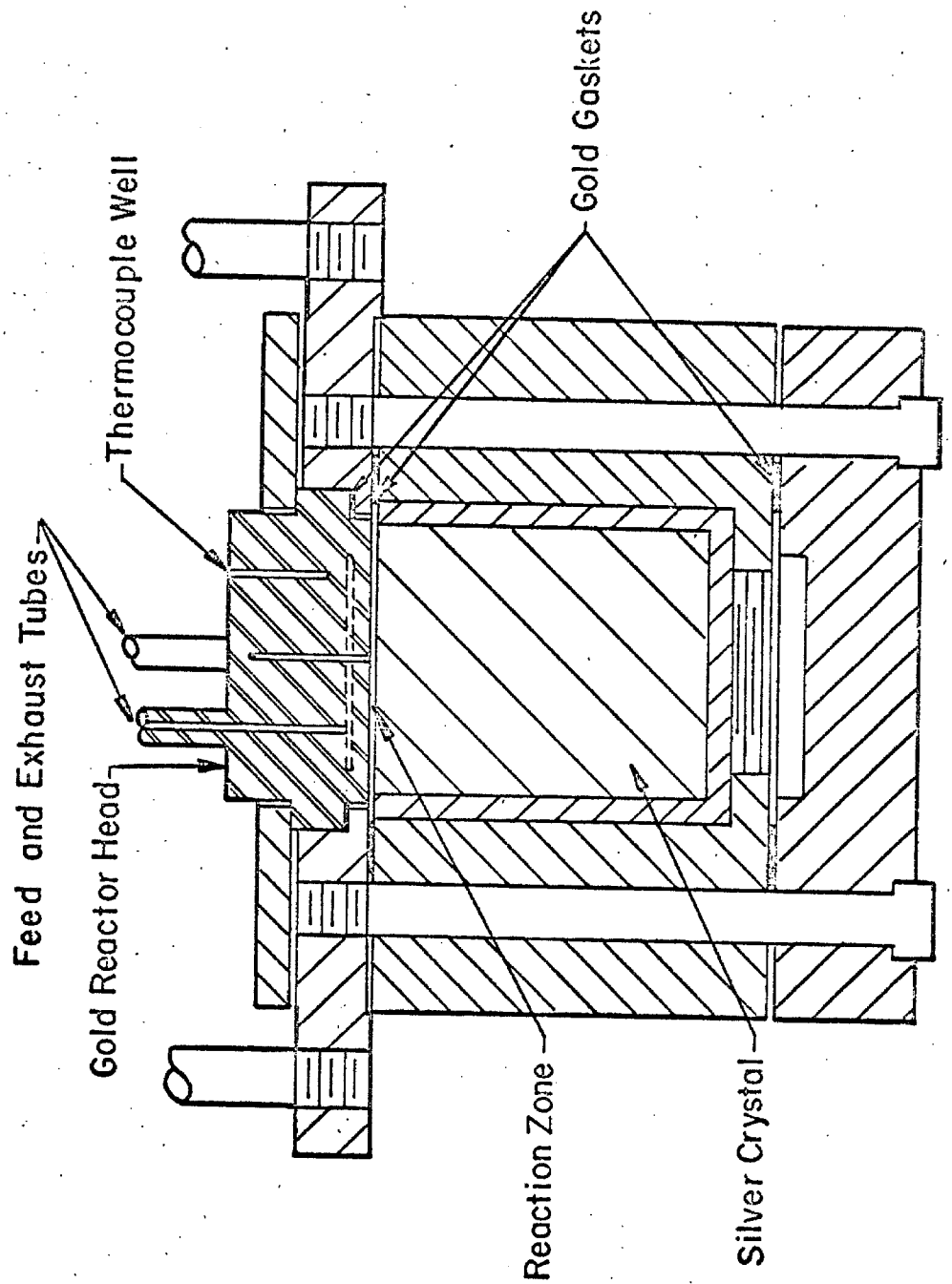

Figure 4. Sketch of Gold-Surface Reactor
Scale 3:1

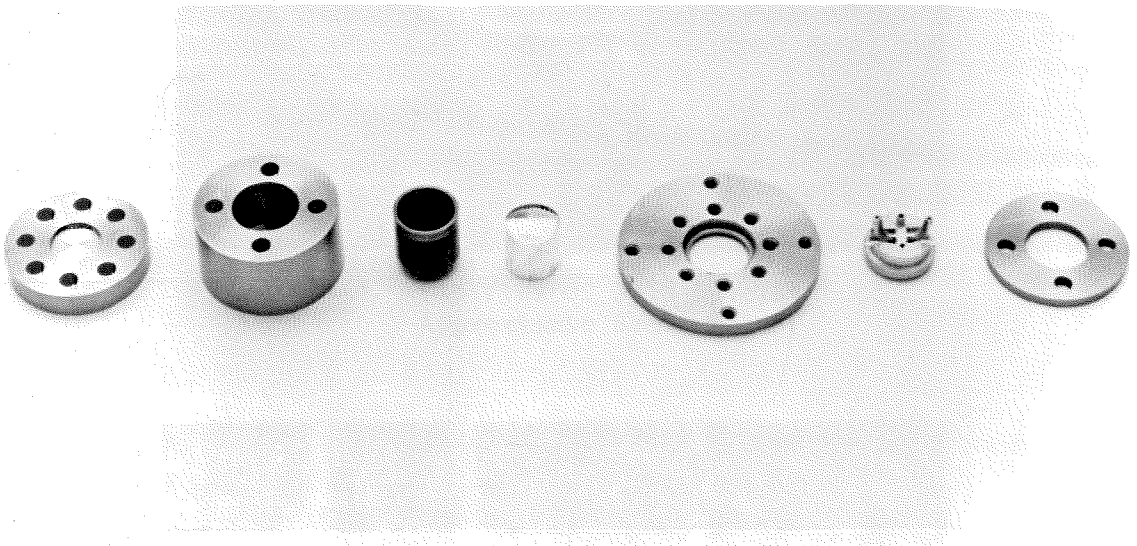

Figure 5. Exploded View of Reactor
Approximate Scale 2:3

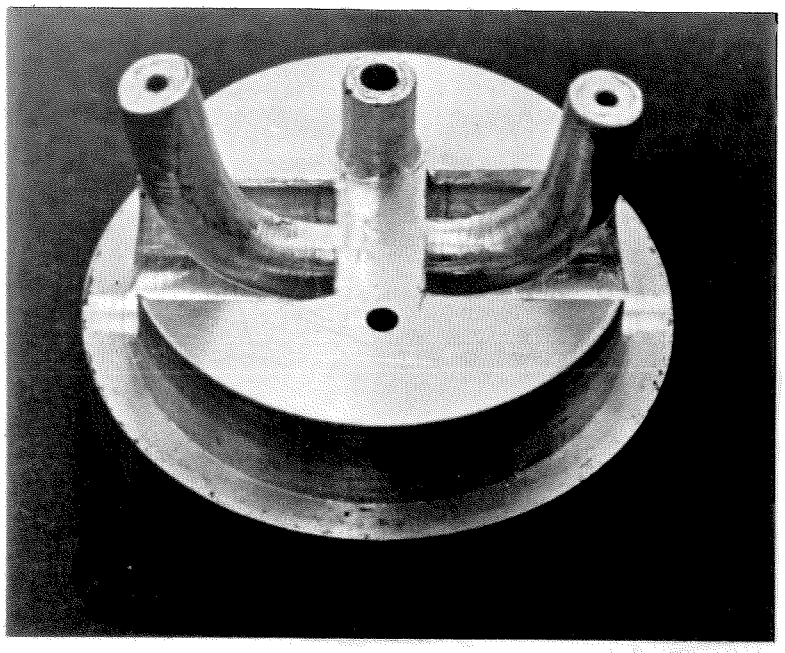

Figure 6-A. Top View of Gold Reactor Head
Approximate Scale 6:1

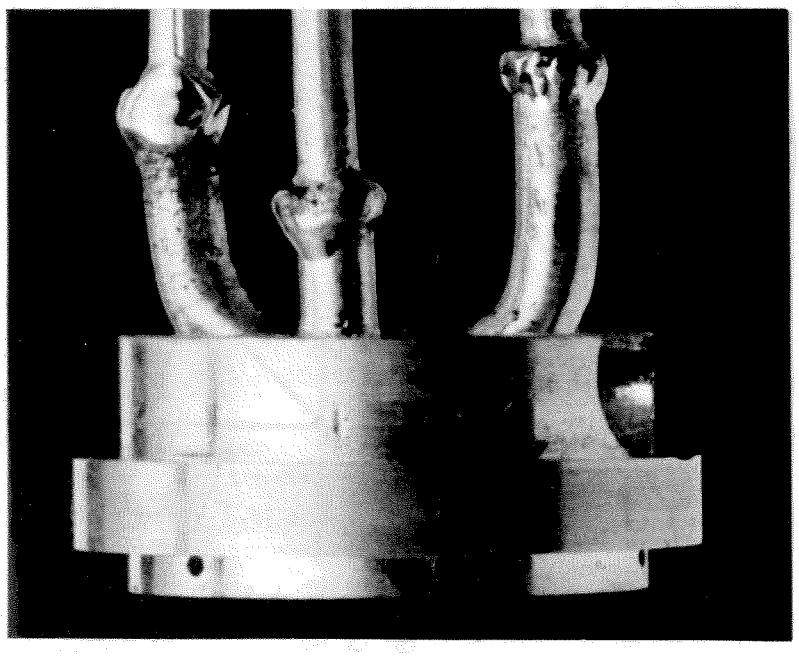

Figure 6-B. Side View of Gold Reactor Head with
Feed and Exhaust Tubes Attached
Approximate Scale 6:1

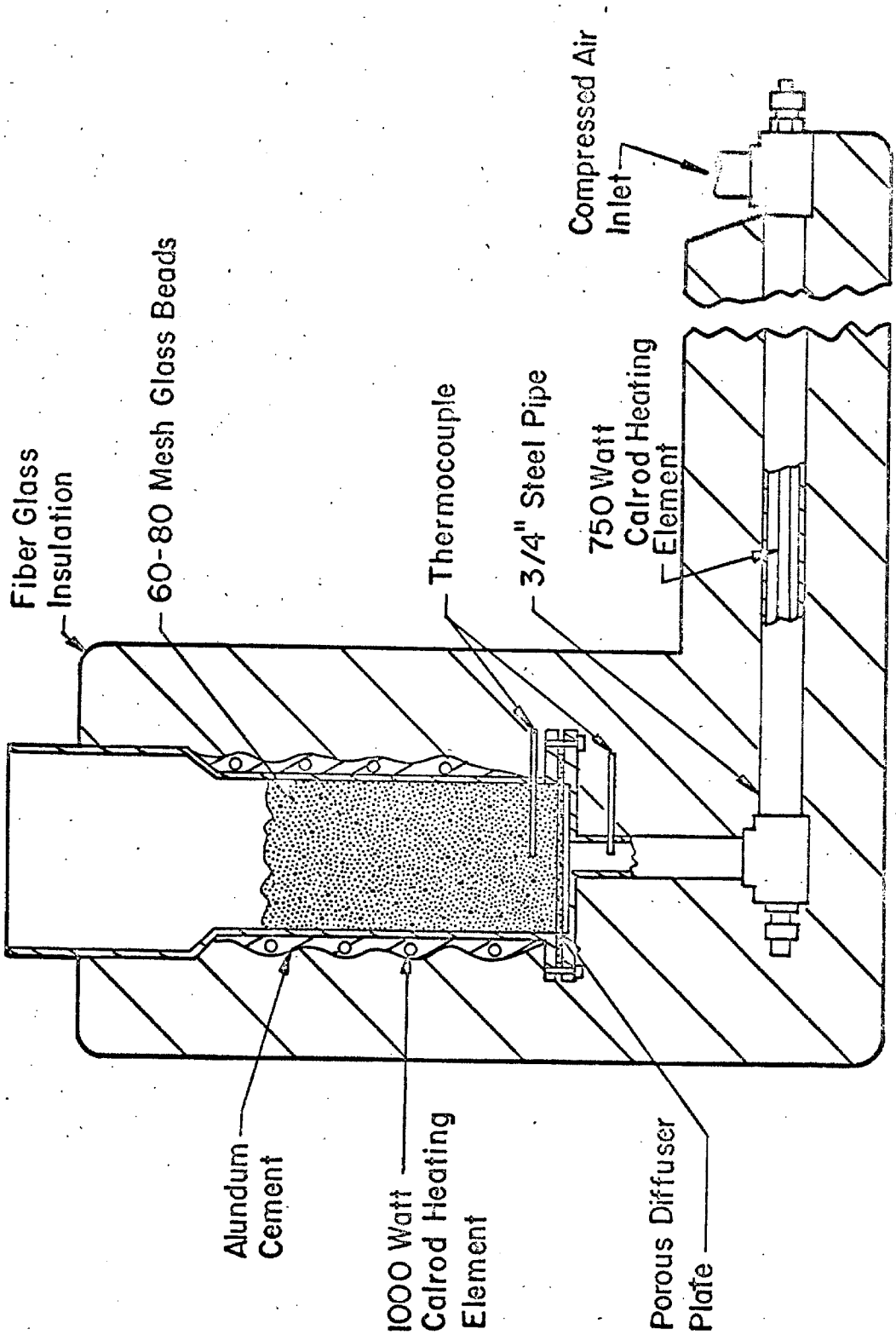

Figure 7. Sketch of Fluidized Bed Temperature Bath
Approximate Scale 1:4

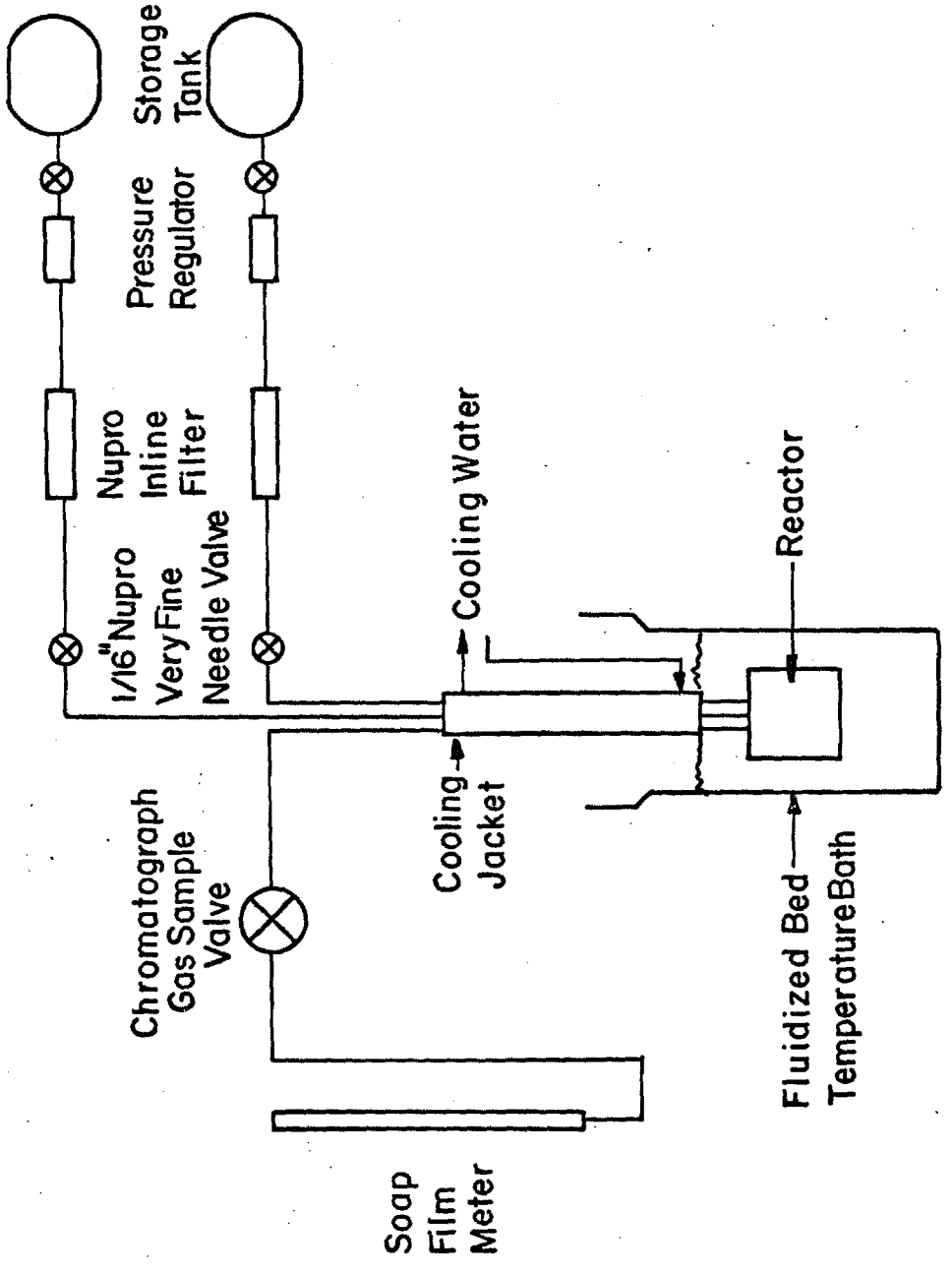

Figure 8. Reactor Flow Diagram

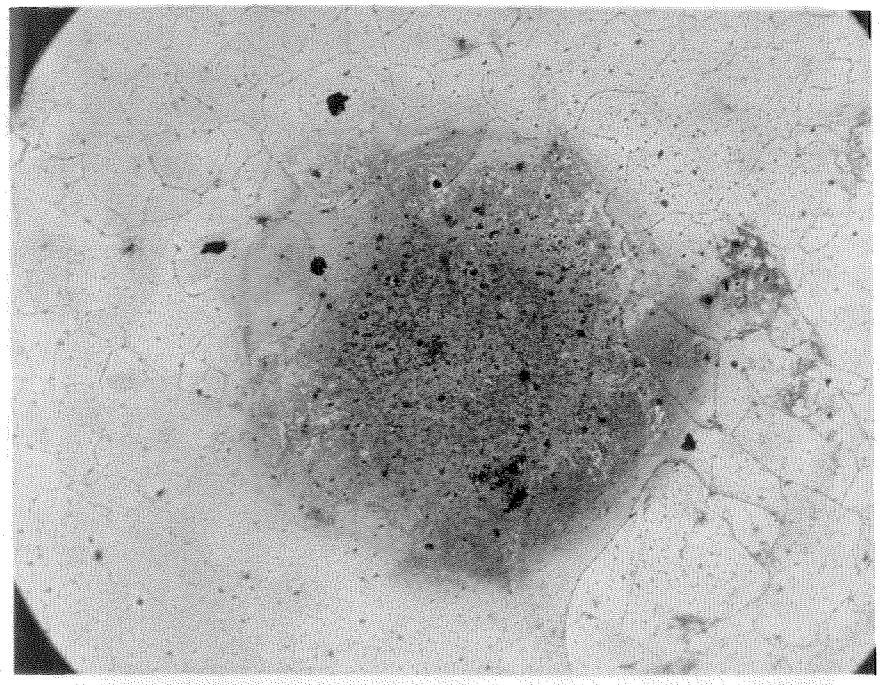

Figure 9. Typical Surface Deposits at Entrance Region of Reactor Feed Stream Crystal 6, ⟨110⟩, Non-strained, Magnification x60

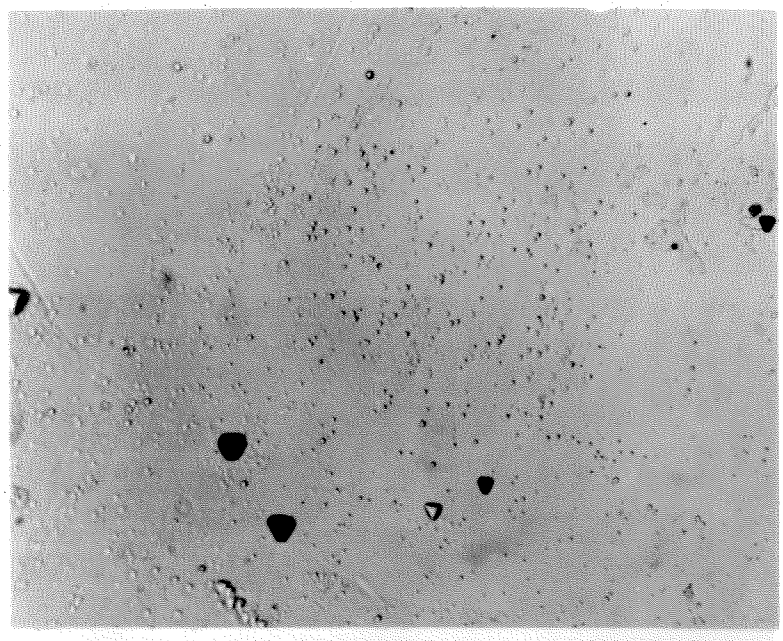

Figure 10-A. Crystal #1, Surface after Etching (111), Non-strained, Before Use in Reactor
Magnification - x300

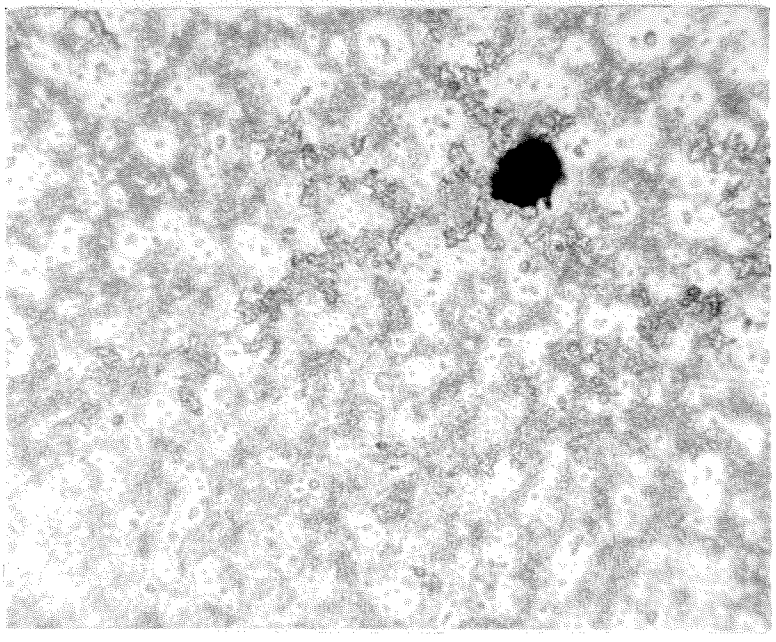

Figure 10-B. Same Location as Figure 10-A
Surface Deposits from Use in Reactor
Magnification - x300

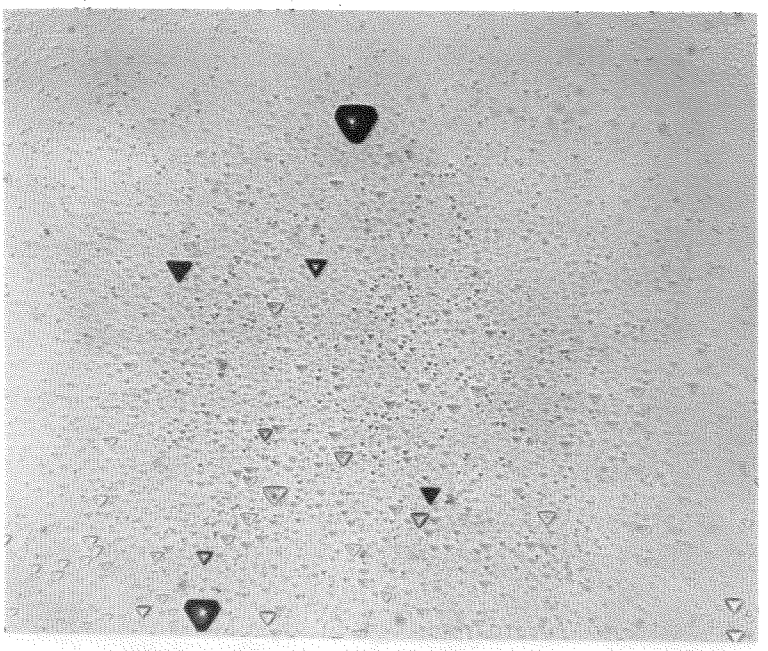

Figure 10-C. Same Location as Figure 10-A Surface Polished and Etched After Use in Reactor Magnification - x 300

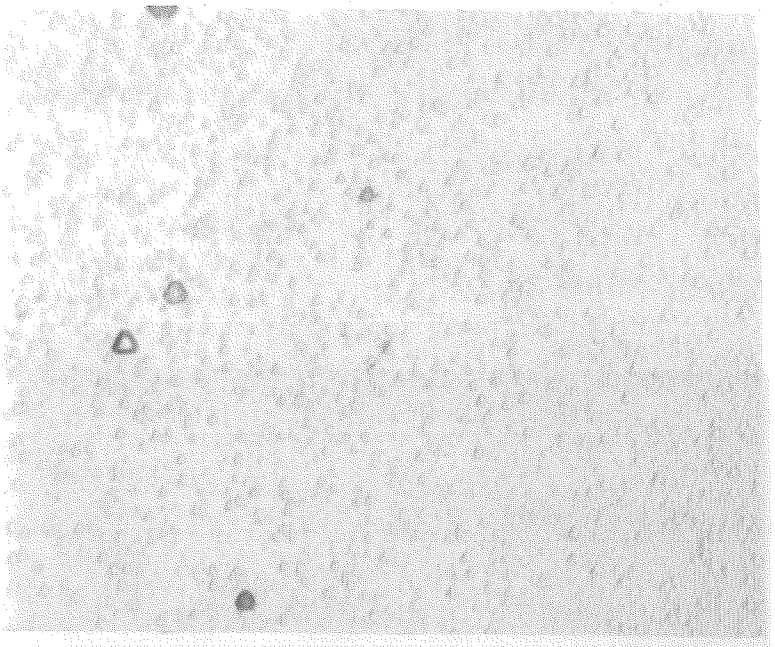

Figure 11-A. Crystal #3, Surface after Etching, ⟨111⟩ , Strained 0.8%, Before Use in Reactor
Magnification - x300

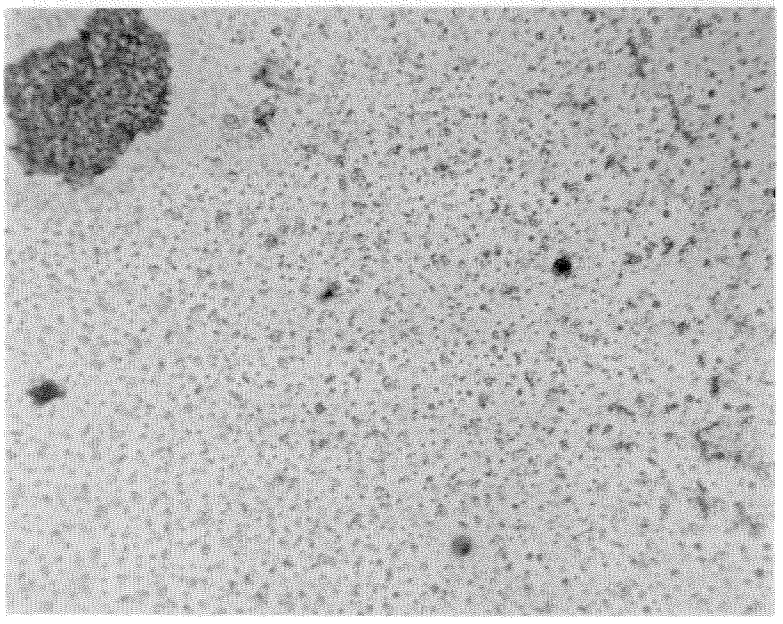

Figure 11-B. Same Location as Figure 11-A Surface Deposits from Use in Reactor
Magnification - x300

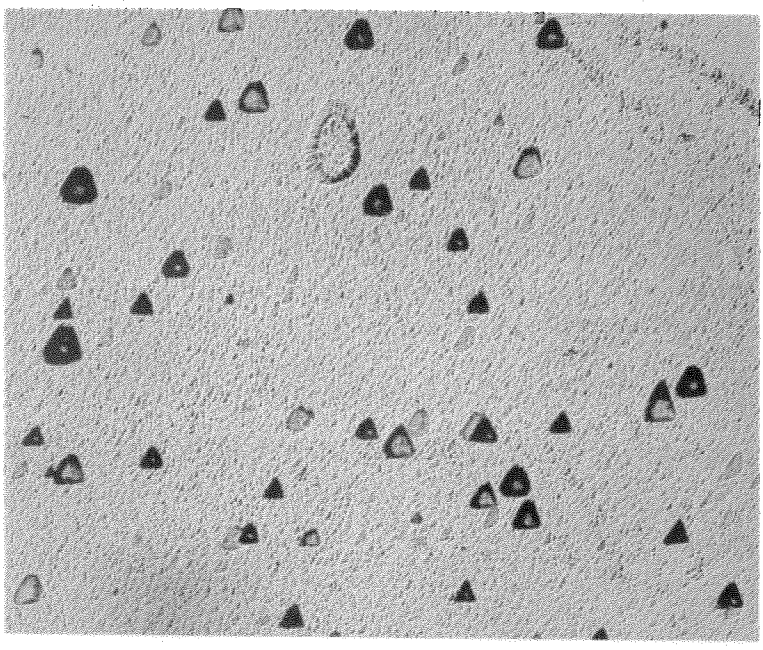

Figure 11-C. Same Location as Figure 11-A Surface Polished and Etched After Use in Reactor Magnification - x300

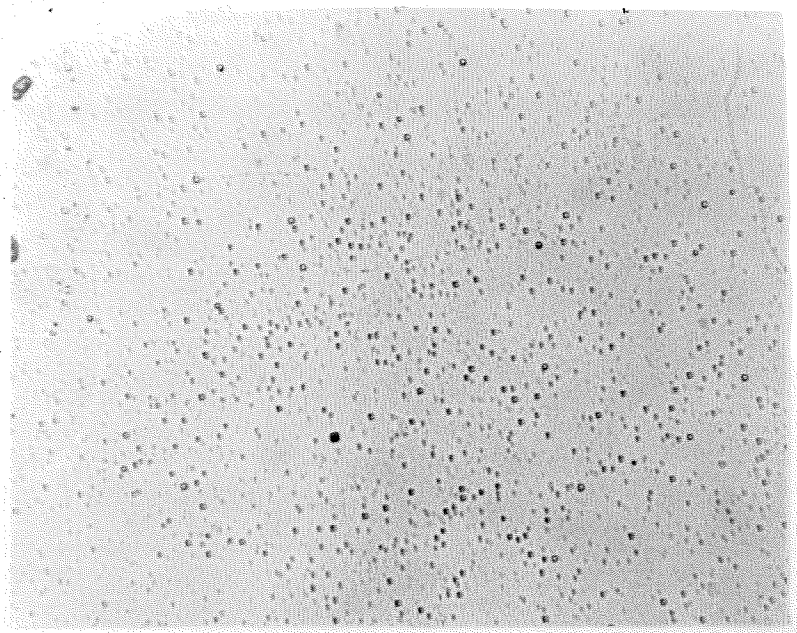

Figure 12-A. Crystal #2, Surface after Etching, ⟨100⟩ , Non-strained, Before Use in Reactor
Magnification - x400

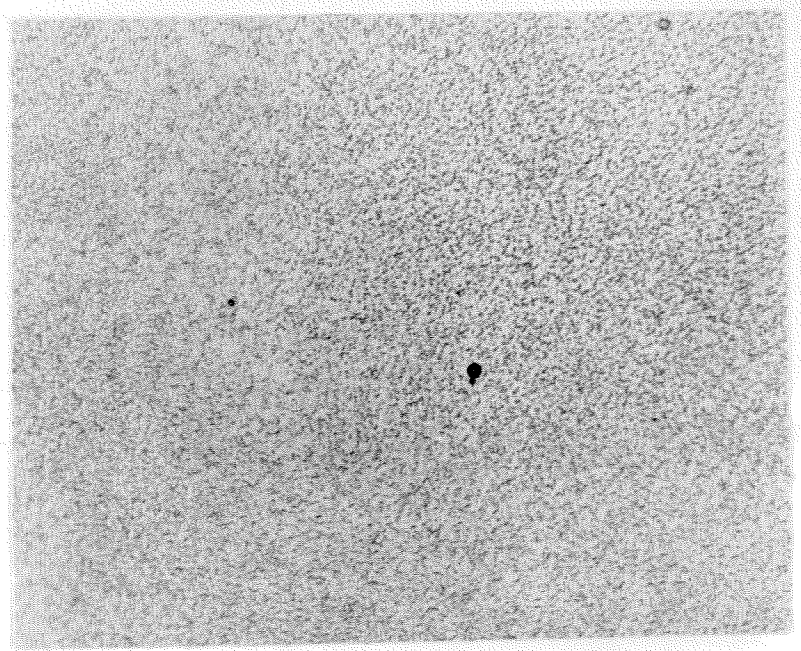

Figure 12-B. Same Location as Figure 12-A
Surface Polished and Etched
After Use in Reactor
Magnification - x300

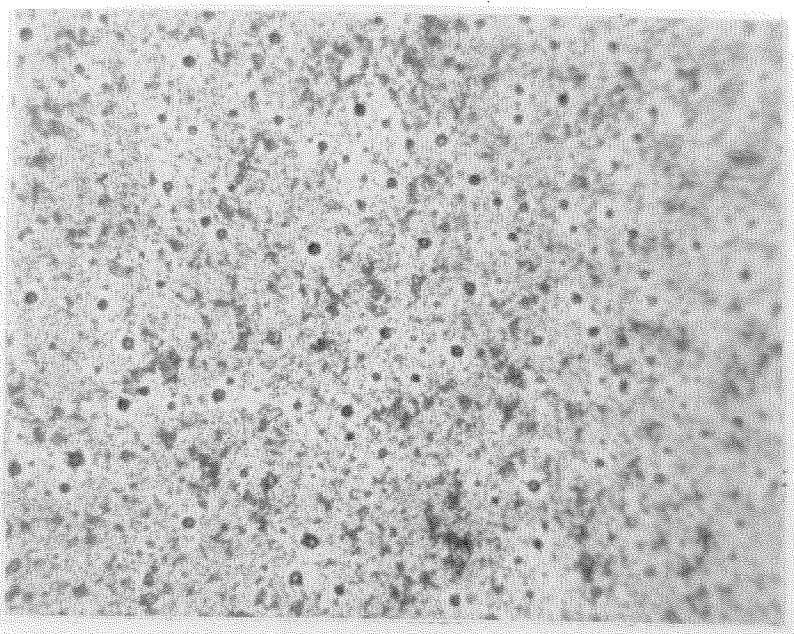

Figure 13-A. Crystal #2, ⟨100⟩ , Non-strained, Surface Deposits from Use in Reactor Magnification - x300

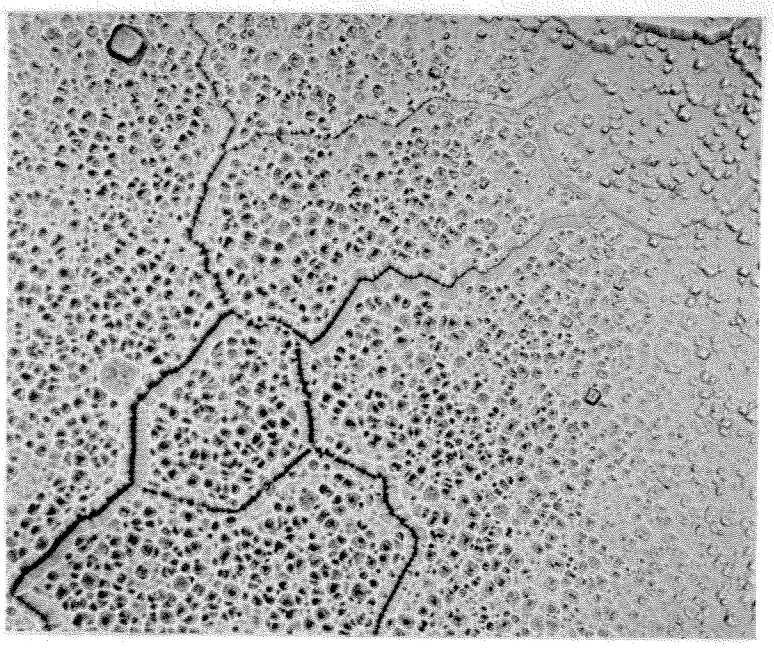

Figure 13-B. Same Location as Figure 13-A Surface Polished and Etched After Use in Reactor Magnification - x300

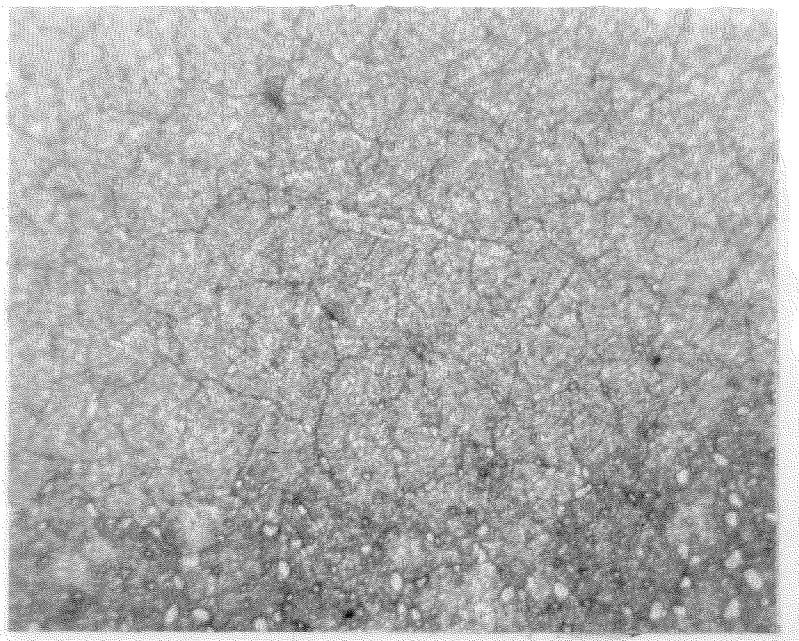

Figure 14-A. Crystal #4, ⟨100⟩ , Strained 0.8%, Surface Deposits from Use in Reactor Magnification - x300

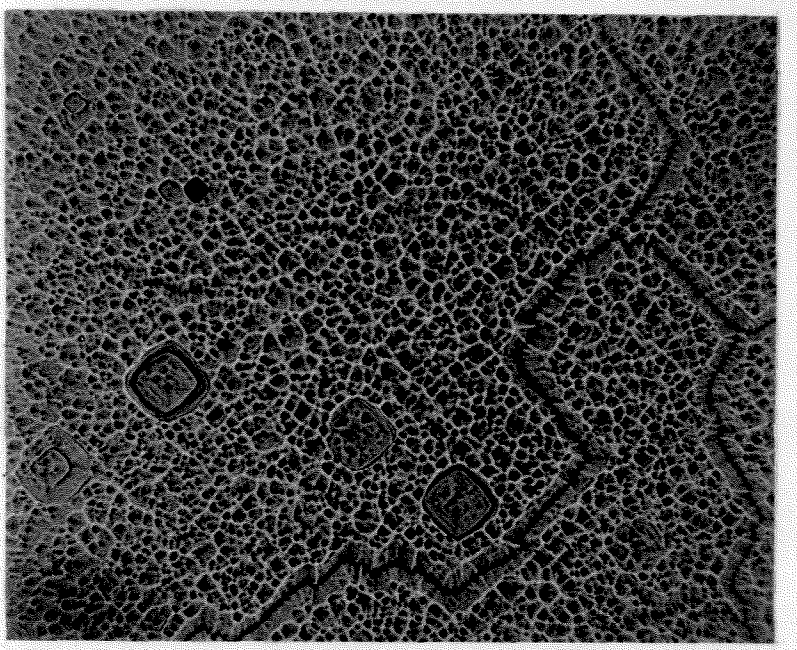

Figure 14-B. Same Location as Figure 14-A Surface Polished and Etched After Use in Reactor Magnification - x300

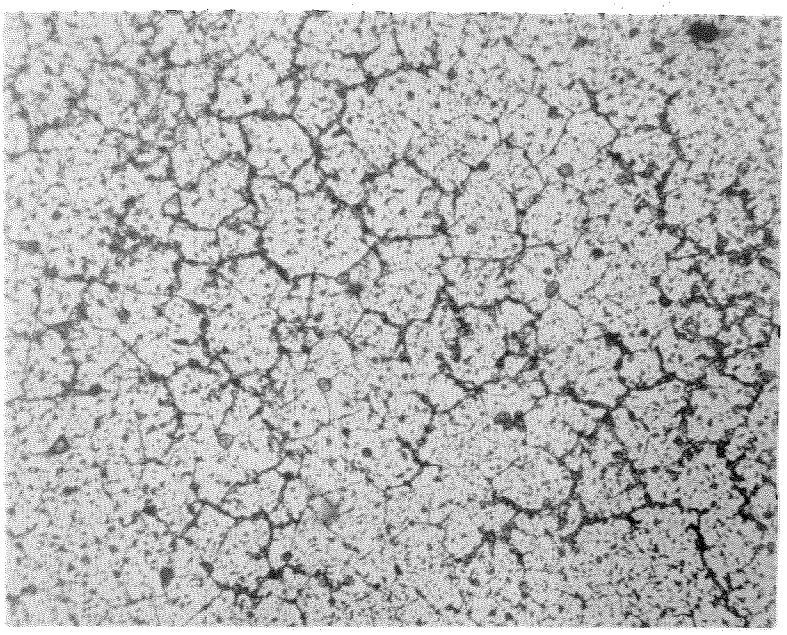

Figure 15-A. Crystal #5, ⟨110⟩, Strained 0.8%, Surface Deposits from Use in Reactor
Magnification - x300

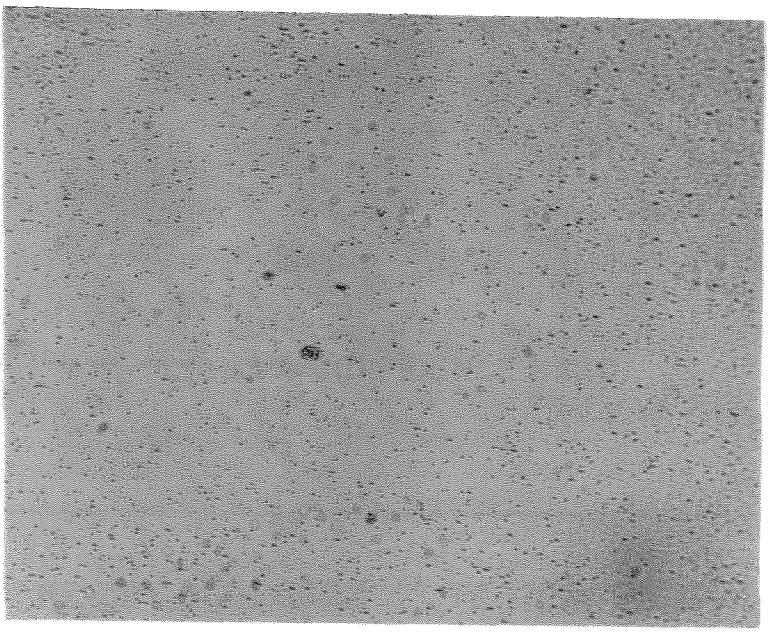

Figure 15-B. Same Location as Figure 15-A
Surface Polished and Etched
After Use in Reactor
Magnification - x300

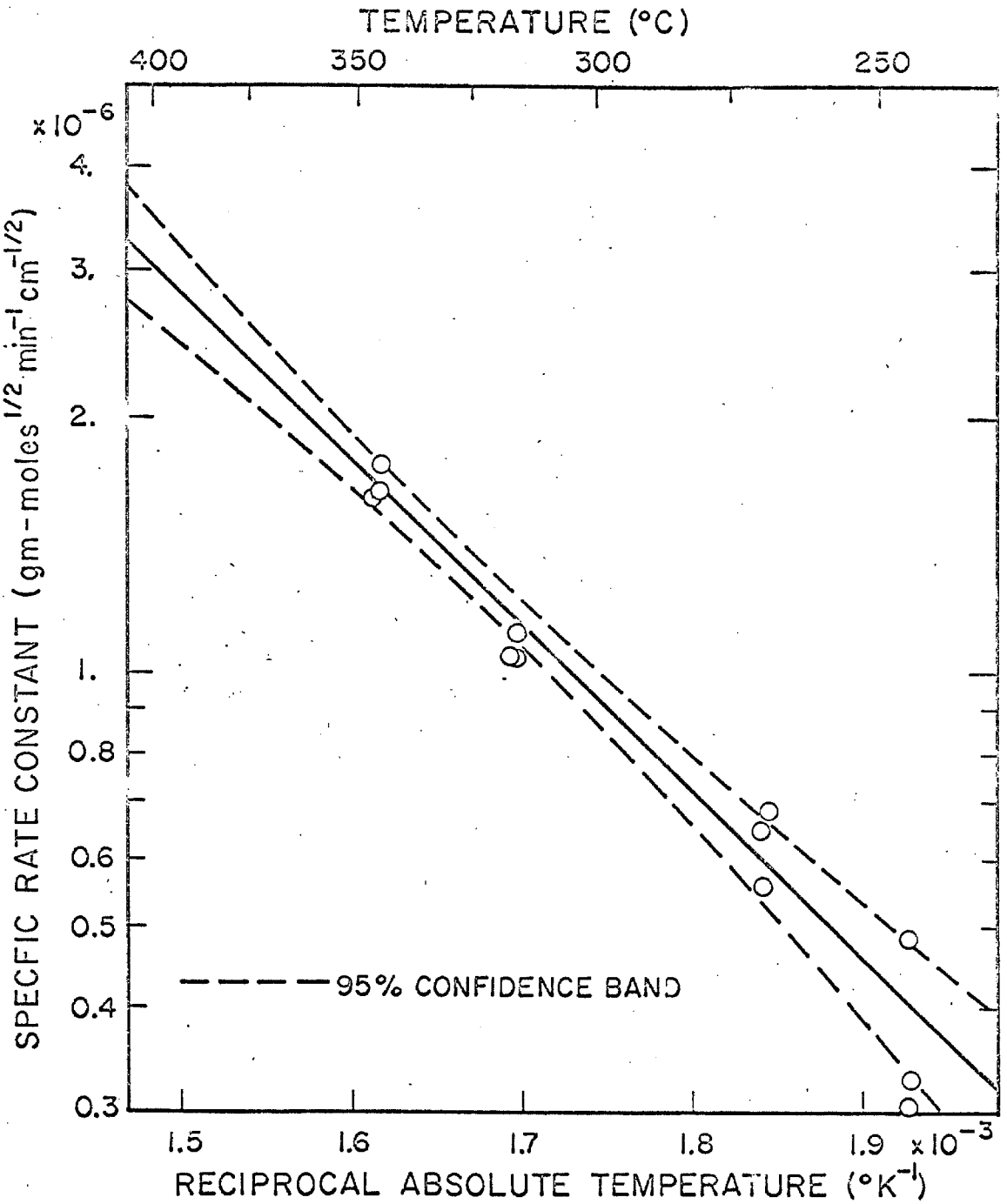

Figure 16. Temperature Dependence of Rate Constant for Production of CO_2 with Ethylene Oxide-Oxygen Feed on Gold, Ethylene Oxide Order - 0, Oxygen Order - 1/2

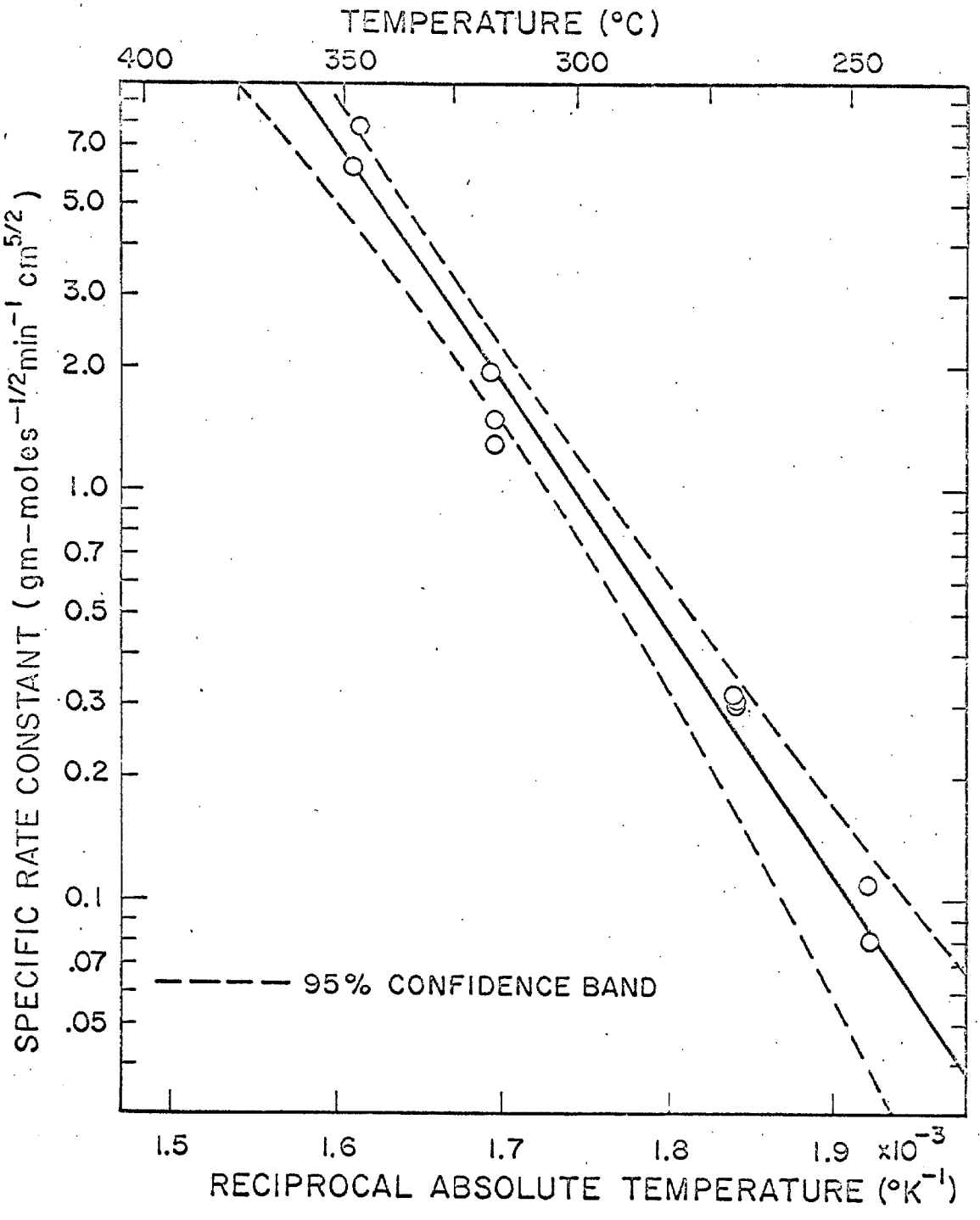

Figure 17. Temperature Dependence of Rate Constant for Production of CO_2 with Ethylene-Oxygen Feed on Gold, Ethylene Order - 1, Oxygen Order - 1/2

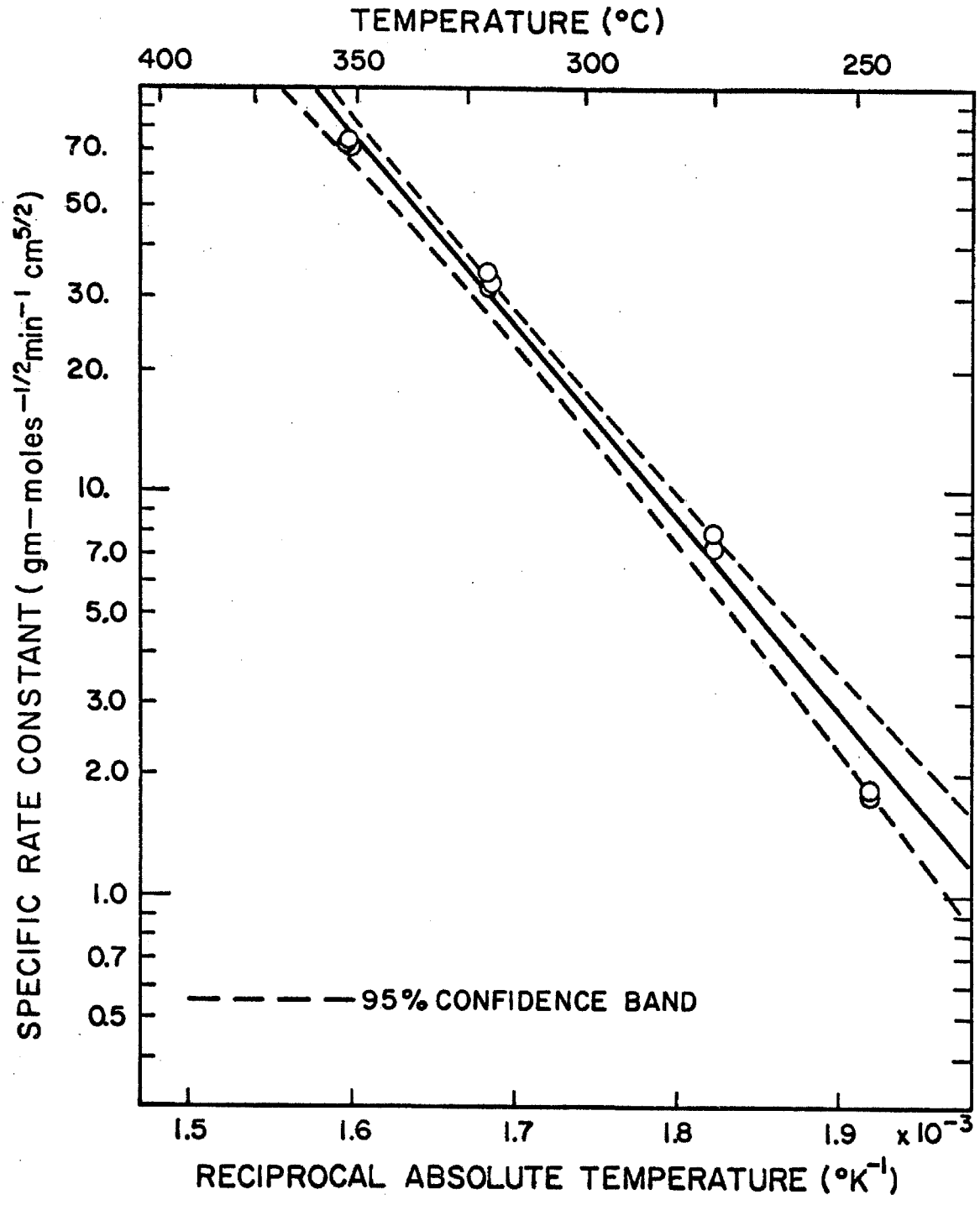

Figure 18. Temperature Dependence of Rate Constant for Production of CO_2 with Ethylene-Oxygen Feed on Crystal #1, (111), Non-strained, Ethylene Order - 1, Oxygen Order - 1/2

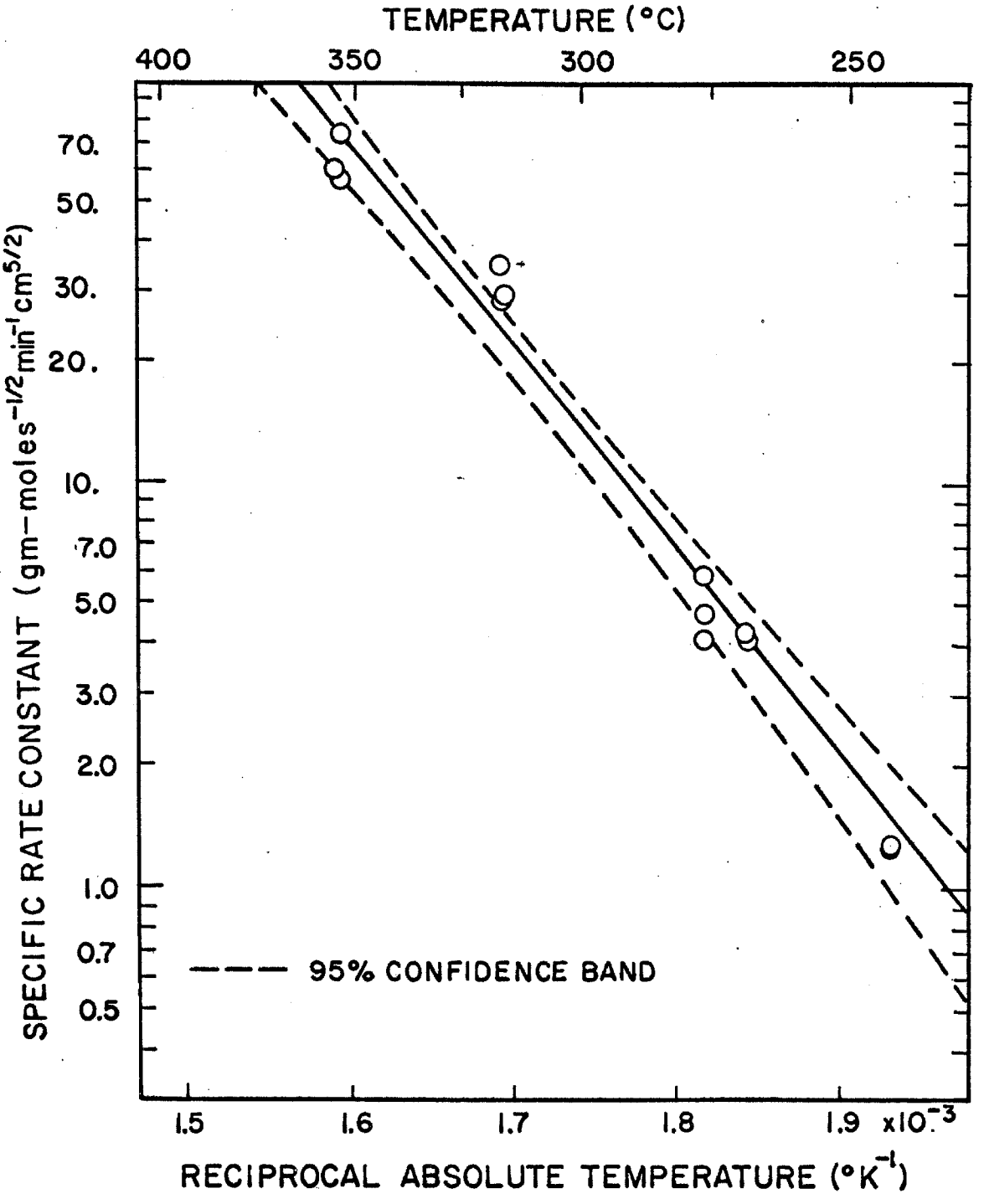

Figure 19. Temperature Dependence of Rate Constant for Production of CO_2 with Ethylene-Oxygen Feed on Crystal #2, (100), Non-strained, Ethylene Order - 1, Oxygen Order - 1/2

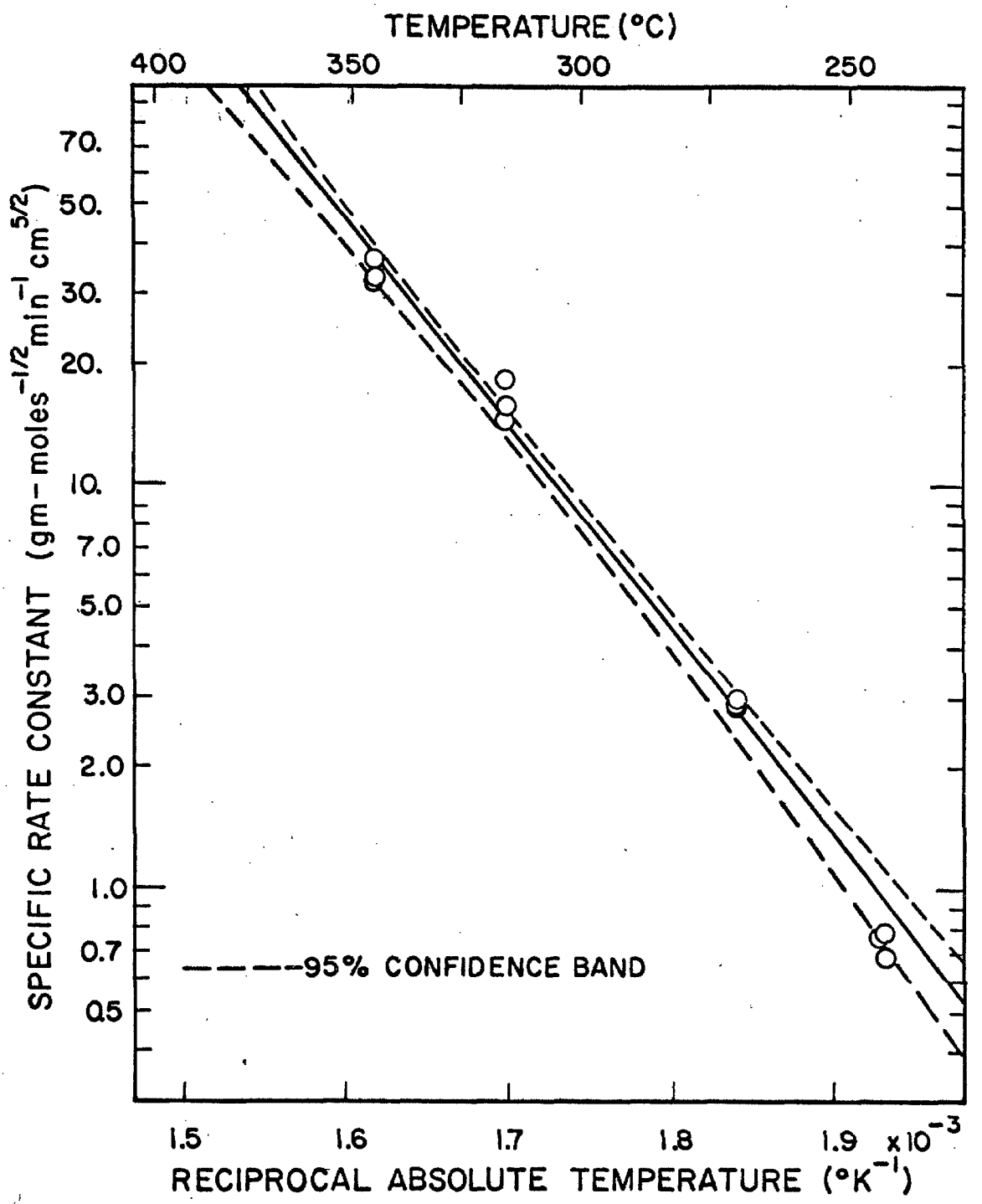

Figure 20. Temperature Dependence of Rate Constant for Production of CO_2 with Ethylene-Oxygen Feed on Crystal #3, (111), Strained 0.8%, Ethylene Order - 1, Oxygen Order - 1/2

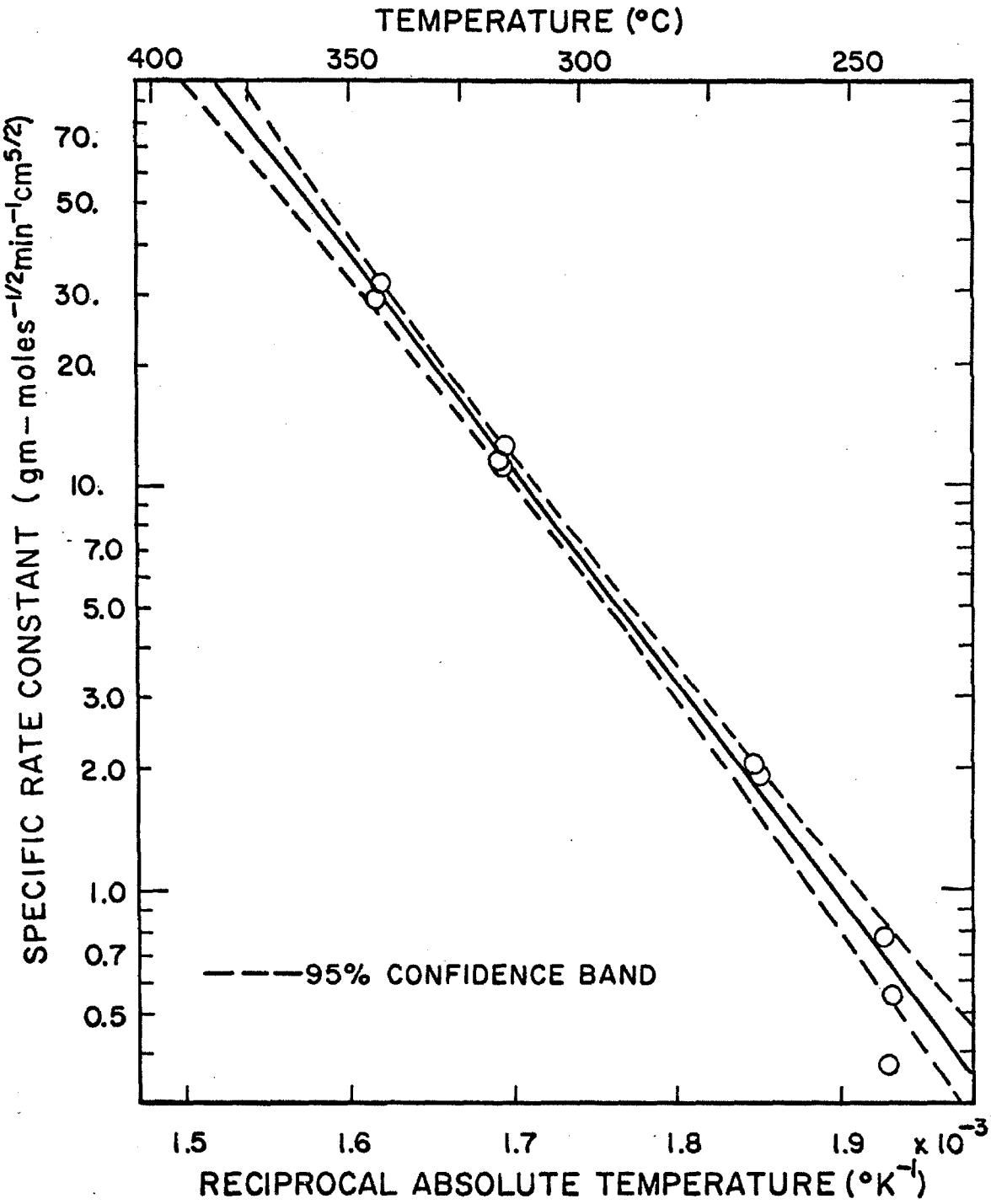

Figure 21. Temperature Dependence of Rate Constant for Production of CO_2 with Ethylene-Oxygen Feed on Crystal #4, (100), Strained 0.8%, Ethylene Order - 1, Oxygen Order - 1/2

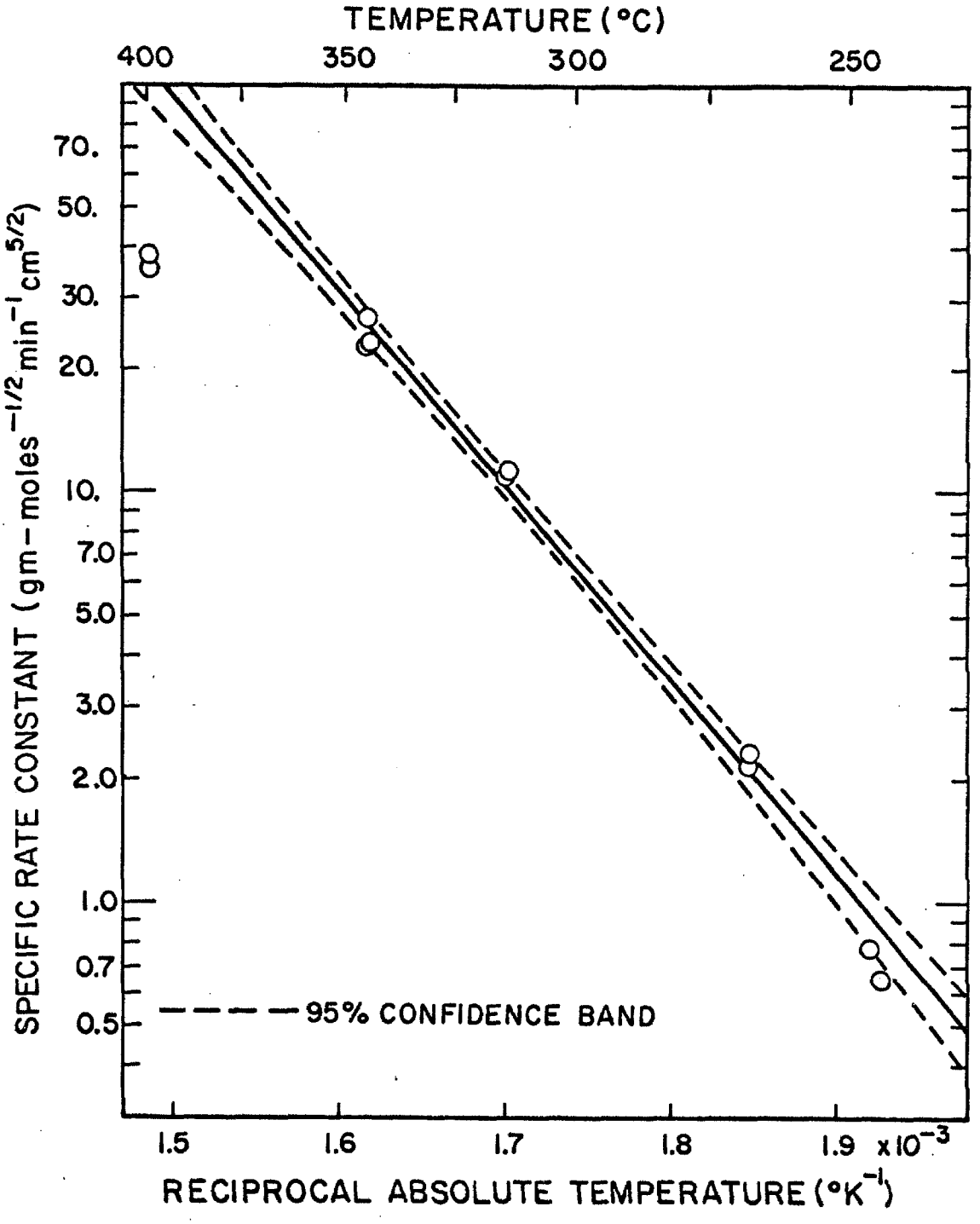

Figure 22. Temperature Dependence of Rate Constant for Production of CO_2 with Ethylene-Oxygen Feed on Crystal #5, (110), Strained 0.8%, Ethylene Order - 1, Oxygen Order - 1/2

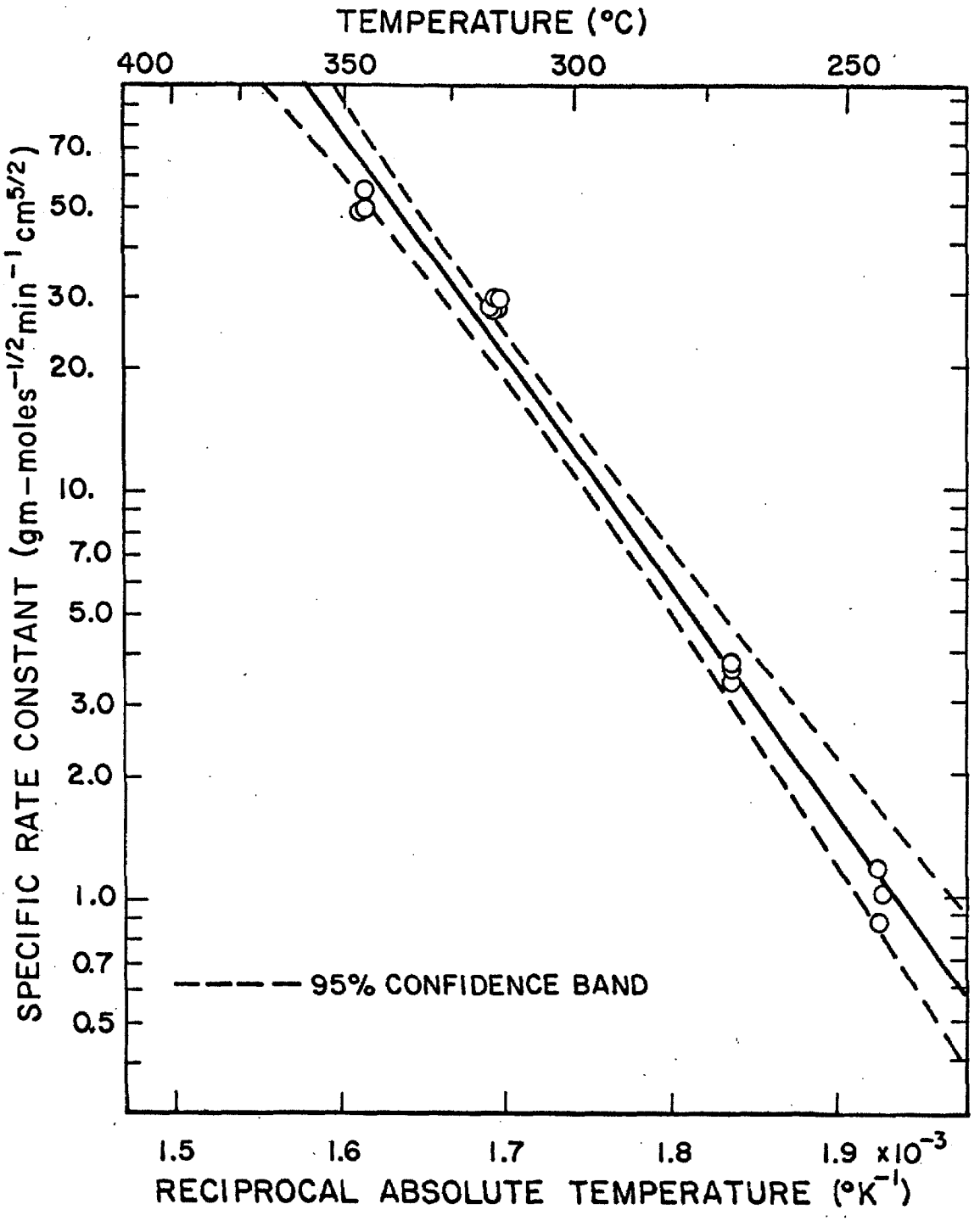

Figure 23. Temperature Dependence of Rate Constant for Production of CO_2 with Ethylene-Oxygen Feed on Crystal #6, (110), Non-strained, Ethylene Order - 1, Oxygen Order - 1/2

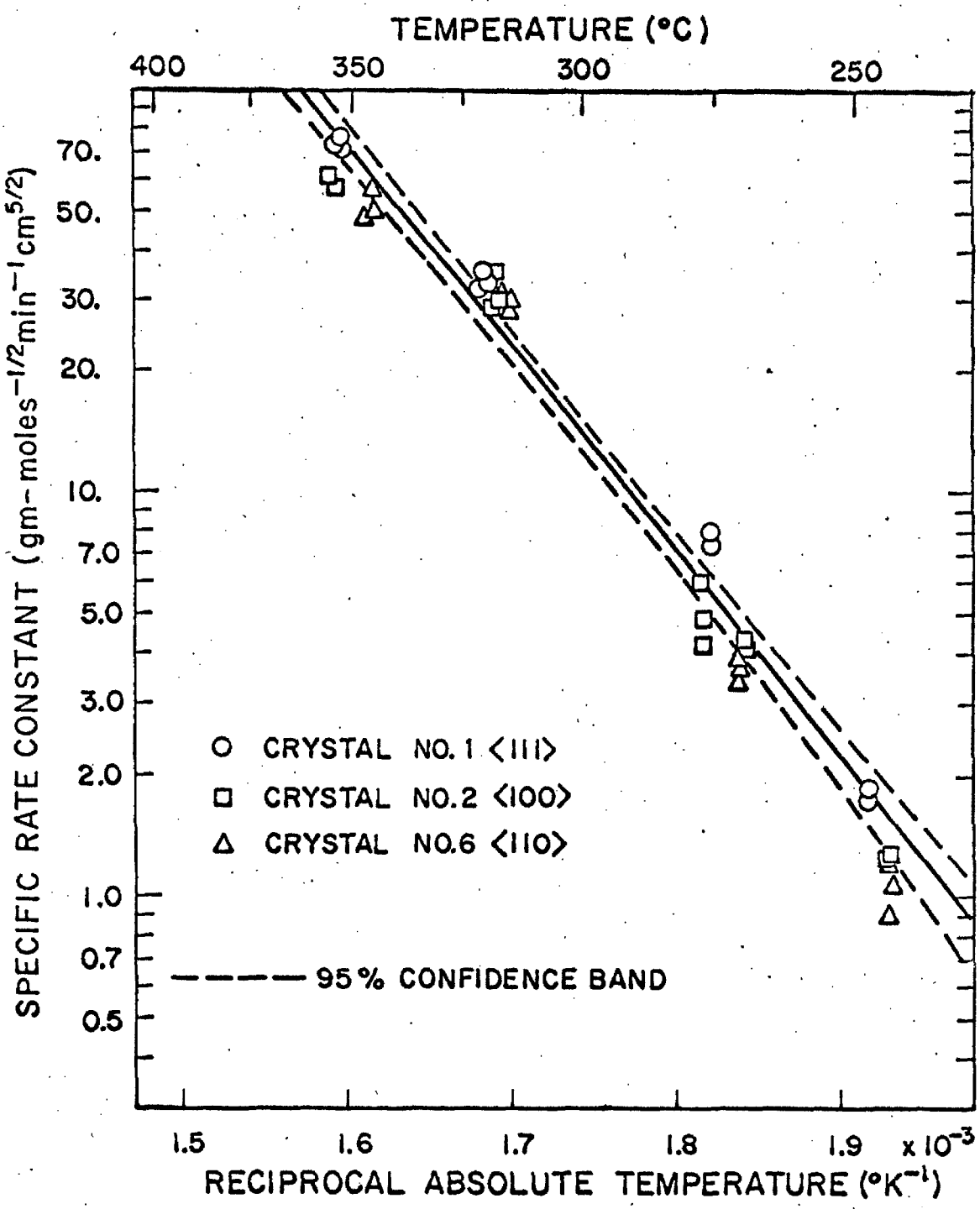

Figure 24. Temperature Dependence of Rate Constant for Production of CO_2, Combined Fit, Crystals #1, #2, and #6, Non-strained, Ethylene Order - 1, Oxygen Order - 1/2

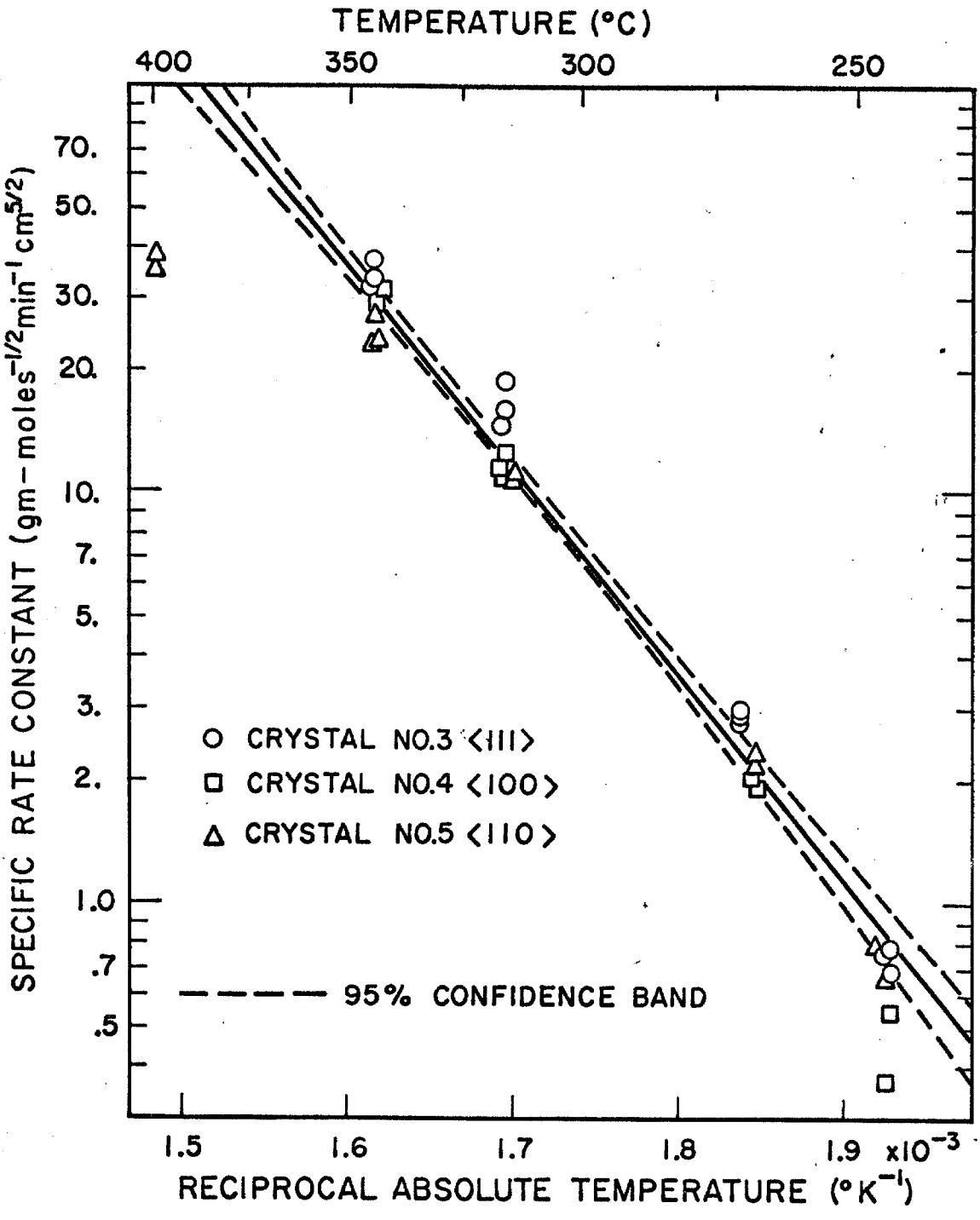

Figure 25. Temperature Dependence of Rate Constant for Production of CO_2, Combined Fit, Crystals #3, #4, and #5. Strained 0.8%, Ethylene Order - 1, Oxygen Order - 1/2

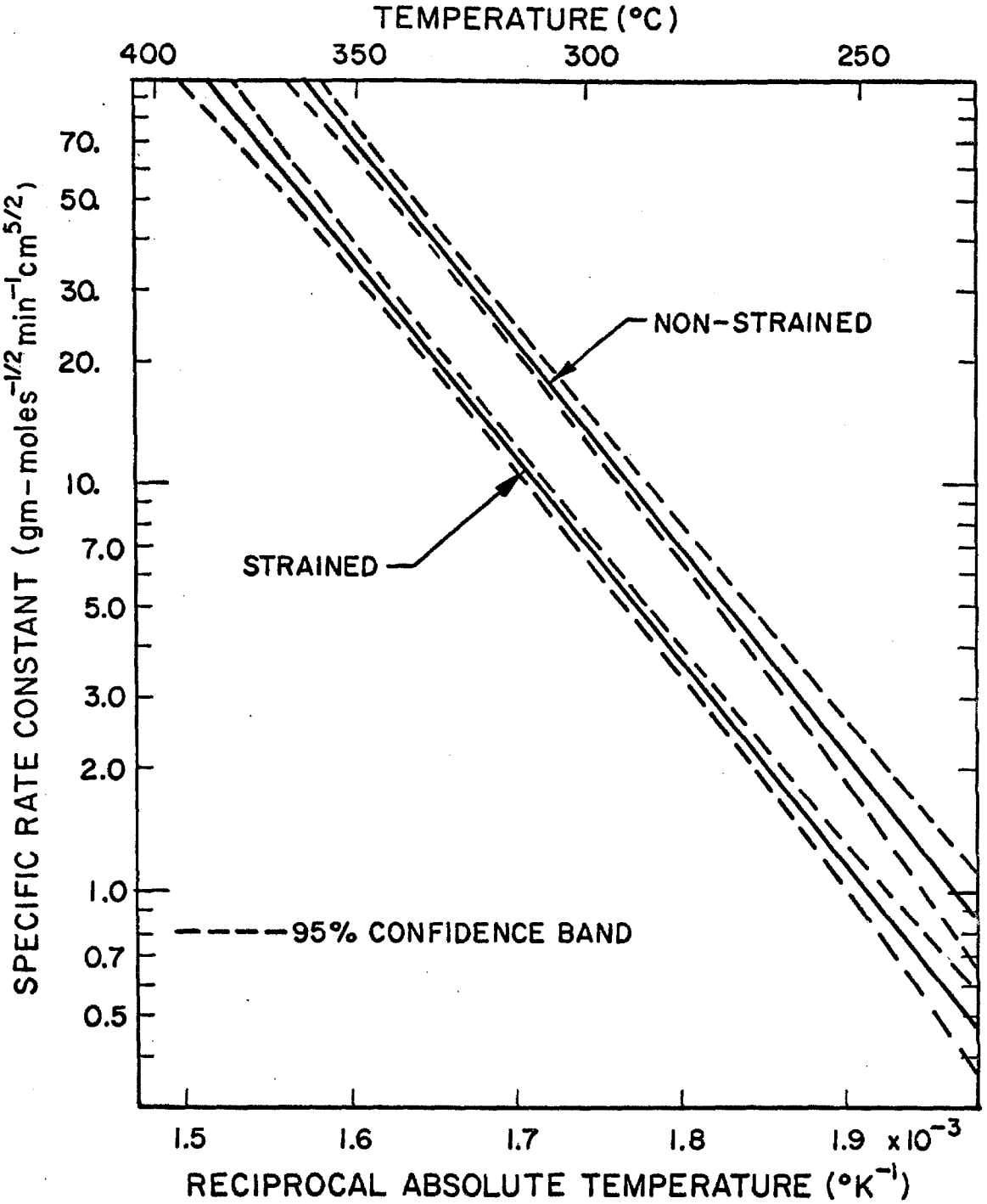

Figure 26. Comparison of Combined Fits for Strained and Non-strained Crystals

APPENDIX A. DEVELOPMENT OF GAS CHROMATOGRAPH

Abstract

A gas chromatograph of high sensitivity was developed for use in a study of the kinetics of the partial oxidation of ethylene on a silver catalyst. The unit consisted of three columns and three detectors. A hydrogen-flame detector of high sensitivity was used for the detection of the oxygenated products of the partial oxidation reaction and a minimum detection limit of 5 ppm for ethylene oxide and acetaldehyde was obtained with a sample size of 1 cc. The minimum detection limit for carbon dioxide was 60 ppm, and the detection limit for carbon monoxide was 200 ppm.

Introduction

Several of the recent studies of the kinetics of the partial oxidation of ethylene on silver catalysts used gas chromatography as the method of analysis of the product gas stream (A-2, A-3, A-10). These applications of gas chromatography had three major disadvantages for the proposed study of the partial oxidation of ethylene on single crystals of silver. They were:

1. Only the main products of the reaction, carbon dioxide and ethylene oxide, were determined in addition to ethylene.
2. Relatively large samples (10 cc.) were required.
3. Sensitivity was only moderate with detection limits of 0.2% by volume.

Estimates of the expected conversion for a flow reactor using a single crystal of silver as a catalyst were calculated from rate data taken from the literature (A-3, A-8). These ranged from 200 ppm to 0.5% of ethylene oxide and 400 ppm to 1.0% of carbon dioxide. Therefore it was necessary to develop a more sensitive gas chromatograph, preferably one using a smaller amount of sample and separating and detecting other possible reaction products such as carbon monoxide, methyl alcohol, ethyl alcohol, and acetaldehyde.

Column Development

Wang (A-12) showed that thermal-conductivity cells in chromatography had minimum detection limits of 50 ppm for compounds such as oxygen, nitrogen, carbon monoxide, and carbon dioxide in a 1 cc. sample. Other authors (A-1) reported the hydrogen-flame-ionization detector could detect quantities of hydrocarbons as low as 0.1 ppm of ethane in a 1 cc. sample. The major problem, then, in developing a gas chromatograph which would meet the requirements for use in the studies of the kinetics of partial oxidation of ethylene on a single crystal of silver was developing columns which gave the desired separation.

The reactants and products of the partial oxidation of ethylene may be divided into the following three categories:

1. Light hydrocarbons and carbon dioxide.
2. Oxygenated hydrocarbon compounds.
3. Light gases - oxygen, nitrogen, methane, and carbon monoxide.

Different types of column packings are required to separate the members of these three groups. A multiple-column arrangement was necessary to obtain the desired results. The group of light gases presented no particular problem since these are easily separated on columns of either Type 5A or Type 13X Linde Molecular Sieve.

Several column packings were qualitatively evaluated for the separation of the group of light gases, ethylene, and carbon dioxide. These were activated charcoal, silica gel, benzyl nitrate saturated with silver nitrate, ethylene glycol saturated with silver nitrate, DC 200-500 silicone oil, and the dimethyl sulfolane, didecyl phthalate-di-n-butyl maleate combination used by Wang (A-12). The solid absorption packings did not give reproducible results for samples with low concentrations. The partition liquids gave various degrees of separation. The column combination developed by Wang gave very good separations with sharp peaks and good reproducibility at low concentrations; so it was used for the separation of the group of light gases, ethylene, and carbon dioxide. This column was also used to check the purity of the ethylene used in the reactor studies.

Tests with various columns showed it was relatively easy to separate ethylene oxide from ethylene when the ethylene oxide concentration was in the range of 1%, but tailing of the ethylene oxide peak became a problem at lower concentrations. The use of an inert support such as Fluoropak 80 or Teflon 6 minimized the tailing of the oxygenated hydrocarbon peaks. Columns of various lengths with packings of DC 200-500 silicone oil, polyethylene glycol 400, Carbowax 20,000, DC 703 silicone oil, XF1150 silicone oil, didecyl

phthalate, and UCON 50 HB 2000 were tried. A compromise was necessary in the selection of a column packing for the separation of ethylene oxide, acetaldehyde, methyl alcohol, and ethyl alcohol because columns which gave good separation of ethylene oxide and acetaldehyde had very long retention times for the alcohols. The long retention times caused spreading of the alcohol peaks. Columns which gave sharp peaks and good separations for the alcohols did not separate the ethylene oxide and acetaldehyde peaks. A 25-foot column packed with 40-60 mesh Teflon 6 coated with 13% of UCON 50 HB 2000 prepared in the manner described by Kirkland (A-7) gave a reasonable compromise for this separation. The performance of this column was much better at 70°C than near room temperature. Several configurations of series, parallel, and switched columns were tried, and the series-parallel arrangement shown in Figure A-1 gave good performance combined with ease of operation.

Apparatus

The gas chromatograph was constructed around a Loenco Model 70 gas chromatograph unit which was purchased from Loe Engineering Co. The original unit was equipped with a single thermistor thermal conductivity detector and a dual hydrogen-flame-ionization detector. A Cary Model 31 electrometer was used with the hydrogen flame detector. The basic unit was modified by the addition of a fan in the detector oven to improve the temperature control and uniformity and the replacement of the thermistor detector with a thermal conductivity-cell equipped with tungsten filaments. An additional

tungsten filament detector was added, and a second column oven was constructed. The hydrogen-flame detector was placed in the separate column oven. A stream splitter was constructed from stainless steel tubing and Swagelok fittings. A sketch of this splitter is shown in Figure A-3. The replacement of the thermistor detector with the filament detector resulted in a decrease in sensitivity of about one half, but the improvement in the baseline stability helped offset the loss of sensitivity. The additional column oven allowed the operation of the columns at different temperatures. A flow chart showing the arrangement of the columns and detectors is given in Figure A-1. This arrangement was selected from several trial systems with parallel, series, and switched column configurations. The operating conditions for the system are tabulated in Table A-1.

A Wilkins Electrolytic Hydrogen Generator was used as the source of hydrogen for the hydrogen-flame detectors. A column, 1 in. I. D. and 12 in. long, of molecular sieve was used to dry the hydrogen stream from the generator to prevent condensation of water in the line to the flame detector. Helium for the carrier gas and compressed air for the hydrogen-flame detectors were obtained from commercial cylinders. Columns, 1 in. I. D. and 6 in. long, of molecular sieve were placed in the helium and compressed air lines.

The restrictors furnished by Loenco to control the flow of air and hydrogen did not perform satisfactory and were replaced by 1/8 in. Nupro Fine Needle valves. Fischer-Porter rotameters were placed in the hydrogen and air lines to measure the flow rates

to the hydrogen-flame detectors. The addition of the rotameters to the inlet gas streams leading to the flame detectors greatly simplified the problem of matching the gas flows to the two detectors.

Temperature programming of the columns was not necessary for this work so use of the dual-hydrogen-flame detector system was not necessary. However tests of the dual-flame detector with temperature programming showed it was very effective in canceling the baseline shift due to increased column bleed with increased temperature.

Gas samples were introduced into the unit through a Loenco linear gas-sample-valve. A vacuum pump and manometer were connected to the sample inlet system to allow introduction of samples from sample bombs at or below atmospheric pressure. A second gas sample valve was used to introduce samples from the exhaust stream of the reactor. A flow diagram of the sample introduction system is shown in Figure A-2.

The stability of the columns used in the unit was very good. Column I was performing satisfactory after 18 months of continuous use, and column III showed no appreciable change after 6 months of service. The section of column II packed with Type 13X Molecular Sieve served as a trap to protect the more efficient column of Type 5A Sieve from moisture and bleed of partition liquid from column I. Column II without the trap section required reactivation after about six weeks of service, but the same column with the trap section did not require activation after nine months of service.

The output of the thermal-conductivity detectors was recorded on potentiometric recorders with full scale sensitivities of 1 mv. The output of the hydrogen-flame detector was recorded on a potentiometric recorder with a full scale sensitivity of 10 mv. Each recorder was equipped with an integrator.

Retention times for the various compounds are given in Tables A-4. Retention times for twenty-seven compounds on Column III are included as the results of an attempt to identify unknown compounds which were found in the exhaust gas from the reactor experiments.

Calibration

Use of a gas chromatograph as a quantitative analytical instrument requires the knowledge of the sensitivity of the detectors to the various compounds in the sample. In some cases where the results can be normalized, it is only necessary to know the relative response for the compounds, but in cases where normalization is not possible, knowledge of the absolute response of the detector is required. In cases where more than one detector is used it is necessary to either use absolute response factors or to know the ratio of the sensitivities of the detectors if normalization is possible. Wang (A-12) found that the absolute response of a thermistor detector could vary as much as a factor of three with changes in operating conditions, but relative response factors were constant within limits of experimental error over the same range. Thus, it was necessary only to deter-

mine the absolute response of the detector for one component and calculate the absolute response for the others from the relative response factors. Wang used a mixture of 5% nitrogen in helium for the calibration for his work. A mixture of 5% methane in helium was selected as the calibration standard for this work because methane was the only compound eluted from each column which gave a response on each detector.

Messner (A-9) determined relative response factors for a large number of compounds relative to benzene in both thermistor and filament detectors and concluded the relative response factor was independent of type or design of thermal-conductivity detector. Wang (A-12) determined relative response factors for oxygen, methane, carbon monoxide, carbon dioxide, ethylene, and other saturated and unsaturated hydrocarbons of four or less carbon atoms relative to nitrogen in a thermistor type of thermal-conductivity cell. His results agreed reasonably with the Messner's values when converted to the same reference gas.

Mixtures of helium containing about 5% methane as an internal standard and various amounts of oxygen, nitorgen, carbon dioxide, carbon monoxide, ethylene, or ethylene oxide were made in 30 ℓ. stainless steel tanks by evacuating the tanks and measuring the pressure change in the tanks after each addition of each gas. Matheson's C. P. grade methane, carbon monoxide, carbon dioxide, ethylene, Bone Dry grade carbon dioxide, 99.7% minimum purity ethylene oxide, Linde's 99.7% minimum purity nitrogen, 99.5% minimum

purity oxygen, and 99.99% minimum purity helium were used in the calibration mixtures.

The changes of absolute pressure in the tanks were measured on either a manometer filled with silicone oil or mercury. DC 200-50 silicone oil was used in the oil manometer. The height of the fluid in the manometers was measured to ± 0.05 cm. with a cathetometer. Manometers which indicated the absolute pressure in the system were necessary because atmospheric pressure in the lab varied considerably during the time required to mix a sample. The oil-manometer design developed by Hayward (A-6) was used to allow complete outgassing of the manometer fluid. Very erratic behavior of the manometer containing silicone oil was observed when the fluid was not completely outgassed.

The composition of the resulting gas mixture was calculated from the series of total pressure changes during the mixing process by four different methods of handling the equation of state of a multicomponent gas mixture. These were:

1. Ideal gas.
2. Dalton's Law of Additive Pressures and Compressability Factors.
3. Amagat's Law of Additive Volumes and Compressability Factors.
4. Kay's Pseudocritical Constant Method.

The compositions of the mixtures calculated from each of these four methods agreed to three significant figures which was better than the expected experimental accuracy so the value obtained from the ideal

gas calculation was used as the composition of the mixture.

Wang (A-12) defined the absolute response of a detector as:

$$K_i = n_i/A_i \qquad \text{(A-1)}$$

The relative response of a component was defined as:

$$N_i = K_i/K_{std} \qquad \text{(A-2)}$$

Therefore the number of moles of a component that passed through the detector was given by:

$$n_i = K_{std}N_iA_i = N_i\left(\frac{A_i}{A_{std}}\ n_{std}\right) \qquad \text{(A-3)}$$

Wang's results showed the relative response factor N_i was a linear function of A_iK_{std} for hydrogen and various C-4 hydrocarbons and was a constant for the light gases and hydrocarbons up to C-4's.

The experimental results from this work were fit to a second order equation with the multi-variable, least-squares method described by Deming (A-4). The equation had the form:

$$n_i = L_i + N_i\left(\frac{A_i}{A_{std}}\ n_{std}\right) + M_i\left(\frac{A_i}{A_{std}}\ n_{std}\right)^2 \qquad \text{(A-4)}$$

$$n_i = PVy_i/RT \qquad \text{(A-5)}$$

where the peak areas, sample temperature, and sample pressure were considered to have possible experimental errors. This least squares method is discussed in more detail in Appendix D. The

constant term in the equation allows for the possible loss of a component on the column, and the second order term corresponds to the non-linear behavior of the relative response factor. Only the linear coefficient was found to be statistically significantly different from zero at the 95% confidence level for the compounds studied in this work. The values of the relative response factor of a given component for different calibration mixtures were averaged using Deming's least-squares method with the relative response factor and the mole fraction of the component and of methane considered to have possible errors. Experimental uncertainties of the mole fractions were calculated from estimates of the accuracy of the pressure measurements, and the standard deviation of the relative response factors was obtained from the first least-squares fit. These were used to weight the average so the earlier calibration data where the experimental accuracy of the composition of the gas mixture was lower could be combined with data taken later when the accuracy had been increased by the use of the manometers which indicated the absolute pressure of the system and the increased sensitivity of the manometer filled with silicone oil. The values of the relative response factors with their 95% confidence limits are given in Table A-3. Values of relative response factors for acetaldehyde, an unsaturated four carbon hydrocarbon, and a six carbon hydrocarbon which were found in small amounts in the exhaust gas from the reactor experiments were estimated for the hydrogen-flame detector from data given by Sternberg (A-11) and Ettre (A-5). These

estimated values are also given in Table A-2.

Results and Conclusions

The main result of this work in chromatography was the development and calibration of a gas chromatograph unit for use in a study of the kinetics of the partial oxidation of ethylene on silver. The major requirements imposed by the proposed kinetic study on the performance of the unit were satisfied. These requirements were:

1. High sensitivity.
2. Small sample size.
3. Analysis for possible reaction products in addition to the main products and reactants.

The unit has the minimum detectable limits shown in Table A-5 for a gas sample of 1 cc. measured at room conditions. Retention times for various hydrocarbon compounds are given in Table A-4. Relative response factors for the unit are given in Table A-2.

In addition to the main objectives of the study, the independence of the relative response factor on the type and design of thermal conductivity cell proposed by Messner (A-9) and confirmed by Wang (A-12) was further substantiated. The values of the relative response factor determined in this study are compared with the values of Wang and messner in Table A-3. These agree within the experimental error for most of the compounds studied. The linearity of the relative response factors for oxygen, nitrogen, carbon monoxide, carbon dioxide, and ethylene over a wide range of concentrations

which Wang reported for the thermistor, thermal-conductivity detector was also observed for the tungsten-filament, thermal-conductivity detector.

Recommendations

The gas chromatograph described in this report worked very satisfactorily during the kinetic studies of the partial oxidation of ethylene on silver, but certain changes could be made to improve its performance.

(1) The signal to noise ratio of Detectors I and II was sufficiently high to allow the output signal from these detectors to be amplified as much as a factor of 10 and still give a reasonably stable baseline. DC amplifiers have been obtained for this purpose and should be added to the output circuits of these detectors.

(2) Three unknown compounds in the reactor exhaust stream were observed on Detector III in low concentrations (about 1 ppm.). These were tentatively identified as an unsaturated four carbon hydrocarbon and two six carbon hydrocarbons. The addition of another flow splitter and hydrogen-flame detector at the end of Column I could probably detect the low concentrations of these unknown compounds. This additional detector would give retention times on another column which should give a more definite identification of these compounds.

(3) The separation of acetaldehyde and ethylene oxide on Column III was adequate for the concentrations of acetaldehyde

encountered in the experimental phase of this project, but could be inadequate for large concentrations. Further work on a column for this separation could be very beneficial.

NOMENCLATURE

A - Chromatogram peak area, integrator units

K - Absolute detector response, gm. moles/integrator unit

L - Constant in equation A-4, gm. moles

M - Constant in equation A-4, 1/gm. moles

N - Relative response factor, dimensionless

n - Amount of component in sample, gm. mole

P - Sample pressure, cm. of mercury

R - Gas constant, 62,361 cm.^{4}/gm. mole ^oK

T - Temperature of sample, ^oK

V - Volume of sample, cc.

y - Mole fraction

Subscripts

i - refers to component i

std - refers to standard component

REFERENCES

A-1. Amberg, C. H., Echigoya, E. and Kugawic, D., Can. J. Chem., 37, 708 (1959).

A-2. Andreatch, A. J. and Feinland, J., Anal. Chem., 32, 1021 (1960).

A-3. Buntin, R. B., Ph. D. thesis, Purdue Univ., Lafayette, Indiana (1961).

A-4. Deming, W. E., "Statistical Adjustment of Data," John Wiley and Sons, Inc., New York, New York (1938).

A-5. Ettre, L. S., "Gas Chromatography," Chapt. 21, p. 307, Academic Press, Inc., New York, New York (1962).

A-6. Hayward, A. T. J., J. Sci. Instrum., 40, 173 (1963).

A-7. Kirkland, J. J., Anal. Chem., 35, 2003 (1963).

A-8. Kummer, J. T., J. Phys. Chem., 60, 666 (1956).

A-9. Messner, A. E., Rosie, D. M., and Argabright, P. A., Anal. Chem., 31, 230 (1959).

A-10. Nault, L. G., Bolme, D. W., and Johanson, L. N., I & E. C. Process Design and Development, 1, 285 (1962).

A-11. Sternberg, J. C., Gallaway, W. S., and Jones, D. T. L., "Gas Chromatography," Chapt. 18, p. 231, Academic Press, Inc., New York, New York (1962).

A-12. Wang, Y. L., Ph. D. thesis, Calif. Inst. of Tech., Pasadena, Calif. (1963).

Table A-1

DESCRIPTION OF COLUMNS AND CHROMATOGRAPH OPERATING CONDITIONS

Carrier gas - Helium

Sample size - 1 cc.

Total carrier gas flow rate - 60 cc./min., 27°C, 1 atm.

Carrier splitting ratio - 5:1 parts by volume, Columns I &II:Column III

Column I - 8 ft. of 1/4 in. copper tubing packed with 30% di-n-butyl maleate on 30-60 mesh Chromosorb P followed by 35 ft. of 1/4 in. copper tubing packed with 3.5% didecyl phthalate, 33% dimethyl sulfolane on 30-60 mesh Chromosorb P; Column temperature - 30°C.

Column II - 4 ft. of 1/4 in. copper tubing packed with 30-60 mesh Linde Molecular Sieve Type 13X followed by 5 ft. of 1/4 in. copper tubing packed with 30-60 mesh Type 5A Molecular Sieve; Column temperature - 30°C.

Column III - 25 ft. of 1/8 in. stainless steel tubing packed with 13% UCON 50 HP 2000 on 40-60 mesh Teflon 6 Molding Powder; Column temperature - 65°C.

Detector I - Tungsten-filament, thermal-conductivity cell, 120 ma. bridge current, temperature - 55°C.

Detector II - Tungsten-filament, thermal-conductivity cell, 120 ma. bridge current, temperature - 55°C.

Detector III - Hydrogen-flame-ionization detector
Hydrogen flow rate - 12 cc./min.; 27°C, 1 atm.
Air flow rate - 250 cc./min; 27°C, 1 atm.
Collection voltage - 300 volts
Electrometer input resistor - 10^{10} ohms
Temperature - 65°C

Table A-2

RELATIVE RESPONSE FACTORS

Component	Sample Quantity (gm. -moles $\times 10^8$)	No. of Samples	Relative Response Factor	95% Confidence Limit
Nitrogen	2.07 - 577.5	59	0.8521	±0.0407
Oxygen	1.64 - 166.6	45	0.9271	0.0622
Carbon monoxide	1.08 - 32.1	38	0.8294	0.0444
Carbon dioxide	2.59 - 56.9	70	0.7732	0.0135
Ethylene	9.90 - 1131.	70	0.7196	0.0129
Ethylene oxide	0.83 - 43.0	61	1.1916	0.0390
Acetaldehyde			1.000[a]	
Unsaturated C_4 hydrocarbon			0.241[a, b]	
C_6 hydrocarbon			0.145[a, b]	

[a]Estimated from data given by Sternberg, J. C., Gallaway, W. S. and Jones, O. T. L., "Gas Chromatography," Chapt. 18, p. 231, Academic Press Inc., New York, New York (1962).

[b]Estimated from data given by Ettre, L. S., "Gas Chromatography," Chapt. 21, p. 231, Academic Press Inc., New York, New York (1962).

Table A-3

COMPARISON OF RELATIVE RESPONSE FACTORS

Component	This Work	Wang[a]	Messner[b]
Nitrogen	0.852	0.899	0.855
Oxygen	0.927	0.963	0.897
Carbon monoxide	0.829	0.914	0.855
Carbon dioxide	0.773	0.763	0.752
Ethylene	0.720	0.724	0.752

[a]Wang, Y. L., Ph. D. thesis, Calif. Inst. Tech., Pasadena, Calif. (1963).

[b]Messner, A. E., Rosie, D. M., and Argabright, F. A., Anal. Chem., 31, 230 (1959).

Table A-4

TABLE OF RETENTION TIMES
(Column Operating Conditions Given in Table A-1)

Column I

Oxygen, Nitrogen, Methane, Hydrogen Carbon Monoxide[a]	7.96 minutes
Ethane, ethylene[a]	9.29
Carbon dioxide	10.65
Acetylene	18.0
Methyl acetylene	38.0
Butadiene	45.0

Column II

Oxygen	9.6
Nitrogen	11.4
Methane	12.9
Carbon monoxide	23.5

Column III

Hydrocarbons

Methane	3.90
Ethane, ethylene[a]	4.24
Acetylene	5.19
Propane	4.83
Methyl acetylene	11.0
Isobutane	5.64
Normal butane	6.19
1-Butene	6.68
Trans-2-butene	7.30
Cis-2-butene	7.97
Isobutylene	6.48
Butadiene	8.34

[a]Components eluted as one peak.

Table A-4 (Continued)

Normal pentane	9.6
2, 2 dimethyl butane	11.3
Normal hexane	16.1
Hexene	17.7
3-hexyne	38.7
Oxygenated hydrocarbons	
Methyl alcohol	20.1
Ethyl alcohol	34.1
Acetic acid	43.1
Ethylene oxide	13.2
Acetone	25.3
Methyl-ethyl ketone	52.0
Diethyl ketone	81.4
Acetaldehyde	11.9
Ethyl ether	13.3

Table A-5

ESTIMATED MINIMUM DETECTION LIMITS
(1 cc. Sample)

Detector I

Ethylene - 60 ppm

Carbon dioxide - 60 ppm

Detector II

Oxygen - 80 ppm

Nitrogen - 80 ppm

Methane - 120 ppm

Carbon monoxide - 200 ppm

Detector III

C-4 hydrocarbons - 0.3 ppm

C-6 hydrocarbons - 0.5 ppm

Acetaldehyde - 5 ppm

Ethylene oxide - 5 ppm

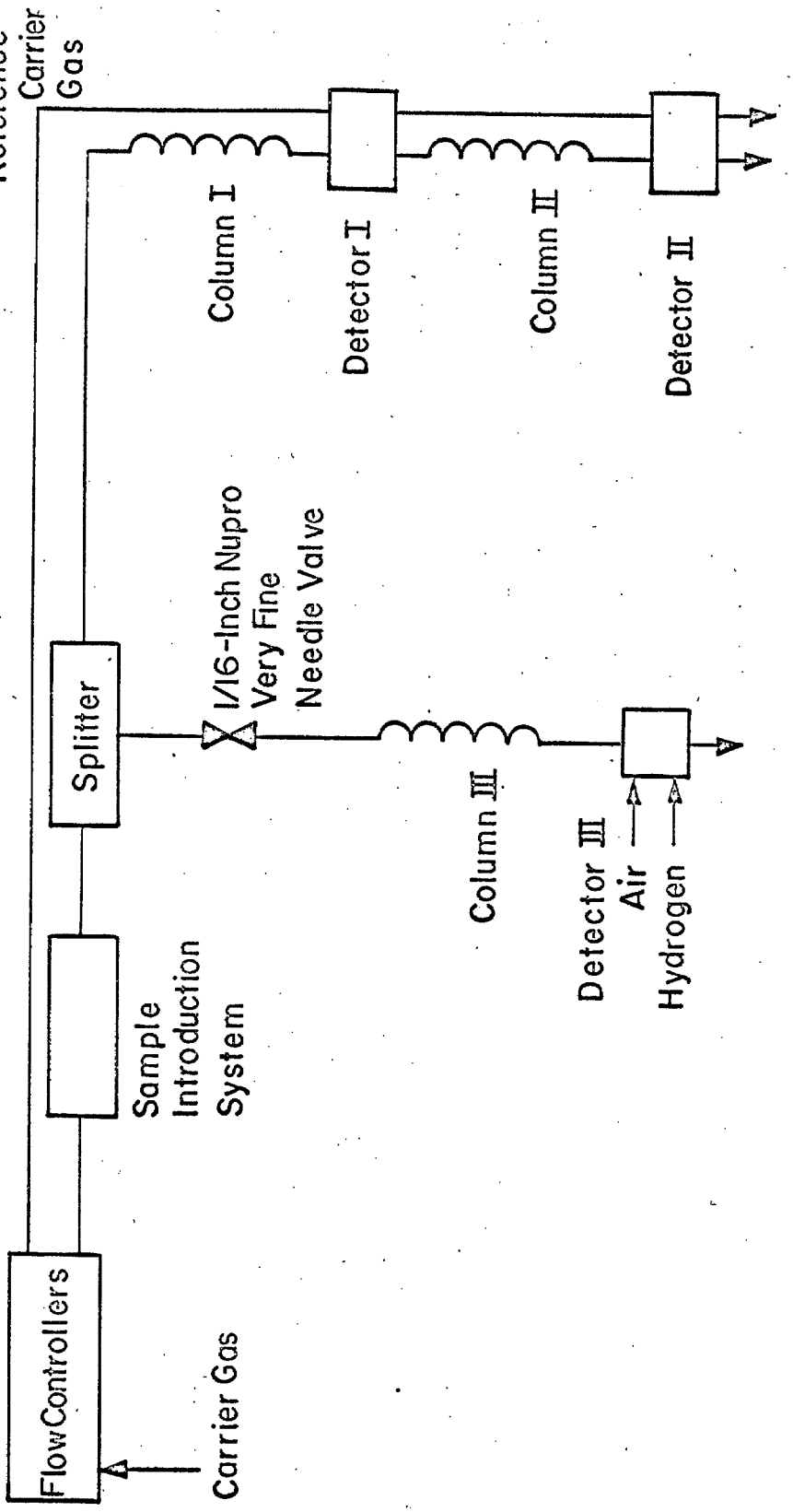

Figure A-1. Flow Chart of Chromatograph

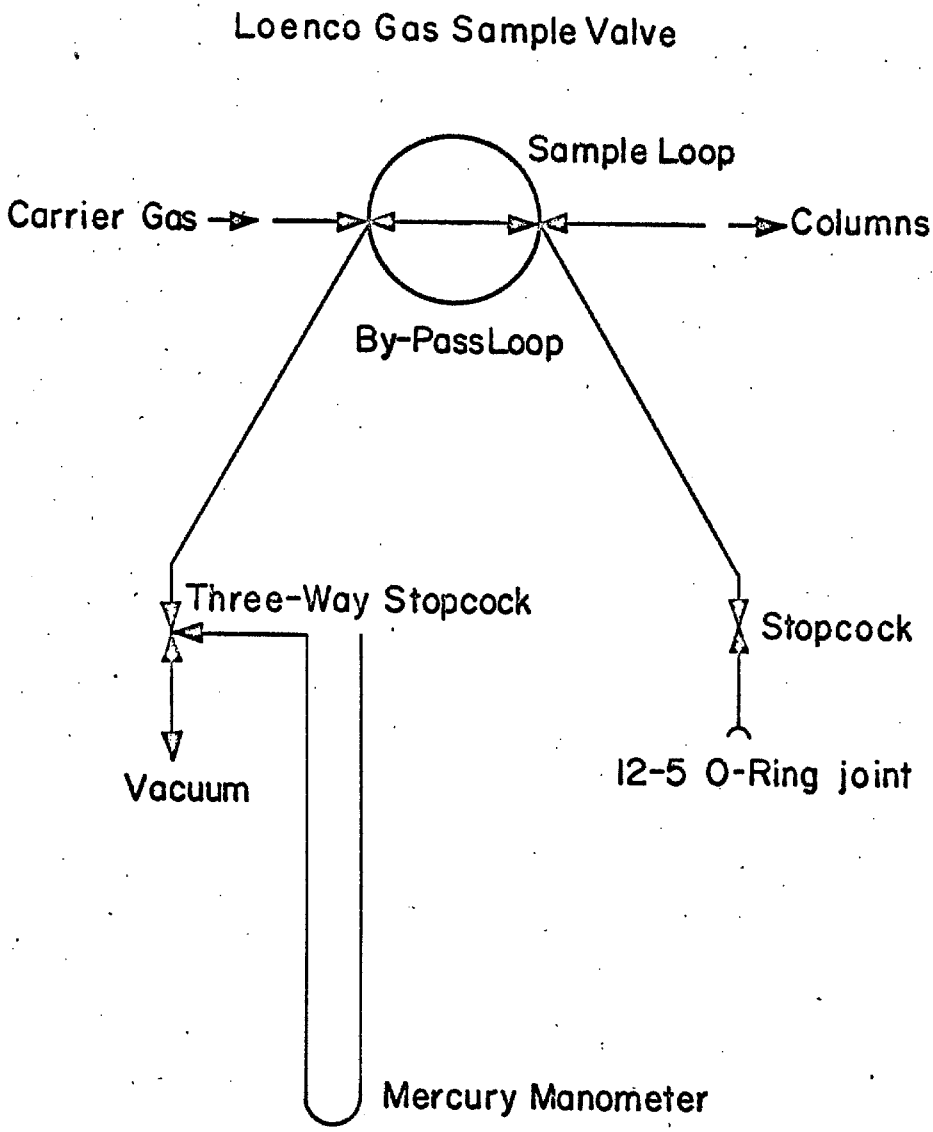

Figure A-2. Flow Chart of Sample Introduction System

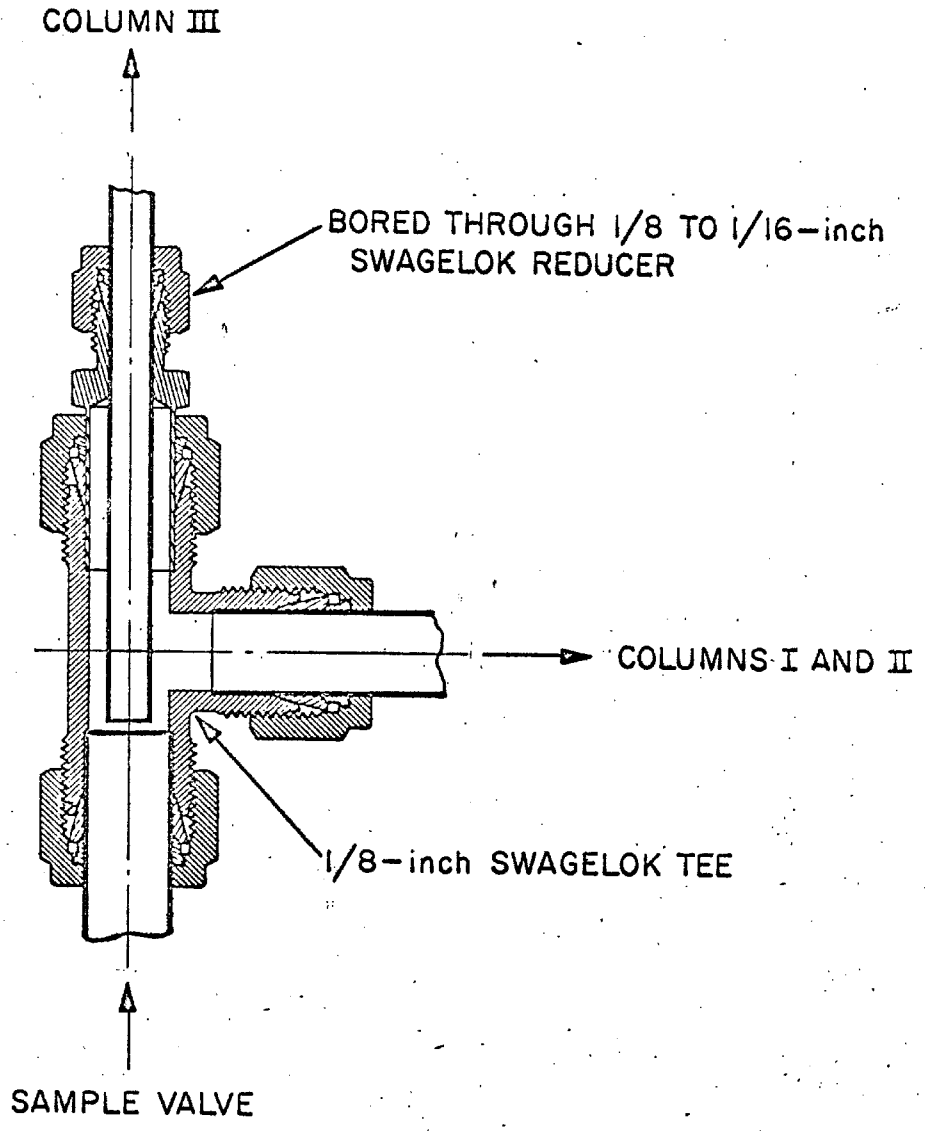

Figure A-3. Sketch of Flow Splitter

APPENDIX B. EFFECTS OF DIFFUSION IN A RADIAL FLOW REACTOR

One of the major objectives in the design of the reactor for use in the kinetic studies of the partial oxidation of ethylene on a single silver crystal was to provide a flow geometry with sufficient symmetry to allow a detailed mathematical study of the effects of the flow pattern and diffusion on the results of the kinetic experiments. The reactor design selected had a parallel disc geometry with the reactant gas feed at the center of one disc and flow in the radial direction to the edges of the discs. Single silver crystals for use in the reactor were obtained in the form of cylinders with a diameter of 1/2 in. and a length of 1/2 in. They had been grown with a particular crystal plane parallel to the cylindrical face of the crystal. This surface was polished and used as the catalyst. The crystal was mounted in the reactor with its axis coinciding with the axis of the parallel disc geometry and the other disc was constructed of quartz in the original reactor design and of gold in the second reactor design in attempts to obtain a non-catalytic surface. In the original design the total disc diameter was twice the diameter of the silver crystal and in the second design it was only slightly larger than the crystal diameter. The effects of flow and diffusion in this reactor geometry are discussed in this appendix. As a result of these calculations a change in reactor size in addition to a change in construction material was made in the design of the second reactor.

Velocity Profile

Bird, Stewart, and Lightfoot (B-1) have discussed the following differential equation which describes the steady, laminar, incompressible, radial flow of a Newtonian fluid between parallel discs neglecting entrance effects:

$$\frac{1}{2}\rho\phi^2\left(\frac{1}{r_2^2}-\frac{1}{r_1^2}\right)=P_1-P_2+\mu\ln\left(\frac{r_2}{r_1}\right)\frac{d^2\phi}{dz^2} \qquad \text{(B-1)}$$

$$\phi = rv_r \qquad \text{(B-2)}$$

Boundary Conditions

$$\phi = 0, \quad z = \pm z_o\ ; \quad \frac{d\phi}{dz} = 0, \quad z = 0 \qquad r_1 \leq r \leq r_2$$

They presented the solution of this differential equation for the "creeping flow" case where the non-linear term representing the inertia of the fluid is neglected:

$$\phi_{cf} = \frac{z_o^2(P_1 - P_2)}{2\mu \ln r_2/r_1}\left[1-\left(\frac{z}{z_o}\right)^2\right] \qquad \text{(B-3)}$$

Equation B-1 was solved numerically by an iterative procedure based on the method described by Fox (B-3) for solution of two-point boundary value problems. The results for a representative case are shown in Figure B-1. The per cent error introduced by the use of the creeping flow solution and the error introduced if the exact solution is approximated by a parabolic profile with the same average value are shown in Figure B-2. The results show that in the range of flow rates used in the microreactor about 0.6% error is introduced by the use of the

creeping-flow approximation for radial flow between parallel discs, and only about 0.1% error is introduced by the use of a parabolic approximation with the same average value as the exact solution. Since the average velocity could be calculated directly from measurements of the volumetric flow rate, the parabolic approximation was the most convenient for use in estimation of the flow pattern in the reactor as well as a very good approximation to the exact solution. This approximation was used in the calculation of the effects of diffusion of the reactants and products to and from the catalyst surface. An estimate of the distance required to establish a velocity profile that was fully developed was obtained from Schlichting (B-5) for the entrance region for linear flow between flat plates. This value of 7×10^{-7} in. shows the entrance effects to be very small for parallel plates under these conditions so it seems reasonable to assume the entrance effects may be neglected in the radial-flow, parallel disc geometry.

Diffusion

The following assumptions were made about the conditions in the parallel-disc microreactor for the consideration of the effects of diffusion on the observed kinetic results:

1. No entrance effects.
2. Laminar flow.
3. Uniform temperature.
4. Steady state.
5. Symmetry about the axis of the reactor.

6. Low conversion and therefore uniform viscosity, specific volume, and diffusion coefficients.

7. No effect of diffusion on the velocity profile.

The partial differential equation describing a material balance on component i is given by:

$$-\nabla \cdot \vec{m}_i + R_i = \frac{\partial \sigma_i}{\partial t} \tag{B-4}$$

which reduces to the following equation for steady state:

$$-\nabla \cdot \vec{m}_i + R_i = 0 \tag{B-5}$$

The mass flux of component i expressed in terms of the Fick diffusion coefficient is:

$$\vec{m}_i = \sigma_i \vec{v} - D_{F,i} \nabla \sigma_i \tag{B-6}$$

Equations B-5 and B-6 can be combined with the assumptions to give:

$$-\frac{D_{F,i}}{r} \frac{\partial}{\partial r}\left(r \frac{\partial \sigma_i}{\partial r}\right) - D_{F,i} \frac{\partial^2 \sigma_i}{\partial z^2} + \frac{1}{r} \frac{\partial}{\partial r}(\sigma_i v_r) = -R_i \tag{B-7}$$

with the boundary conditions:

$$\sigma_i = \sigma_{i,o} \quad \text{at} \quad r = r_1 \quad , \quad -z_o \leq z \leq z_o$$

$$\frac{\partial \sigma_i}{\partial z} = 0 \quad \text{at} \quad z = -z_o , \quad r > 0$$

$$\frac{\partial \sigma_i}{\partial z} = \frac{R_s}{D_{F,i}} \quad \text{at} \quad z = z_o , \quad r_c > r > 0$$

When diffusion in the direction of flow is neglected, the homogeneous reaction is zero, and the velocity profile is assumed to be flat the

following definitions of dimensionless variables may be made, which reduce equation B-7 to the following differential equation and accompanying boundary conditions:

$$\eta = \frac{2\pi D_{F,i} r^2}{z_o Q} \tag{B-8}$$

$$\psi = \frac{\pi r_c^2 D_{F,i}}{z_o Q} \left(\frac{\sigma_i - \sigma_{i,o}}{\sigma_{i,\infty} - \sigma_{i,o}} \right) \tag{B-9}$$

$$\omega = \frac{z}{z_o} \tag{B-10}$$

$$\frac{\partial \psi}{\partial \eta} = \frac{\partial^2 \psi}{\partial \omega^2} \tag{B-11}$$

$$\psi = 0 \quad \text{at} \quad \eta = 0 \ , \quad -1 \leq \omega \leq 1$$

$$\frac{\partial \psi}{\partial \omega} = 0 \quad \text{at} \quad \omega = -1 \ , \quad \eta \geq 0$$

$$\frac{\partial \psi}{\partial \omega} = 1 \quad \text{at} \quad \omega = 1, 0 \leq \eta \leq \frac{2\pi D_{F,i} r_o^2}{z_o Q}$$

Equation B-11 with its boundary conditions was solved with the use of Laplace transforms to give:

$$\psi - \frac{\eta}{2} = \left(\frac{1+\omega}{2} \right)^2 - \frac{1}{3} - \frac{4}{\pi^2} \sum_{n=1}^{\infty} \frac{(-1)^n}{n^2} \cos \left[n\pi \left(\frac{1+\omega}{2} \right) \right] \exp \left[\frac{n^2 \pi^2 \eta}{4} \right] \tag{B-12}$$

Figure B-3 shows the dimensionless concentration profiles obtained from this solution.

When the parabolic velocity profile was substituted into equation B-7 and the same dimensionless variables were defined, the

following partial differential equation was obtained with the same boundary conditions as equation B-11:

$$\frac{3}{2}(1 - \omega^2)\frac{\partial \psi}{\partial \eta} = \frac{\partial^2 \psi}{\partial \omega^2} \qquad \text{(B-13)}$$

This equation was solved numerically on the IBM 7094 Digital Computer using a method described by Longwell (B-4). The dimensionless concentration profiles obtained from the numerical solution are shown in Figures B-4. Figures B-3 and B-4 show the concentration profile is fully developed for η greater than 8 and the variation in ψ across the slit is from 4.67 to 5.67 for the flat velocity profile and from 4.76 to 5.76 for the parabolic velocity profile. The value of η at the outer radius of the silver crystal was in the range of 2400 so the variation in ψ was a change in the fifth place which indicated diffusion across the slit was sufficiently rapid to not affect the kinetic results obtained from the reactor.

In the cases considered above, it was assumed that diffusion in the radial direction, the direction of flow, could be neglected and diffusion across the slit was considered. The other extreme case for flow between parallel discs will be considered now: If it is assumed that diffusion in the axial direction is very rapid so that gradients in the axial direction may be neglected and the velocity profile is flat, then equation B-7 reduces to:

$$-\frac{D_{F,i}}{r}\frac{d\sigma_i}{dr}\left(r\frac{d\sigma_i}{dr}\right) + \frac{Q}{4\pi z_o r}\frac{dr_i}{dr} = -R_i \qquad \text{(B-14)}$$

where the volumetric rate term now includes any catalytic reactions

on the surfaces of the discs expressed in volumetric units. In the exhaust region where $R_i = 0$ equation B-5 gives:

$$(r\dot{m}_{i,r}) = c \tag{B-15}$$

Therefore the combination of equation B-15 and B-6 gives:

$$\sigma_i v - D_{F,i} \frac{d\sigma_i}{dr} = \frac{c}{r} \tag{B-16}$$

Equation B-16 can be integrated by the use of an integrating factor to give:

$$\sigma_i = \frac{c_1 4\pi z_o D_F}{Q} + c_2 r^{\left(\frac{Q}{4\pi z_o D_{F,i}}\right)} \tag{B-17}$$

Since the concentration must be finite as the radius goes to infinity, $c_2 = 0$; therefore the concentration must be uniform from the region where the reaction rate drops to zero to the exhaust of the reactor. A material balance across the interface between the reacting region and the non-reaction region shows that the derivative of the concentration is zero at this point in the reacting region if the diffusion coefficient is non-zero. Studies of the partial oxidation of ethylene on silver reported in the literature have indicated that in the range of conditions of interest the reactions other than the ones occurring on the silver surface were negligible. So equation B-14 was solved for the case where the reaction rate was uniform in the catalytic region and was zero in the remainder of the reactor. The reaction rate was considered uniform because planned experimental work would use excess amounts of reactants and the expected conversion

was low. Equation B-14 can be rearranged into the form:

$$\frac{d^2\sigma_i}{dr^2} - \frac{A}{r}\frac{d\sigma_i}{dr} = -\frac{R_i}{D_{F,i}} \qquad \text{(B-18)}$$

where

$$A = \frac{Q}{4\pi z_o D_F} - 1 = \beta - 1$$

This equation can be integrated by the use of an integrating factor to give:

$$c \rightarrow y^2 \quad \text{as} \quad A \rightarrow \infty \qquad \text{(B-19)}$$

$$c = y^2(1 - 2 \ln y) \qquad A = 1 \qquad \text{(B-20)}$$

$$c = \frac{2}{1 - A} y^{1+A} - \frac{1 + A}{1 - A} y^2 \qquad A \neq 1 \qquad \text{(B-21)}$$

where:

$$c = \frac{\sigma - \sigma_{i,o}}{\sigma_{i,\infty} - \sigma_{i,o}} \quad , \quad y = \frac{r}{r_c}$$

The average change in the concentration in the reactor can be based on either an area average or a radial average which can be determined from the radial concentration profiles. These average values are given by:

$$c_{avg,\ radial} = \frac{A + 4}{3(A + 2)} \qquad \text{(B-22)}$$

$$c_{avg,\ area} = \frac{A + 5}{2(A + 3)} \qquad \text{(B-23)}$$

Radial concentration profiles calculated from equations B-19, B-20, B-21 are shown in Figure B-5. Average values of the concentration

change as a function of η are shown in Figure B-6. The expected operating conditions of the reactor gave a value of β of about 0.5 which shows diffusion in the radial direction could be important in the interpretation of the kinetic results obtained from this reactor.

Preliminary experimental runs in the microreactor indicated that there were unexpected side reactions of the ethylene oxide in the reactor so the combined effects of the side reactions removing component i and diffusion in the direction of flow were investigated. A first-order reaction was assumed for the side reaction, and the catalytic reaction rate was assumed to be uniform over the surface of the crystal. The analytic solution equation B-18 for this case consisted of some rather unusual Bessel's functions which would be difficult to evaluate; so solutions were obtained numerically on the IBM 7094 Digital Computer using the method of solving two-point, boundary-value, differential equations described by Fox (B-3). Results of the numerical solution with a catalytic rate of production estimated from the results for the partial oxidation of ethylene given by Buntin (B-2) and a first-order rate constant estimated from the preliminary experimental runs for the rate of disappearance of ethylene oxide are given in Figure B-7.

These results showed the concentration profile over the catalyst was greatly affected by the side reaction in the remainder of the reactor when the effects of diffusion were taken into consideration. Continuation of the solution out to the exhaust of the reactor and from the outer radius of the crystal to the end of the sample tubes showed with this rate of disappearance of ethylene oxide the amount which would appear

in a sample or in the exhaust stream would be only 1 to 3% of the amount which would be obtained with no side reactions. These results indicated the reactor design would have to be changed if ethylene oxide was to be detected in the reactor. Two changes were made to try to reduce the undesired reactions of the ethylene oxide. The first was a change of material for use in the construction of the new reactor. A literature search showed gold was probably less active as an oxidation catalyst than most metals so gold was selected for the material for use in the head of the reactor and the feed and exhaust tubes. The second change was to reduce the total area in the reactor so there would be a larger fraction of the reactor area used as the catalyst for the desired reactions and a smaller fraction available for undesired, side reactions. Calculations of the concentration profile with the new design showed that if gold had the same catalytic activity as quartz for the reactions causing the disappearance of ethylene oxide then the concentration at the outer radius of the catalyst would be reduced only 2% and the value obtained at the exhaust of the reactor would be 92% of the value at the edge of the catalyst. This concentration profile is shown in Figure B-8. Later experiments showed the rate of ethylene oxide oxidation on gold was greater than on quartz and ethylene oxide could only be detected in very small amounts in the exhaust of the second reactor.

Numerical solution of equation B-7 for the combined case with diffusion in the axial direction and in the radial direction was attempted but no results were achieved due to instabilities in the methods used.

Discussion of Results and Conclusions

The results of the solution of the non-linear, differential equation which describes the steady, laminar, incompressible, radial flow of a Newtonian fluid between parallel discs neglecting entrance effects showed a parabolic velocity profile gave a very good approximation to the exact solution when the average velocity of the parabolic profile was the same as the average of the exact profile. An estimate of the distance required to establish a fully developed flow profile for the expected reactor conditions showed entrance effects were negligible.

Consideration of diffusion in the axial direction to and from the catalyst surface showed that for the geometry of the reactor and the expected range of experimental conditions, diffusion in the axial direction was sufficiently rapid so that there should have been no effect on the rate of the surface reactions.

Diffusion in the direction of flow was found to have a significant effect on the radial concentration profile for the expected range of operating conditions. Side reactions of the products of the reaction downstream from the catalyst were neglected in this calculation, and correction curves for converting the total concentration change to the average concentration over the surface of the catalyst were calculated.

The effects of diffusion in the direction of flow combined with reactions of the desired products on surfaces downstream from the catalyst were considered in the reactor geometry used in the original design when preliminary experimental reactor runs indicated these

reactions were large enough to seriously affect the amount of product in the reactor exhaust stream. These calculations showed the side reactions were large enough to almost completely remove the desired product of the reaction. Calculations based on the same operating conditions and rates of reaction showed the new reactor design should have greatly reduced this effect.

Results were not obtained for attempted numerical solutions of the case of diffusion in the axial and radial directions because of instabilities in the methods used to obtain the solutions. The results of the studies of diffusion in the axial and radial directions separately indicated that the reactor would be operating in a range where axial diffusion effects were very small and radial diffusion effects were large. Therefore radial concentration profiles obtained neglecting axial diffusion were considered adequate for use in making any necessary corrections to the kinetic results obtained from the new reactor.

REFERENCES

B-1. Bird, R. B., Stewart, W. E., and Lightfoot, E. N., "Transport Phenomena," p. 114, John Wiley & Sons, Inc., New York, New York (1960).

B-2. Buntin, R. R., Ph. D. thesis, Purdue University (1961).

B-3. Fox, L., "The Numerical Solution of Two Point Boundary Problems in Ordinary Differential Equations," Oxford Univ. Press, London (1957).

B-4. Longwell, P. A., A. I. Ch. E. Journal, 3, #3, 353 (1957).

B-5. Schlichting, H., "Boundary Layer Theory," p. 147, McGraw-Hill Book Co., Inc., New York (1955).

NOMENCLATURE

A - dimensionless parameter defined in eq. B-18

c - dimensionless concentration

d - differential operator, dimensionless

D_F - Fick diffusion coefficient, cm.^{2}/min.

ln - natural logaritm, dimensionless

$\dot{m}$ - material flux, lb./ft.^{2} sec.

P - pressure, lb./ft.^{2}

Q - volumetric flow rate, ft.^{3}/sec.

r - radius, ft.

r_c - radius of catalyst, ft.

R - specific volumetric reaction rate, lb./ft.^{3} sec.

R_s - specific surface reaction rate, lb./ft.^{2} sec.

t - time, sec.

v - velocity, ft./sec.

V - dimensionless velocity, v/v_{max}

y - dimensionless radius, r/r_c

z - axial distance, ft.

z_o - one half of distance between discs, ft.

β - radial flow Peclet Number, $Q/4\pi z_o D_F$

δ - partial differential operator

η - dimensionless radial distance, $2\pi D_{Ei} r^2/z_o Q$

μ - viscosity, lb. sec./ft.^{2}

ρ - density, lb. sec.^{2}/ft.^{4}

σ - concentration, lb./ft.^{3}

ϕ - flow variable, v/r, ft.^{2}/sec.

ψ - dimensionless concentration, $(\pi r_c^2 D_{F,i}/z_o Q)\{(\sigma_i-\sigma_{io})/(\sigma_{i\infty}-\sigma_{io})\}$

ω - dimensionless disc spacing, z/z_o

Subscripts

1 - at the inner radius of the discs

2 - at the outer radius of the discs

i - refers to component i

r - component of vector in radial direction

cf - creeping flow case

o - initial value

∞ - refers to value at the exhaust of the reactor

Superscripts

$\rightarrow$ - denotes a vector

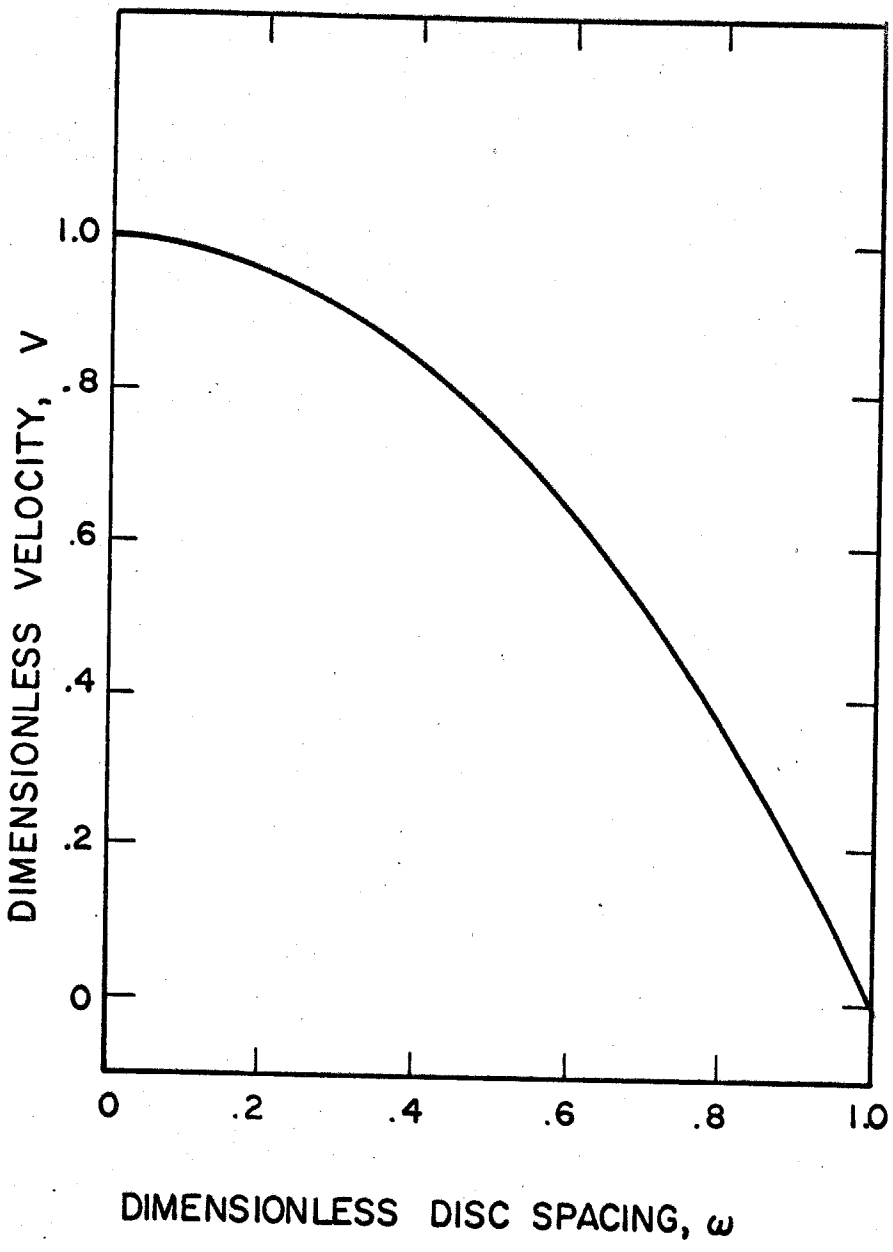

Figure B-1. Typical Velocity Profile

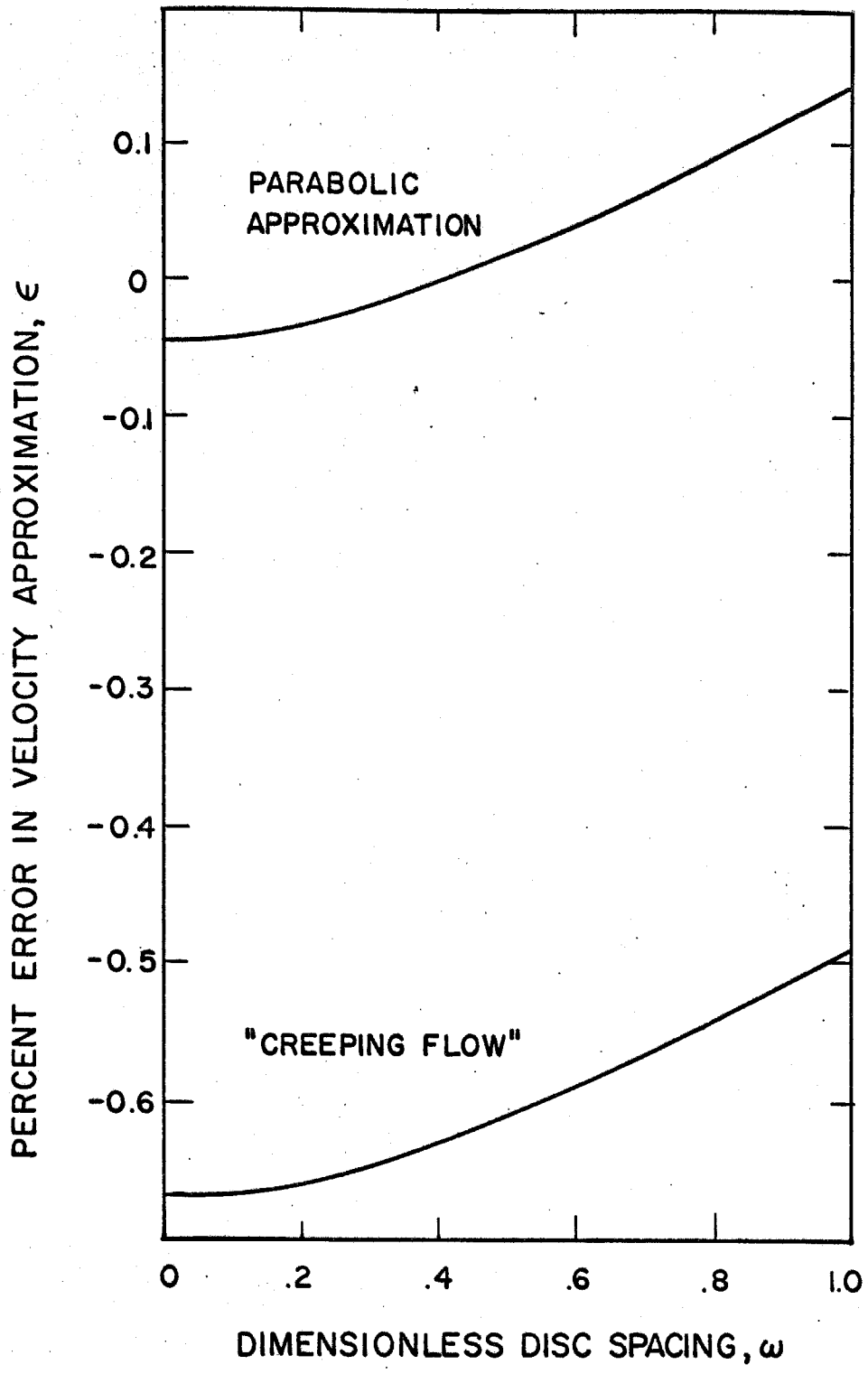

Figure B-2. Error of Velocity Distribution Approximations

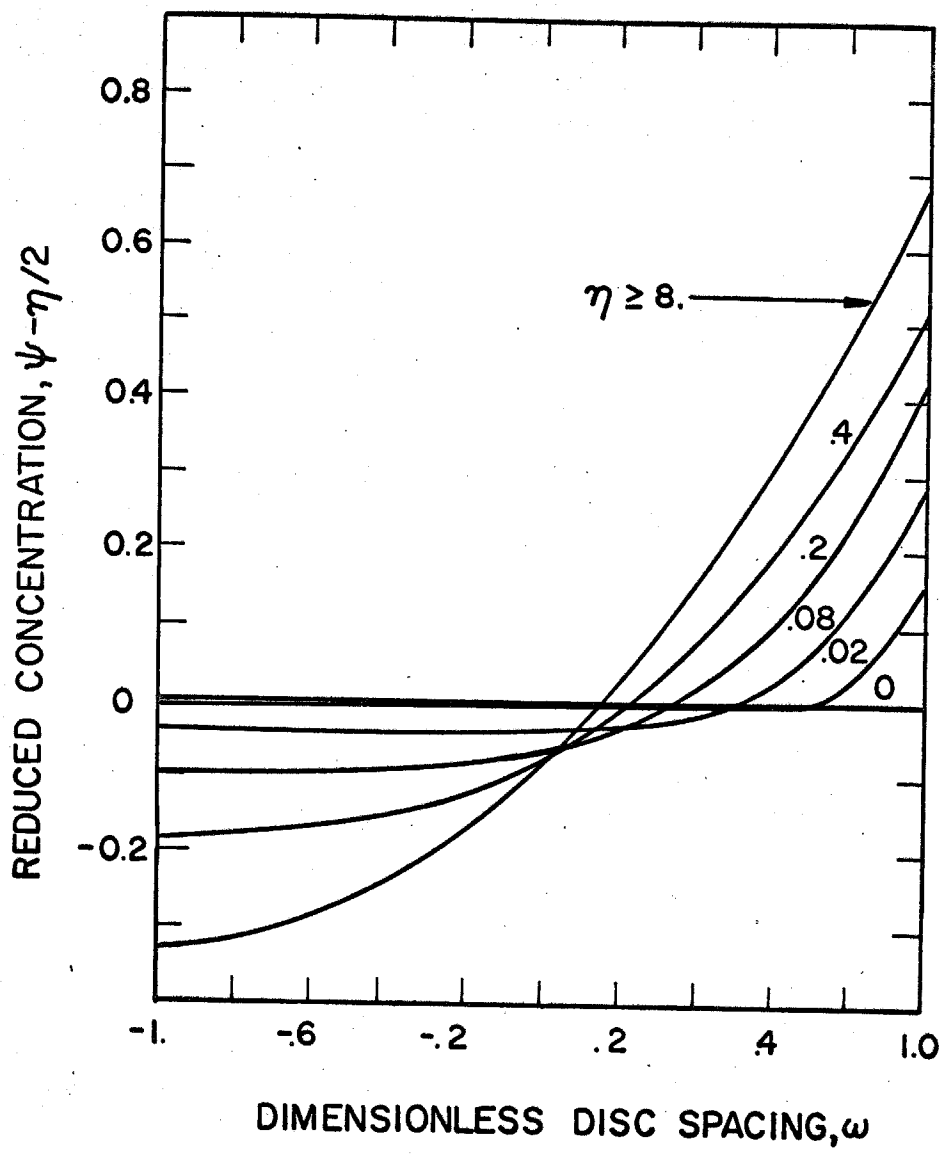

Figure B-3. Reduced Axial Concentration Profile,
Flat Velocity Distribution
No Side Reactions

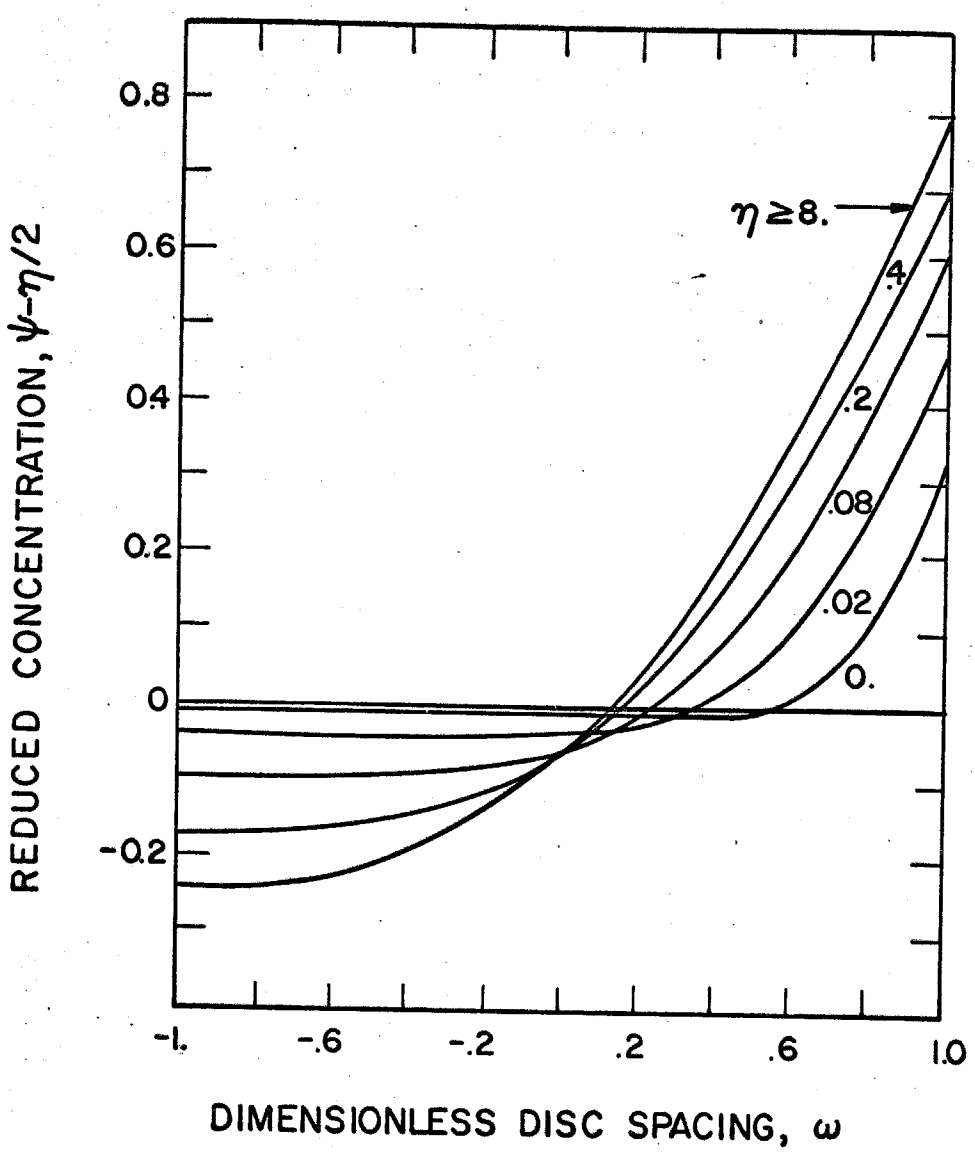

Figure B-4. Reduced Axial Concentration Profile, Parabolic Velocity Distribution No Side Reactions

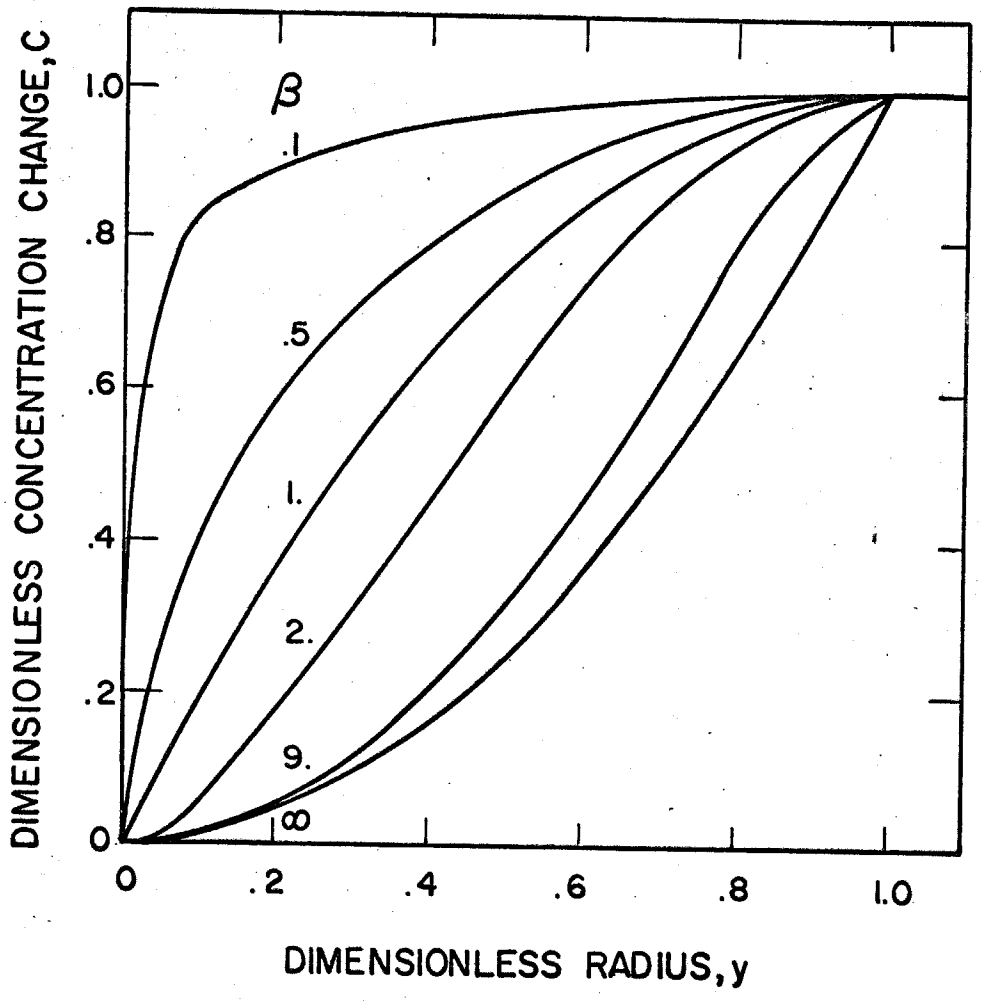

Figure B-5. Radial Concentration Profile
No Side Reactions

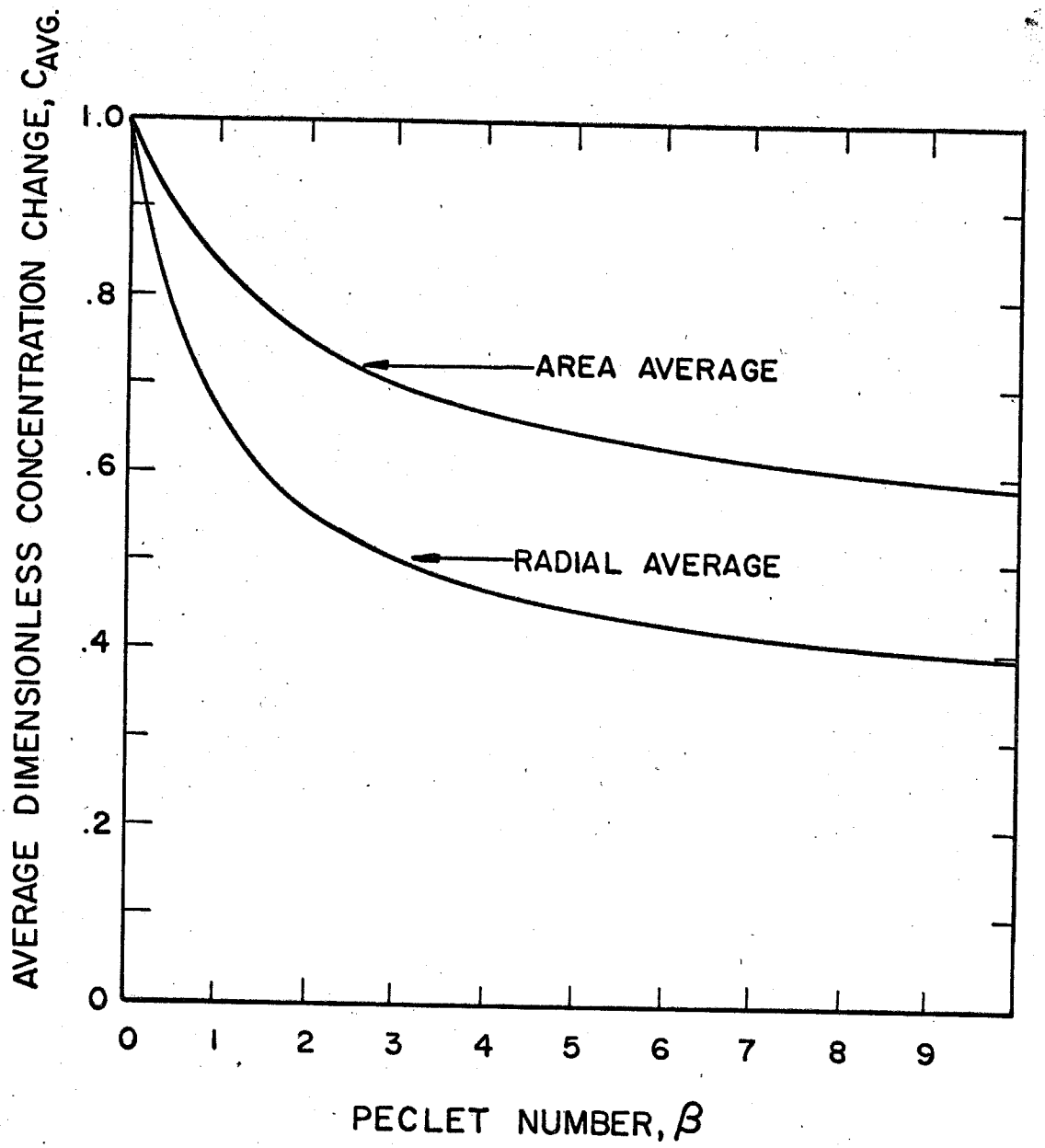

Figure B-6. Effect of Peclet Number on Average Radial Concentration Change
No Side Reactions

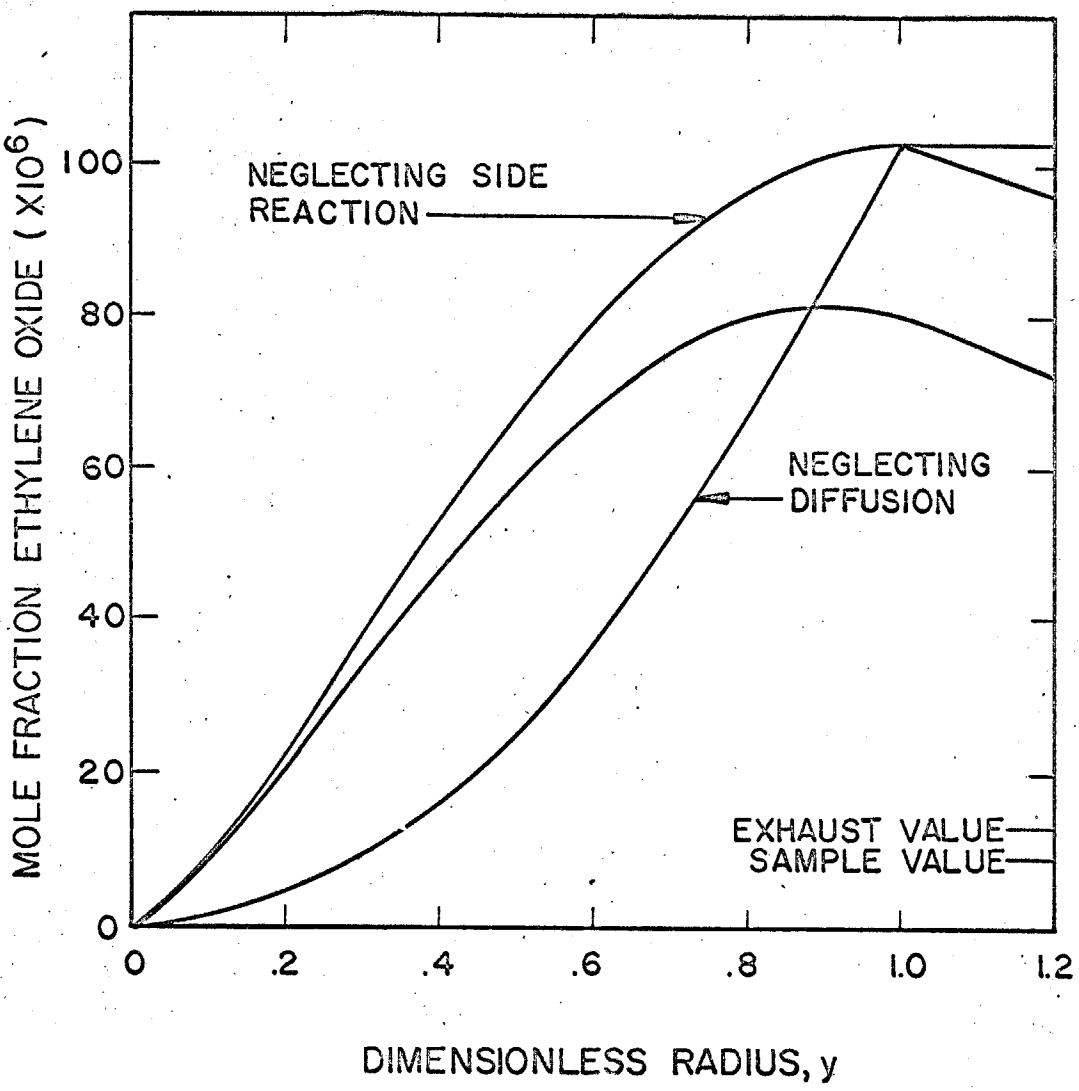

Figure B-7. Calculated Effect of Side Reaction and Radial Diffusion on Radial Concentration Profile, Original Reactor Geometry

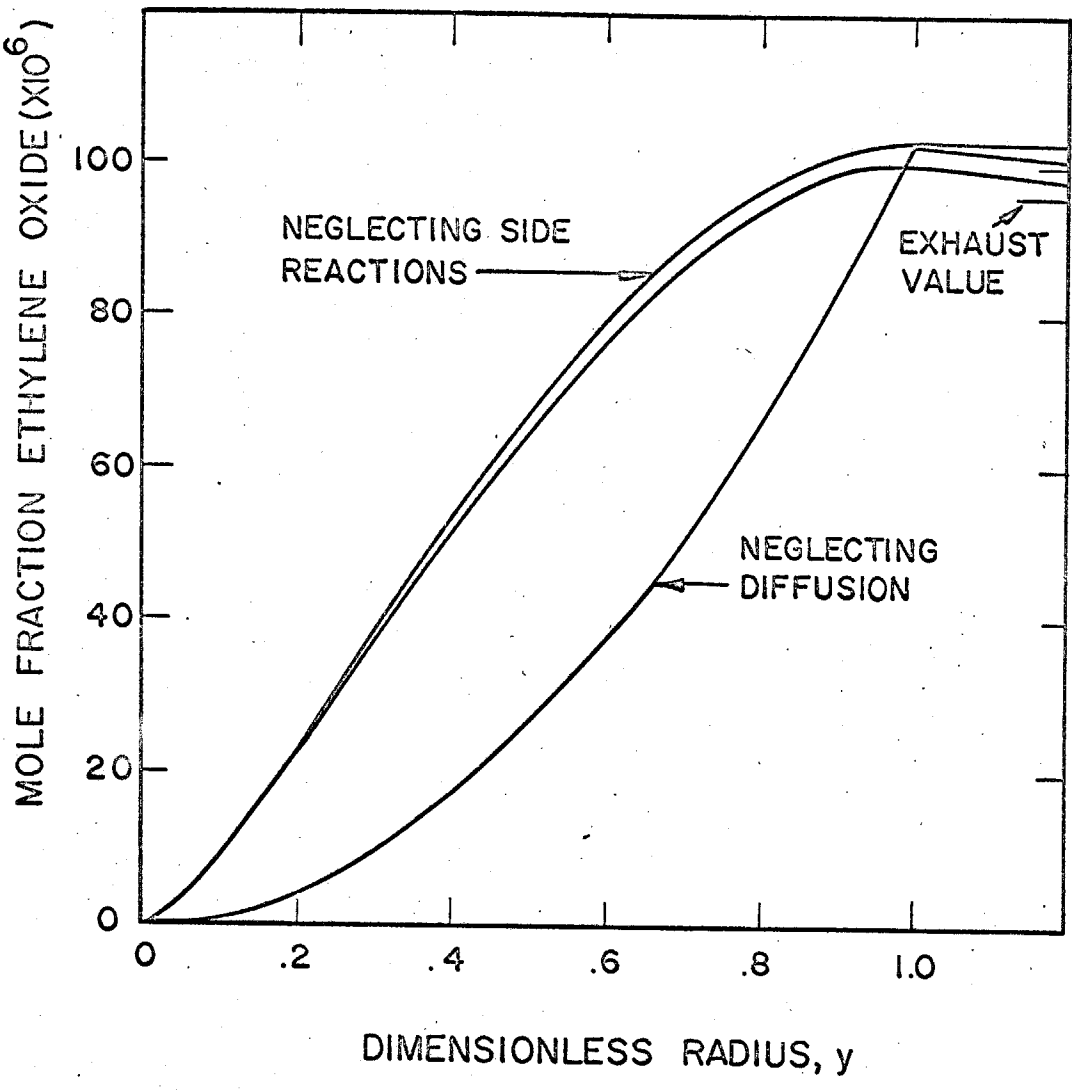

Figure B-8. Calculated Effect of Side Reaction and Radial Diffusion on Radial Concentration Profile, Second Reactor Geometry

APPENDIX C. POLISHING AND ETCHING OF SILVER CRYSTALS

Introduction

The study of the partial oxidation of silver on single crystals with particular emphasis on the effects of the crystallographic orientation of the surface of the silver crystal exposed as the catalyst and the dislocation density of the exposed surface required careful preparation of the silver surface. The method used to prepare the surface of the crystal for etching or for use in the reactor and etching technique is discussed in this Appendix.

Source of Crystals

The crystals used in this work were purchased from the Unimet Company, Arlington, Massachusetts. They had been grown as 1/2 in. cylinders from silver with a minimum purity of 99.99%. The crystals were reported by the manufacturer to be oriented with a specified crystal plane within $\pm 2^{o}$ of normal to the axis of the cylinder. The crystals were cut into half-inch lengths by the manufacturer with an electric-spark, cutting device to minimize the amount of strain introduced into the surfaces. Three crystallographic orientations, (100), (110), and (111), were purchased for use in the study. The reactor design was selected so that a crystal only required polishing of the end of the cylinder prior to use in the reactor.

Polishing of Crystals

A chemical polish had been developed by Levinstein and Robinson (C-3) for use on single silver crystals prior to etching for measurement of dislocation density. Their application of the chemical polish required mechanical preparation of the surface before polishing. Gilpin and Worzala (C-2) developed a method for chemical polishing silver crystals which produced a flat, strain-free surface with rapid removal of silver. A nylon-covered polishing wheel was used to circulate a modified version of the Levinstein polishing solution over the surface of the crystal. The crystal was held in light contact with the wheel by a spring-loaded shaft. The specimen was rotated slowly. They suggested the use of a solution of 100 ml. of saturated CrO_3, 800 ml. of water, and 45 ml. of 10% HCl for the rapid rate of removal of metal with minimum attack of the polishing cloth. This method of polishing silver crystals removed the metal at a rate of 0.001 in./min. No other preparation of the surface was necessary to produce a polished surface for either use in the reactor or for etching purposes. The crystals were washed in concentrated NH_4OH after the polishing step to remove silver chromate and silver chloride which might have remained on the surface. Both compounds are soluble in concentrated NH_4OH (C-1).

Etching of Crystals

Levinstein and Robinson (C-3) had described a method of etching to reveal dislocations in additon to a chemical polishing method.

Their basic etching solution contained 5 parts by volume of concentrated NH_4OH and 2 parts of 30% H_2O_2. Samples were etched for 5 to 45 seconds in this solution. A modified solution for producing smaller etch pits on crystal surfaces with high dislocation densities was also suggested and contained 5 parts concentrated NH_4OH, 1 part 30% H_2O_2, and 0.08 part by volume of a solution containing 5 gm. CrO_3, 25 ml. of water, and 0.5 ml. of concentrated HCl. Levinstein and Robinson investigated the relationship between etch pits produced by these solutions and dislocations and reported a one-to-one correspondence.

Only the (100) and (111) crystal planes were mentioned in the paper by Levinstein and Robinson. Attempts to etch the (110) crystal plane with these solutions were made during this work, and apparently the (110) plane was not attacked by these solutions. The polishing solutions did work on the (110) plane as well as on the other two planes. The etching solution produced pits with shapes characteristic of the crystal plane; square pits were produced on the (100) plane and equilateral triangles were produced on the (111) surface. The etching solution was also sensitive to angular deviations from the (111) crystal plane. A maximum of 2.5 degrees deviation from the (111) plane was allowable for the pits to still have a distinguishable shape was reported by Levenstein and Robinson.

Photomicrographs

Photomicrographs of the etched silver crystals were made using a Bausch and Lomb Model DM metallurgical microscope and a

Bausch and Lomb Model L camera. The camera was equipped with a 4 × 5 in. Polaroid Land film holder. Polaroid Type 55 P/N film was used with this holder to produce both a Polaroid print and a negative. The microscope was equipped with a micrometer stage to allow positioning of the silver crystal for photomicrographs of the same area before and after an operation.

Dislocation Density

Five areas of 0.0625 in.^{2} each were selected at random on the photomicrographs. The average of the number of etch pits in these areas was converted to a value for the density of etch pits by multiplying by the square of the magnification of the photomicrograph and dividing by the area in sq. cm. If a one-to-one correspondence of etch pits to dislocations is assumed, then the dislocation density is equal to the etch-pit density.

Results

The chemical-polishing apparatus described by Gilpin and Worzala (C-2) was found to work satisfactorily on the single silver crystals used in this work. The rate of removal of metal was sufficiently rapid that mechanical preparation of the crystals was unnecessary to produce a polished surface on the face of the cylindrical crystal.

The etching solution developed by Levinstein and Robinson was not found to etch the (110) crystal plane of silver. The (100) and (111) crystals obtained from the Unimet Company responded to the etching

solution and gave pits of the appropriate shapes indicating that the crystals were oriented within 2.5° of the specified planes. Etch-pit densities ranged from 3×10^6 to 5×10^6 pits/sq. cm. for the crystals as obtained from the manufacturer and from 4×10^6 to 7×10^6 pits/sq. cm. for crystals which had been strained 0.8% by rolling 0.004 in. parallel to the axis of the cylinder at 45° angles. If a one-to-one correspondence of etch pits to dislocations is assumed then these values of dislocation density and of increase of dislocation density with strain agree reasonably well with the values reported by Levinstein and Robinson (C-4) which were from 5×10^6 to 2×10^7 dislocations/sq. cm. for unstrained crystals and from 2×10^7 to 6×10^7 dislocations/sq. cm. for crystals which were strained 0.8% in shear.

Vreeland (C-5) had some doubts, however, about assuming a one-to-one correspondence of etch pits to dislocations. His doubts were based on difficulties in distinguishing etch pits from the background of the photomicrographs obtained by the author and the lack of certain patterns of etch pits which he felt should be present. A change in the manner the surfaces etched after the crystals were used in the reactor was also used as a basis for his doubts.

REFERENCES

C-1. "Handbook of Chemistry and Physics," 39th Edition, p. 600, Chemical Rubber Publishing Co., Cleveland, Ohio (1958).

C-2. Gilpin, C. B., and Worzala, F. J., Rev. Sci. Instr., 35, 229 (1964).

C-3. Levinstein, H. J., and Robinson, W. H., J. Appl. Phys., 33, 3149 (1962).

C-4. Levinstein, H. J., and Robinson, W. H., "Report of the Conference on the Relations between Structure and Strength in Metals and Alloys," National Physics Laboratory, Teddington, England (1963).

C-5. Vreeland, T., Jr., Associate Professor of Materials Science, California Institute of Technology, conversations with author.

APPENDIX D. DERIVATION OF LEAST SQUARES EQUATIONS

The problem of fitting a function to experimental data arises frequently, and the method of least-squares is one approach. This method mimizes the value of Chi-square for the fit of the function to the data and therefore gives the highest probability on the Chi-square test (D-1).

The usual treatment of the application of the least-squares principle considers functions which are linear with respect to the parameters which are to be determined and assumes only one of the variables has experimental errors which are uniformly distributed over the range of variables (D-2, D-3, D-4). Many situations arise where several variables have experimental errors, or the errors of the variables are not uniformly distributed over the range of the variables or the function is non-linear with respect to the parameters, Deming (D-1) presented a method of applying the principle of least squares to these situations. A derivation of the equations used in this method is presented in this Appendix.

Derivation of Least Squares Equations

Deming (D-1) developed a method for the application of the least-squares principle to the problem of fitting a function to experimental data for the general case of a function which is non-linear with respect to the parameters and several of the experimental variables have errors which are not distributed uniformly over the range of

the variables. Additional constraints on the values of the parameters were also included. This method reduces to the usual least-squares method for the case of a function which is linear with respect to the parameters and only one experimental variable has errors which are uniformly distributed over the range of the variable.

Assume H experimental values of N related variables

$$\begin{array}{ccccc} x(1,1) & \cdots & x(1,n) & \cdots & x(1,N) \\ \vdots & & \vdots & & \vdots \\ x(h,1) & \cdots & x(h,n) & \cdots & x(h,N) \\ \vdots & & \vdots & & \vdots \\ x(H,1) & \cdots & x(H,n) & \cdots & x(H,N) \end{array}$$

and the values of the standard deviation of each of the variables at each experimental point

$$\begin{array}{ccccc} \sigma(1,1) & \cdots & \sigma(1,n) & \cdots & \sigma(1,N) \\ \vdots & & \vdots & & \vdots \\ \sigma(h,1) & \cdots & \sigma(h,n) & \cdots & \sigma(h,N) \\ \vdots & & \vdots & & \vdots \\ \sigma(H,1) & \cdots & \sigma(H,n) & \cdots & \sigma(H,N) \end{array}$$

are given and a function of the N variables and M parameters:

$$F(\vec{X}, \vec{C}) = 0 \qquad \text{(D-1)}$$

is to be fitted to the experimental data with L additional constraints on the values of the parameters:

$$G_1(\vec{C}) = 0$$
$$\vdots$$
$$G_L(\vec{C}) = 0 \qquad \text{(D-2)}$$

Deming (D-1) defined the objective of the least-squares method as finding values of the parameters so that the weighted sum of the squares of the deviations of the variables is a minimum. The weighted sum of the squares of the deviations is defined as

$$S = \sum_{h=1}^{H} \sum_{n=1}^{N} \left[\frac{x(h, n) - X(h, n)}{\sigma(h, n)} \right]^2 \qquad \text{(D-3)}$$

Equation (D-1) taken at each experimental point and equations (D-2) for each constraint on the values of the parameters are considered as constraints on the possible values of the X s and C s, and the problem of minimizing the sum of the squares of the deviations is attacked by the method of Lagrange's undetermined multipliers. First a new function, which is to be minimized, is defined:

$$S' = S + 2 \sum_{h=1}^{H} \lambda_h F_h + 2 \sum_{\ell=1}^{L} \lambda g_\ell G_\ell \qquad \text{(D-4)}$$

At a minimum or maximum of S' the partial derivative of S' with respect to each X, C, and Lagrange multiplier is equal to zero. This gives:

$$\frac{\partial S'}{\partial X_{h, n}} = -2 \omega_{h, n} \Delta x_{h, n} + 2\lambda_h \frac{\partial F}{\partial X_{h, n}} = 0 \qquad \text{(D-5)}$$

$$\frac{1}{2}\frac{\partial S'}{\partial \lambda_h} = F_h = 0 \qquad \text{(D-6)}$$

$$\frac{1}{2}\frac{\partial S'}{\partial \lambda_{2\ell}} = G_\ell = 0 \qquad \text{(D-7)}$$

$$\frac{1}{2}\frac{\partial S'}{\partial C_m} = \sum_{h=1}^{H} \lambda_n \frac{\partial F_h}{\partial C_m} + \sum_{\ell=1}^{L} \lambda g_\ell \frac{\partial G_\ell}{\partial C_m} = 0 \qquad \text{(D-8)}$$

This gives a total of $H \times N + H + L + M$ equations, which in the general case are non-linear, to be solved for the $H \times N$ predicted values of the variables, the M values of the parameters, the H values of λ, and the L values of λg. Deming's approach to this problem was to expand the function F in a Taylor's series about the value of $\vec{x}$ at each experimental point and about an estimate of the values of the parameters. This gives:

$$F = 0 = F(\vec{x}_h, \vec{C}_e) - \sum_{n=1}^{N} \Delta x_{h,n} \left(\frac{\partial F}{\partial X_n}\right)_{h,e} + \sum_{n=1}^{N} \frac{\Delta x_{h,n}^2}{2} \left(\frac{\partial^2 F}{\partial X_n^2}\right)_{h,e} - \cdots - \sum_{m=1}^{M} \Delta C_{m,e} \left(\frac{\partial F}{\partial C_m}\right)_{h,e} + \sum_{m=1}^{M} \frac{\Delta C_{m,e}^2}{2} \left(\frac{\partial^2 F}{\partial C_m^2}\right)_{h,e} - \cdots \qquad \text{(D-9)}$$

A Taylor's series expansion of the constraint equations G about the estimate of the parameters gives:

$$G_{\ell} = 0 = G_{\ell,e} - \sum_{m=1}^{M} \Delta C_{m,e} \left(\frac{\partial G_{\ell}}{\partial C_m} \right)_e + \sum_{m=1}^{M} \frac{\Delta C_{m,e}^2}{2} \left(\frac{\partial^2 G_{\ell}}{\partial C_m^2} \right)_e - \ldots \quad \text{(D-10)}$$

If the Taylor's series expansions for the functions F and the constraint equations are used in equation (D-4) and the second and higher order partial derivative terms are neglected; then equations (D-5), (D-6), (D-7), and (D-8) reduce to the following set of equations which are linear with respect to the Δx's and ΔC's:

$$2\omega_{h,n}\Delta x_{h,n} - 2\lambda_h \left(\frac{\partial F}{\partial X_n} \right)_{h,e} = 0 \quad \text{(D-11)}$$

$$F_{h,e} - \sum_{n=1}^{N} \Delta x_{h,n} \left(\frac{\partial F}{\partial X_n} \right)_{h,e} - \sum_{m=1}^{M} \Delta C_{m,e} \left(\frac{\partial F}{\partial C_m} \right)_{h,e} = 0 \quad \text{(D-12)}$$

$$G_{\ell,e} - \sum_{m=1}^{M} \Delta C_{m,e} \left(\frac{\partial G_{\ell}}{\partial C_m} \right)_e = 0 \quad \text{(D-13)}$$

$$- \sum_{h=1}^{H} \lambda_h \left(\frac{\partial F}{\partial C_m} \right)_{h,e} - \sum_{\ell=1}^{L} \lambda g_{\ell} \left(\frac{\partial G_{\ell}}{\partial C_m} \right)_e = 0 \quad \text{(D-14)}$$

Equation (D-11) can be rearranged to give :

$$\Delta x_{h,n} = \frac{\lambda_h \left(\frac{\partial F}{\partial X_n} \right)_{h,e}}{\omega_{h,n}} \quad \text{(D-15)}$$

Combination of equation (D-12) and equation (D-15) gives:

$$\lambda_h = \frac{\left[F_{h,e} - \sum_{m=1}^{M} \Delta C_{m,e} \left(\frac{\partial F}{\partial C_m}\right)_{h,e}\right]}{D_h} \qquad \text{(D-16)}$$

$$D_h = \sum_{n=1}^{N} \left(\frac{\partial F}{\partial X_n}\right)^2 \Big/ \omega_{h,n} \qquad \text{(D-17)}$$

Substitution of equation (D-16) into equation (D-14) gives:

$$\sum_{h=1}^{H} \left(\frac{\partial F}{\partial C_m}\right)_{h,e} \frac{\left[F_{h,e} - \sum_{m=1}^{M} \Delta C_{m,e} \left(\frac{\partial F}{\partial C_m}\right)_{h,e}\right]}{D_h} + \sum_{\ell=1}^{L} \lambda g_\ell \left(\frac{\partial G_\ell}{\partial C_m}\right)_e = 0 \qquad \text{(D-18)}$$

The set of equations (D-13) and (D-18) may be written in matrix form as:

$$A\vec{z} = \vec{B} \qquad \text{(D-19)}$$

where:

for $1 \leq i \leq M$, $1 \leq j \leq M$

$$a_{ij} = \sum_{h=1}^{H} \left(\frac{\partial F}{\partial C_i}\right)_{h,e} \left(\frac{\partial F}{\partial C_j}\right)_{h,e} \Big/ D_h \qquad \text{(D-20)}$$

$$b_i = \sum_{h=1}^{H} \left(\frac{\partial F}{\partial C_i}\right)_{h,e} F_{h,e} \Big/ D_h \qquad \text{(D-21)}$$

$$z_i = \Delta C_{i,e} \tag{D-22}$$

for $1 \leq i \leq M$, $m \leq j \leq M + L$

$$\ell = j - M$$

$$a_{ij} = - \left(\frac{\partial G_\ell}{\partial C_i} \right)_e \tag{D-23}$$

for $M < i \leq M + L$, $1 \leq j \leq M$

$$\ell = i - M$$

$$a_{ij} = - a_{ji} \tag{D-24}$$

$$b_i = G_{\ell,e} \tag{D-25}$$

$$z_i = \lambda g_\ell \tag{D-26}$$

for $M < i \leq M + L$, $M < j \leq M + L$

$$a_{ij} = 0 \tag{D-27}$$

These linear equations are called the normal equations. Equation (D-19) can be solved by matrix inversion methods and the calculated values of the variables obtained from equations (D-15) and (D-16). The sum of the squares is obtained from:

$$S = \sum_{h=1}^{H} \sum_{n=1}^{N} \omega_{h,n} \Delta x_{h,n}^2 = \sum_{h=1}^{H} \lambda_h^2 \sum_{n=1}^{N} \frac{\left(\frac{\partial F}{\partial X_n} \right)^2}{\omega_{h,n}} = \sum_{h=1}^{H} \lambda_h \sum_{n=1}^{N} \Delta x_{h,n} \left(\frac{\partial F}{\partial X_n} \right)_h \tag{D-28}$$

An estimate of the variance of the fit and the variance of the parameters is given by the following equations (D-1):

$$\sigma^2 = S/(H - M - L) \tag{D-29}$$

$$\sigma^2_{C_m} = a^I_{m,m}\sigma^2 \tag{D-30}$$

The confidence limits for the values of the parameters are given by:

$$CL_{C_m} = t(P, H\text{-}M\text{-}L)\sqrt{\sigma^2_{C_m}} \tag{D-31}$$

Confidence bands for function f, of the parameters may be calculated from the following equation:

$$CL_f = t(P, H\text{-}M\text{-}L)\sqrt{\sigma^2\,(\vec{f'}^T A^I \vec{f'})} \tag{D-32}$$

The only assumption in this method of applying the least-squares principle to curve fitting is that the second and higher order partial derivative terms of the Taylor's series expansions of the function F and the constraint equations may be neglected. A case where this assumption is valid is the one usually considered in least-squares data fitting; the case of fitting a function which is linear with respect to the parameters and a single variable with errors uniformly distributed over its range. The validity of this assumption for the general case will depend on the functions F and G, the magnitudes of the experimental errors, and the original estimate of the parameters. A check should be made to determine if the matrix solution is actually a minimum or maximum because equations (D-11), (D-12),

(D-13), and (D-14) are satisfied in either case. The evaluation of the confidence limits for the parameters or the confidence bands for functions of the parameters assumes the errors in the variables were independent and were distributed with a normal frequency distribution.

A general-purpose subroutine based on this method was written for use on the IBM 7094 Digital Computer. The method has been used for fitting various functions to experimental data. No particular difficulties have been encountered for functions which are linear with respect to the parameters and several variables were considered to have possible experimental errors. The application of the method to functions which were non-linear with respect to the parameters has had a very limited amount of success.

REFERENCES

D-1. Deming, W. E., "Statistical Adjustment of Data," John Wiley and Sons, Inc., New York (1943).

D-2. Hoel, P. G., "Introduction to Mathematical Statistics," 2nd Edition, p. 125, John Wiley and Sons, Inc., New York (1954).

D-3. Lapidas, L., "Digital Computation for Chemical Engineers," p. 323, McGraw-Hill Book Co., Inc., New York (1962).

D-4. Mickley, H. S., Sherwood, T. K., and Reed, C. E., "Applied Mathematics in Chemical Engineering," 2nd Edition, p. 95, McGraw-Hill Book Co., Inc., New York (1957).

NOMENCLATURE

A - Matrix defined in equations (D-19) through (D-27)

B - Vector defined in equations (D-19) through (D-27)

C - Parameter of the function F

ΔC - Difference between estimated value of C and true value of C

CL - Confidence Limit

D - Defined in equation (D-17)

f - A function of the parameters

f' - Vector of partial derivatives of f with respect to the parameters

F - Function which is fitted to the experimental data

G - Constraint function on values of parameters

P - Probability

S - Weighted sum of the squares of the derivatives of the experimental variables defined by equation (D-3)

S' - Weighted sum of squares defined by equation (D-4)

t - Student's t

x - Experimental value of variable

X - Adjusted value of variable

Δx - x - X

z - Vector defined in equations (D-19) through (D-27)

λ - Lagrange multiplier

λg - Lagrange multiplier

σ - Standard deviation

σ^2 - Variance

Superscript

$\rightarrow$ - Denotes vector

Subscripts

s - Refers to value obtained with estimated values of parameters

h - Index refering to experimental points

ℓ - Index refering to constraints

m - Index refering to parameters

n - Index refering to variables

APPENDIX E

PROPOSITIONS

PROPOSITION

A new design for a hydrogen-flame-ionization detector is proposed. This design should have a higher sensitivity than the flame detectors in use at the present time. The increase in sensitivity would result from an increase in flame temperature and a reduction in the volume of the reaction zone of the flame.

The hydrogen-flame-ionization detector measures the ions formed by the combustion or a carbon compound in a hydrogen flame. The sensitivity of the present flame detector design is in the parts per billion range for hydrocarbons (1, 5). The present design is based on the use of a stable, laminar, diffusion flame of hydrogen. This design of flame detector was studied in detail by Desty, Geach, and Goldup (3). Their results indicated the sensitivity of the flame ionization detector was a strong function of the flame temperature, and the ionization efficiency was low with one ion formed per 2,000 carbon atoms. Sternberg, Gallaway, and Jones (4) concluded the ionization was dependent on the rate of energy release per mole of flame gas rather than on the flame temperature. On the basis of these studies, the sensitivity of the flame detector could be increased by reducing the energy losses from the flame and reducing the volume of the reaction zone.

Three large sources of energy loss from the laminar, diffusion flame used in the present flame detector designs exist. One is due to the large excess of air required to provide oxygen for the flame

and to keep the water vapor concentration in the detector cell low. A second large energy loss from the flame is due to conduction along the hydrogen jet. Radiation from the flame to its cooler surroundings is the third large loss of energy from the flame. Reduction of these energy losses would raise the flame temperature and should increase the sensitivity of the detector.

The flame-detector design shown in Figure 1 is based on the design of the free turbulence, vortex burner discussed by Berty (2). Berty reported complete combustion of the fuel in the vortex burner was possible with only a slight excess of air. The vortex burner operated with the flame detached from the fuel jet and concentrated in a small region in the center of the vortex, and the incoming air acted as an insulator between the flame and the burner wall reducing heat losses to the wall. These facts indicate that the flame temperature and the density of energy release in the vortex burner flame would be higher than in the laminar, diffusion type of flame detector.

In conclusion, a design for an increased sensitivity hydrogen flame detector is presented. Arguments for the increased sensitivity are based on an increase in flame temperature due to low heat losses from the flame and a reduction in the volume of the reaction zone of the flame. This design should be considered as a possible way of increasing the sensitivity of hydrogen flame detectors.

References

1. Andreatch, A. J., and Feinland, J., Anal. Chem. 32, 1021 (1960).
2. Berty, T. E., seminar in Ch. E. 291, Fall Term 1961-62, California Institute of Technology, Pasadena, California, and private conversations with the author.

3. Desty, D. H., Geach, C. J., and Goldup, A., "An Examination of the Hydrogen Ionization Detector Using a Diffusion Dilution Apparatus," presented at the Third International Symposium on Gas Chromatography, Edinburg, Scotland, June 1960.

4. Ongkiehong, L., "Investigation of the Hydrogen Flame Ionization Detector," Koninklijke/Shell Laboratorium, Amsterdam, The Netherlands.

5. Sternberg, J. C., Gallaway, W. S., and Jones, D. T. L., "Gas Chromatography," Chapt. 18, Academic Press, New York (1962).

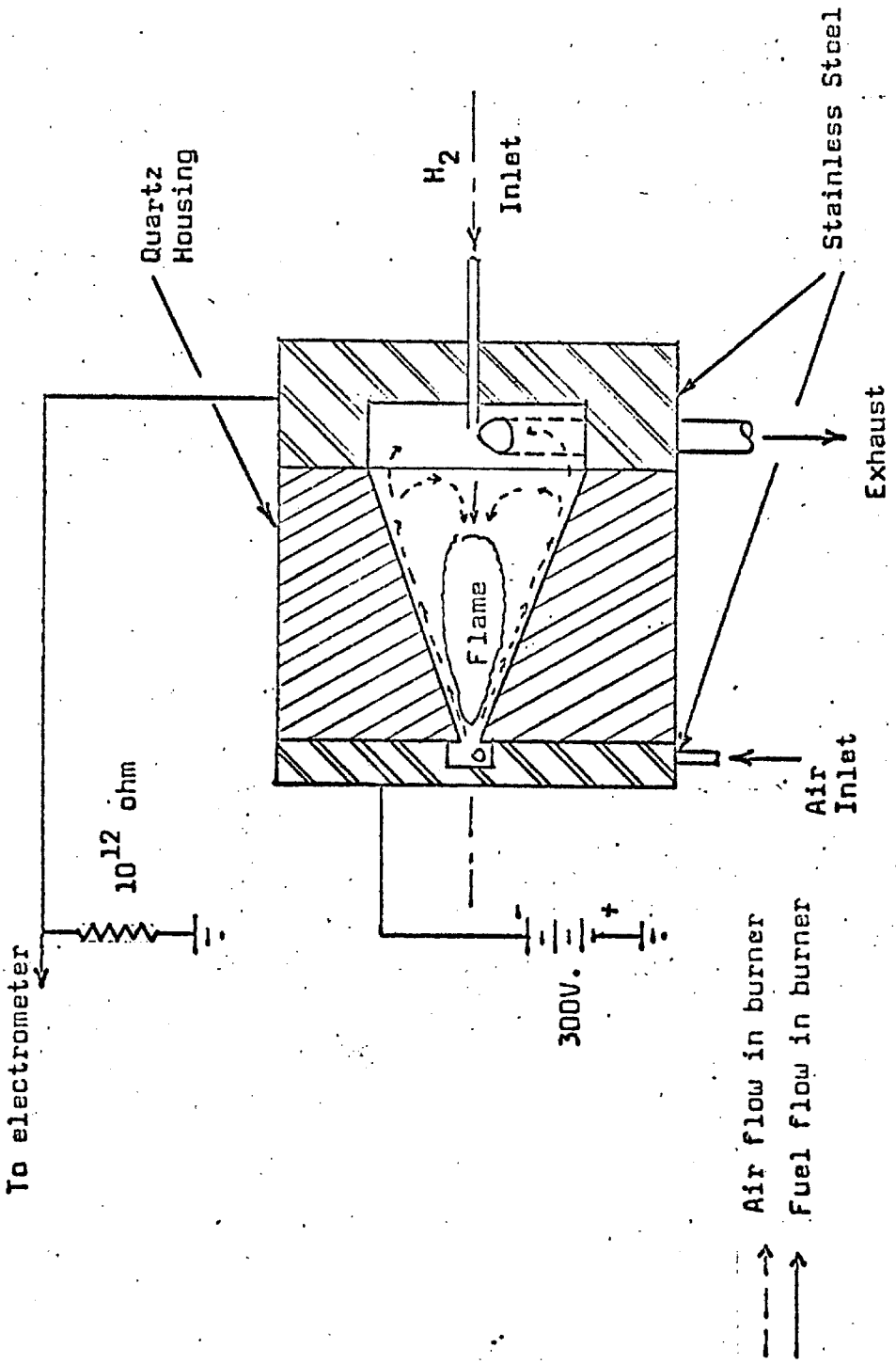

Figure 1. Diagram of Proposed Design for a Hydrogen Flame Ionization Detector

PROPOSITION

A statistical model of the pore structure of porous solids is proposed. This model is used to calculate the tortuosity factor for effective diffusion coefficients in porous solids.

The problem of evaluating an effective diffusion coefficient for diffusion in a porous solid from the Fick diffusivity, the Knudsen diffusivity, or some combination of the two occurs frequently in studies of heterogeneous catalysis. An empirical correction factor, the tortuosity factor, is used to account for the winding, crooked nature of the pore structure.

Wheeler (3) proposed a model of a porous solid where the pores were visualized as randomly oriented cylinders of one fixed diameter which intersected any plane at an average angle of 45°. The path length for diffusion was $1/\sqrt{2}$ longer than the distance normal to the plane, and the cross-sectional area of the pore was $1/\sqrt{2}$ of the projected area of the pore onto the plane. Therefore Wheeler's model gave a tortuosity factor of 1/2. Deryaguin (1) studied the effects of elastic and inelastic collisions of the gas molecules with the wall of the pore on the effective diffusion coefficient. He found the ratio of the diffusion coefficient for elastic collisions to the coefficient for inelastic collisions was 13/9 for a completely random pore structure. Satterfield and Sherwood (2) combined the tortuosity factor and a geometric factor into a single factor for use in empirical correlations of experimentally determined values of effective diffusion coefficients. This factor ranged from 0.1 to 0.9.

The effects of the tortuosity of the pore structure on the

effective diffusion coefficient are more clearly defined if the angle between the axis of a pore and a particular coordinate direction is assumed to have a statistical frequency distribution. A sketch of a pore in spherical coordinates is shown in Figure 1. The diffusional mass flux of component i through the pore in the direction of the axis of the pore expressed in terms of the Fick diffusion coefficient is:

$$\dot{m}_p = - D_i A_p \frac{dC_i}{dL} \tag{1}$$

The radial component of the mass flux through the pore is given by:

$$\dot{m}_r = \dot{m}_p \cos \phi \tag{2}$$

The following equations are obtained from the geometry of the system shown in Figure 1.

$$dr = dL \cos \phi \tag{3}$$

$$A_p = A_s \cos \phi \tag{4}$$

Therefore the component of the mass flux through the pore in the radial direction is related to the gradient of the concentration of component i in the radial direction and the area of the pore normal to the radial direction by:

$$\dot{m}_r = - D_i A_s \frac{dC_i}{dr} \cos^3 \phi \tag{5}$$

If the frequency distribution, $f(\phi)$, of the pore angle is independent of the size and shape of the pores, an average value of $\dot{m}_r$ may be obtained from the following equation:

$$\dot{m}_{r,m} = - D_i A_s \frac{dC_i}{dr} \int_0^{\pi/2} \cos^3\phi \, f(\phi) \, d\phi \qquad (6)$$

The total flux of component i crossing the spherical surface at r is given by:

$$\dot{m}_t = \sum \dot{m}_{r,m} = - 4\pi r^2 D_{i,e} \frac{dC_i}{dr} \qquad (7)$$

The porosity of the solid, θ, is related to the sum of the projected pore areas by the following equation:

$$4\pi r^2 \theta = \sum A_s \qquad (8)$$

Substitution of equations (6) and (8) into equation (7) gives the following relationship for the effective diffusion coefficient:

$$D_{i,e} = \theta D_i \int_0^{\pi/2} \cos^3\phi \, f(\phi) \, d\phi \qquad (9)$$

The following results were obtained by evaluating the integral in equation (9) for two assumed frequency distributions:

Frequency Distribution	Average Pore Angle	Tortuosity Factor	
		Wheeler's Model	This Model
$f(\phi) = 2/\pi$	45^o	0.50	0.424
$f(\phi) = 4/\pi - 8\phi/\pi^2$	30^o	0.75	0.630

The differences in the values obtained for the tortuosity factor by use of the two models are about 15%.

A model of the pore structure for porous solids has been

proposed in terms of a statistical frequency distribution function for the angle between the axis of the pore and a coordinate direction of the solid. The value of the model was demonstrated by using it to calculate the effects of the tortuosity of the pores on the effective diffusion coefficient.

References

1. Deryaguin, B., Compt. rend. acad. sci., U. S. S. R. 53, 623 (1946).

2. Satterfield, C. N., and Sherwood, T. K., "The Role of Diffusion in Catalysis," p. 12, Addison-Wesley Publishing Co., Inc., Reading, Mass. (1963).

3. Wheeler, A., "Catalysis," II, p. 129, Reinhold Publishing Corp,, New York (1955).

Nomenclature

A_p - Normal cross-sectional area of pore, cm.^{2}

A_s - Projected cross-sectional area of pore, cm.^{2}

C_i - Concentration of component i, gm./cm.^{3}

D_i - Pore diffusivity of component i, cm.^{2}/sec.

$D_{i,e}$ - Effective radial diffusivity for component i, cm.^{2}/sec.

d - Differential operator, dimensionless

L - Distance measured along axis of pore, cm.

$\dot{m}_p$ - Diffusion flux of component i through pore, gm./sec.

$\dot{m}_r$ - Radial component of $\dot{m}_p$, gm./sec.

$\dot{m}_{r,m}$ - Average of $\dot{m}_r$, gm./sec.

$\dot{m}_t$ - Total diffusion flux of i through spherical surface at radius r, gm./sec.

r - Radius of spherical surface, cm.

θ - Porosity of particle

ϕ - Angle between pore axis and radial coordinate direction

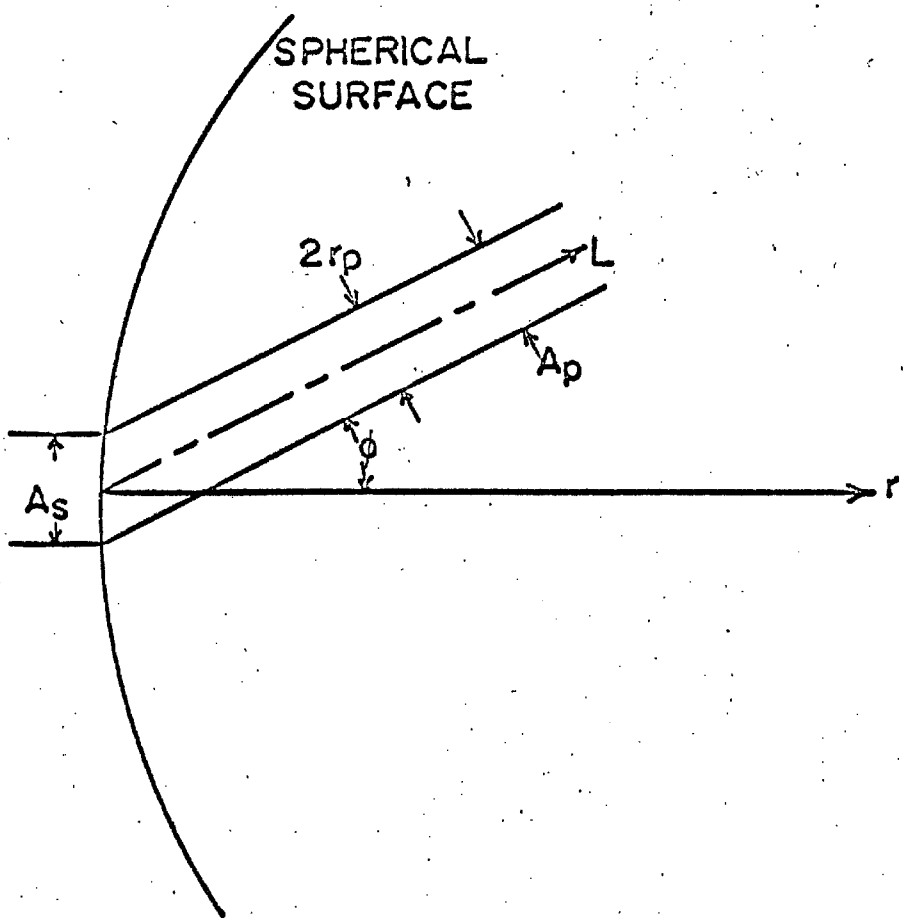

Figure 1. Sketch of Pore Geometry

PROPOSITION

The conversion for a zero-order chemical reaction in a back-mixed, flow reactor with a macrofluid feed may be increased by the addition of a recycle loop to the reactor.

Levenspiel (1) discussed a statistical model for the residence time in a chemical reactor. He developed analytic expressions for the conversion of a macrofluid in a flow reactor with complete back-mixing. A macrofluid was defined as a fluid which separated into aggregates which maintained their identity during their stay in the reactor. The following expressions were developed for zero, first, and second-order reactions with no volume change associated with the reaction.

Zero-order

$$\frac{C}{C_o} = 1 - R + Re^{-1/R} \tag{1}$$

First order

$$\frac{C}{C_o} = 1/(1 + R) \tag{2}$$

Second-order

$$\frac{C}{C_o} = (1/R)e^{1/R}ei(1/R) \tag{3}$$

$$R = \frac{kV}{v} C_o^{n-1} \tag{4}$$

If a recycle loop is added to the reactor as shown in Figure 1,

and the volume of the loop is negligible compared to the reactor volume; the following equations may be used to describe the system:

$$v/v_f = 1/(1 - B) \tag{5}$$

$$C_o = BC + C_f(1 - B) \tag{6}$$

For a first-order reaction combination of equations (2), (4), (5), and (6) gives

$$C/C_f = 1/(1 + kV/v_f) = 1/(1 + R_f) \tag{7}$$

Equation (7) shows the conversion for a first-order reaction is not affected by the fraction of the total flow which is recycled. An iterative procedure was used to solve the equations for the zero and second-order cases. The conversion for the second-order case decreased with increased recycle rate. The zero-order case showed an increase in conversion with increased recycle rate. The results for the zero-order case are shown in Figure 2. A large increase in conversion was obtained for $R_f = 1$ and B greater than 0.5. This method of increasing conversion could have application to specific industrial problems.

References

1. Levenspiel, O., "Chemical Reaction Engineering," p. 317, John Wiley and Sons, Inc., New York (1962).

Nomenclature

B - Fraction of total reactor flow recycled, dimensionless

C - Concentration of reactant, gm. moles/ℓ.

e - Base of natural logarithms, dimensionless

ei - Exponential integral

k - Reaction rate constant, gm. moles (gm. moles/ℓ.)$^{-n}$/min.

n - Reaction order, dimensionless

R - Parameter defined in equation (4), dimensionless

v - Volumetric flow rate, ℓ./min.

V - Reactor volume, ℓ.

Subscripts

f - Refers to feed

o - Refers to inlet of reactor

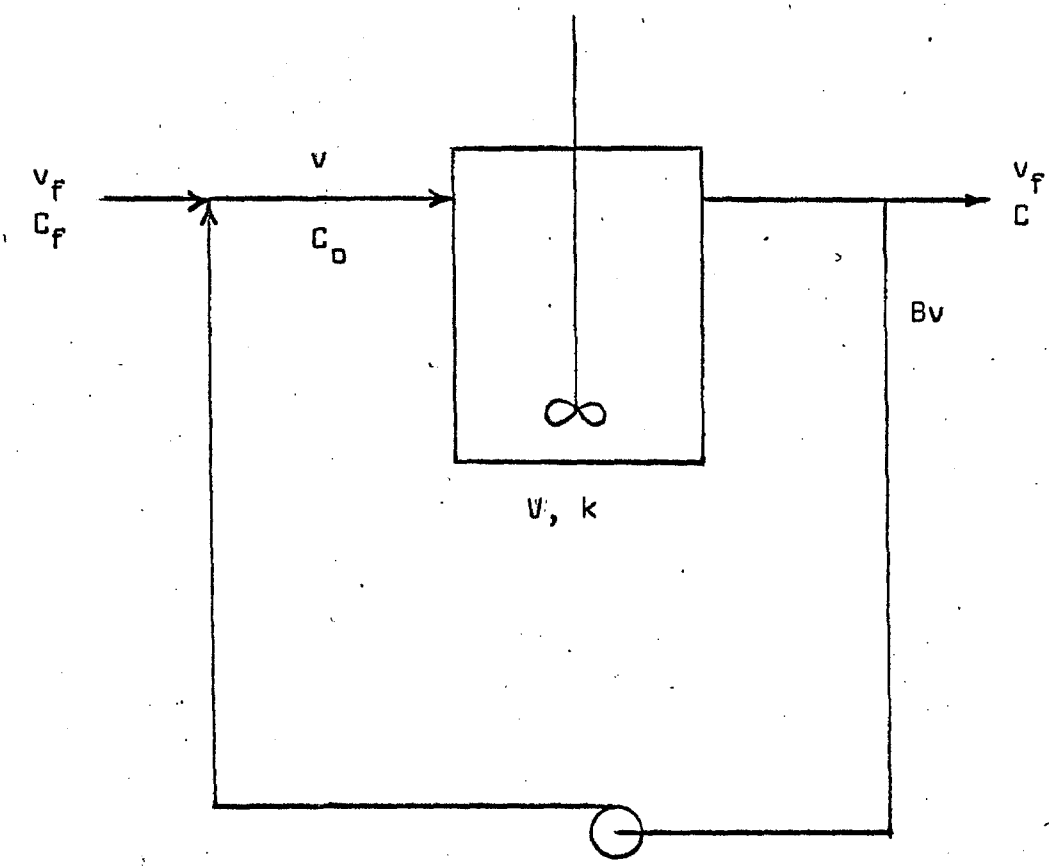

Figure 1. Flow Chart for Reactor with Recycle

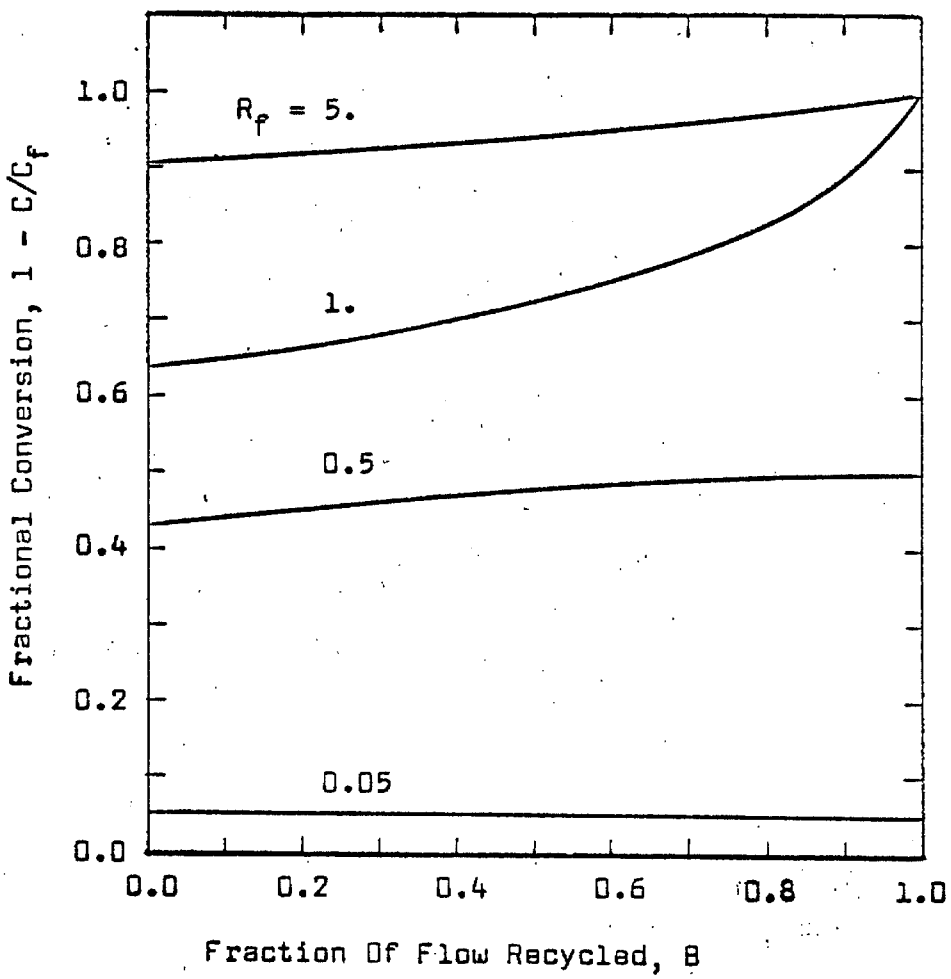

Figure 2. Effect of Recycle on Conversion of Zero-order Reaction

PROPOSITION

The problem of obtaining a solution of the differential equations describing a general set of first-order chemical reactions in a closed, constant volume system can be simplified by use of the law of conservation of matter.

Matsen and Franklin (2) and Frost and Pearson (1) have discussed in detail the application of matrix methods to the problem of obtaining the solution of the differential equations for a general set of first-order reactions in a closed, constant volume system. They have shown the simultaneous differential equations describing the behavior of the concentrations of n components in such a system as a function of time can be written in matrix form as follows:

$$\dot{\vec{c}} = A\vec{c}, \quad t > 0 \tag{1}$$

$$\vec{c} = \vec{c}^{\,o}, \quad t = 0 \tag{2}$$

$$a_{ii} = -\sum_{\substack{j=1 \\ i \neq j}}^{n} k_{ij}, \tag{3}$$

$$a_{ij} = k_{ji} \tag{4}$$

The solution of the problem in matrix form is straightforward, theoretically, but is often very difficult in practice. Calculation of the n eigenvalues of the matrix A is required for the solution. This calculation becomes more difficult as n increases.

The law of conservation of matter for this system may be written as:

$$\sum_{i=1}^{A} c_i = \sum_{i=1}^{n} c_i^o \tag{5}$$

This equation may be used to reduce the number of equations in the original system by one. The resulting system of equations in matrix form is:

$$\dot{\vec{c}} = B\vec{c} + \vec{d} \quad , \quad t > 0 \tag{6}$$

$$\vec{c} = \vec{c}^{\,o} \quad , \quad t = 0 \tag{7}$$

$$c_n = \sum_{i=1}^{n} c_i^o - \sum_{i=1}^{n-1} c_i \tag{8}$$

$$b_{ii} = - \sum_{j=1}^{n} k_{ij} - k_{ni} \quad , \quad i \neq j \tag{9}$$

$$b_{ij} = k_{ij} - k_{ni} \tag{10}$$

$$d_i = k_{ni} \sum_{j=1}^{n} c_j^o \tag{11}$$

The solution of this matrix equation requires the calculation of n-1 eigenvalues. Thus application of the law of conservation of matter reduced the dimension of the matrix and the corresponding number of eigenvalues by one. This reduction could greatly simplify the calculations necessary to use this method.

References

1. Frost, A. A., and Pearson, R. G., "Kinetics and Mechanism," p. 173, John Wiley and Sons, Inc., New York (1961).

2. Matsen, F. A., and Franklin, J. L., J. Am. Chem. Soc., 72, 3337 (1950).

Nomenclature

A - Matrix with elements defined in equations (3) and (4)

a - Elements of A matrix

B - Matrix with elements defined in equations (9) and (10)

b - Elements of B matrix

c - Concentration, gm. moles/cc.

d - Vector defined in equation (11)

k_{ij} - First order rate constant for component i reacting to produce component j, 1/sec.

t - Time, sec.

Superscripts

$\cdot$ - Denotes derivative with respect to time

o - Denotes initial conditions

$\rightarrow$ - Denotes vector

PROPOSITION

A method for numerically differentiating experimental data is proposed. This method fits a polynomial of degree two by the method of least squares to seven data points and evaluates the derivative at the central point.

In the analysis of experimental data, numerical differentiation is often necessary, but only a brief discussion of the problems which are involved is found in the literature (2). However numerical differentiation of smooth, tabulated functions is discussed in detail (1, 2). The numerical methods for differentiating smooth data or tabulated values of functions generally reduce to fitting a polynomial of degree N-1 to N points and calculating the derivative from this polynomial. Such a procedure is of limited value when applied to data which has errors because the errors in the data tend to be magnified by the differentiation process and produce large errors in the values of the derivative. This can be seen in the results shown in Tables 1 and 2 for the cases where the number of points equals the number of constants in the polynomial.

A method for numerically differentiating experimental data was proposed by the author and used by Nebeker (4) and Morrison (3). This procedure fitted a polynomial of degree two by the method of least squares to seven data points and evaluated the derivative from the polynomial. The choice of the use of a second-degree polynomial and seven data points was based on the semi-quantitative argument which follows:

1. A second-degree polynomial should fit short segments of a curve reasonably well.

2. The value of Student's "t", a measure of the statistical uncertainty associated with a given fit because of the amount of data used, decreases rapidly as the number of degrees of freedom increase from zero to four and decreases much slower as the number of degrees of freedom increase above four. This indicates there is little statistical advantage gained by increasing the number of degrees of freedom above four and in practice the fit might be worse since a larger segment of the data would be involved. Therefore it was reasoned that a second-degree polynomial fitted to seven data points should give a reasonably good value for the derivative.

To obtain further evidence to support the use of this procedure for differentiating experimental data two sets of "experimental" data were generated by adding random normal deviates with $\sigma = 0.1$ to values of an algebraic function. The "experimental" data were numerically differentiated using the least-squares procedure, and the value of the derivative which was obtained was compared to the value of the derivative of the algebraic function. The root-mean-square (RMS) errors of the derivative obtained by the use of several different combinations of the number of data points and the degree of the polynomial are shown in Tables 1 and 2. These results show little difference in the errors of the derivatives using either first or second-degree polynomials, but a decrease of about 50% in the value of the RMS error is obtained when the number of degrees of freedom are increased

from 2 to 4. The RMS error of the derivative was 0.016 for a first-degree polynomial and 0.0013 for a second-degree polynomial when the procedure was applied to smooth values of the function $y = \exp(-x)$. This would indicate the use of the second-degree polynomial is more desirable since it gave a much better result for the case of smooth data.

These calculations gave further evidence of the value of the use of a least-squares fit of a second-degree polynomial to seven experimental data points for calculating the derivative of the experimental data at the central point. When the data points are equally spaced with respect to the independent variable, the procedure gives the following equation for the calculation of the derivative:

$$y_i' = \frac{1}{28\,\Delta x} \sum_{j=-3}^{j=3} j\, y_{i+j} \qquad (1)$$

In cases where the data are not equally spaced, the usual least-squares calculations are made and the derivative calculated from the resulting fit.

In conclusion a semi-quantitative argument and results of a numerical study are presented to support this proposal that a second-degree polynomial fitted to seven experimental data points by the method of least squares is a satisfactory procedure for differentiating experimental data. For the case of equally spaced values of the independent variable the procedure reduces to a simple algebraic expression for the derivative.

References

1. Lapidus, L., "Digital Computation for Chemical Engineers," p. 42, McGraw-Hill Book Company, Inc., New York (1962).

2. Mickley, H. S., Sherwood, T. K., and Reed, C. E., "Applied Mathematics in Chemical Engineering," p. 25, McGraw-Hill Book Company, Inc., New York (1957).

3. Morrison, M. E., Ph. D. Thesis, California Institute of Technology, Pasadena, California (1965).

4. Nebeker, E. B., Ph. D. Thesis, California Institute of Technology, Pasadena, California (1965).

Table 1

Comparison of Root-mean-square Error of Derivative

$y = 1 - x$
$\sigma = 0.1$

Number of Constants	Number of Points						
	2	3	4	5	6	7	8
1	1.00	1.00	1.00	1.00	1.00	1.00	1.00
2	2.98	1.48	0.91	0.63	0.53	0.41	0.39
3		1.65	1.58	1.29	0.90	0.81	0.74
4			2.88	1.85	1.77	1.35	1.17
5				3.45	1.83	1.69	1.75
6					5.26	2.74	1.49
7						7.74	4.07
8							12.1

Table 2

Comparison of Root-mean-square Error of Derivative

$y = \exp(-x)$
$\sigma = 0.1$

Number of Constants	Number of Points							
	2	3	4	5	6	7	8	9
1	0.66	0.66	0.66	0.66	0.66	0.66	0.66	0.66
2	2.32	1.50	1.11	0.82	0.72	0.64	0.51	0.45
3		1.70	1.50	0.98	0.74	0.51	0.68	0.65
4			2.23	1.93	1.82	1.35	1.09	0.89
5				2.22	1.84	1.96	1.78	1.13
6					2.91	2.10	1.92	1.61
7						4.28	2.44	1.62
8							7.62	3.15
9								13.7